NASA CR 137767

STOL AIRCRAFT TRANSIENT GROUND EFFECTS

PART II. EXPERIMENTAL TECHNIQUES FEASIBILITY STUDY

J. P. Crowder, M. I. Goldhammer, and D. N. Smyth

DOUGLAS AIRCRAFT COMPANY

LONG BEACH, CALIFORNIA

Prepared for:

NATIONAL AERONAUTICS AND SPACE ADMINISTRATION

NASA AMES RESEARCH CENTER

CONTRACT NAS2-8653

1. Report No.	2. Government Accession No.	3. Recipient's Catalog No.
NASA CR 137767		

4. Title and Subtitle	5. Report Date
STOL AIRCRAFT TRANSIENT GROUND EFFECTS PART II. EXPERIMENTAL TECHNIQUES FEASIBILITY STUDY	November, 1975
	6. Performing Organization Code
7. Author(s)	8. Performing Organization Report No.
J. P. Crowder, M. I. Goldhammer, D. N. Smyth	
	10. Work Unit No.
9. Performing Organization Name and Address	11. Contract or Grant No.
Douglas Aircraft Company 3855 Lakewood Blvd. Long Beach, California 90846	NAS2-8653
	13. Type of Report and Period Covered
12. Sponsoring Agency Name and Address	Contractor Report
National Aeronautics and Space Administration Washington, D. C. 20546	14. Sponsoring Agency Code

15. Supplementary Notes
NASA Project Engineer, D. G. Koenig, Large Scale Aerodynamics Branch, Ames Research Center, Mountain View, California

16. Abstract The importance of aerodynamic ground effect phenomena on STOL aircraft is well known, but there is evidence that the transient effects of STOL aircraft landing and takeoff maneuvers are not adequately predicted by present experimental methods which preclude correct simulation of aircraft attitude and the dynamics associated with changing altitude. This study examines procedures for simulating such transient effects and a basis is developed for selection of an experimental approach based on considerations of simulation requirements, experimental techniques, facilities, and costs.

The results of this study are generally applicable to STOL aircraft employing any of the following powered lift systems:

- o Externally blown flap
- o Upper surface blown flap
- o Augmentor wing
- o Internally ducted jet flap

Simulation requirements are established for a nominal STOL configuration representative of these powered lift systems. Scaling relationships are developed to apply the simulation requirements to model test situations.

Procedures for the extraction of aerodynamic forces from the measured data are discussed. Various means of expressing the aerodynamic data in forms convenient for use in performance or stability and control applications are described.

Five different experimental techniques are presented that depend on two different types of experimental facilities, wind tunnels and test tracks, and involve different types of model motion. Engine simulation techniques are reviewed and the results of

17. Key Words (Suggested by Author(s))	18. Distribution Statement
STOL Aircraft Aerodynamics Ground Effect Experimental Techniques Transients	Continued on back of page

19. Security Classif. (of this report)	20. Security Classif. (of this page)	21. No. of Pages	22. Price*
Unclassified	Unclassified	141	

*For sale by the National Technical Information Service, Springfield, Virginia 22151

a preliminary sizing study are presented to establish preferred model size and test speed trends.

Candidate facilities are reviewed and general considerations of model support provisions are analyzed. Five experimental systems are selected for detailed study that include three different facilities; the NASA Langley V/STOL Wind Tunnel, the NASA Ames 40- by 80-foot Wind Tunnel, and the NASA Langley Vortex Research Facility Test Track.

A technical and cost evaluation of the five experimental systems is conducted to establish the feasibility of accomplishing the experimental objectives and the cost of doing so.

Finally, the factors pertinent to selecting the experimental approach are reviewed and summarized.

An experimental approach is recommended utilizing the NASA Langley Vortex Research Facility in a two-phase program. Prior to commencing this program, a pilot program is suggested, utilizing existing model and instrumentation equipment, to demonstrate the feasibility of the experimental procedure and to acquire preliminary data for correlation with analytical methods.

FOREWORD

The results of a study on STOL aircraft transient ground effects are presented. This study consisted of two concurrent tasks which are reported on separately as Parts I and II.

Part I. Fundamental Analytical Study - The objective of this task was to establish, through a fundamental analytical study, a theoretical framework for the development of methods for predicting aerodynamic characteristics of STOL aircraft in ground effect.

Part II. Experimental Techniques Feasibility Study - The objective of this task was to investigate the feasibility of conducting transient model tests of STOL aircraft simulating takeoff, approach, and landing, to enable, in terms of facility, testing techniques and cost, an experimental approach to be selected.

This study, conducted under the technical direction of D. N. Smyth of the Powered Lift Technology Development Section, Aerodynamics Subdivision of the Douglas Aircraft Company, was sponsored by the NASA Ames Research Center under Contract NAS2-8653. Mr. J. P. Crowder was the principal investigator for the Experimental Techniques Feasibility Study and Mr. M. I. Goldhammer served as the principal investigator for the Fundamental Analytical Study. The NASA project engineer was Mr. David Koenig of the Large Scale Aerodynamics Branch.

The authors gratefully acknowledge the contributions made by Mr. R.L. Jones in the design and layout of the models and support mechanism developed for the Feasibility Study. He was assisted in these endeavors by Mr. R. Ferris, whose contributions are also appreciated. A number of other people contributed to various phases of the work reported herein for which the authors are grateful.

TABLE OF CONTENTS

	Page
LIST OF ILLUSTRATIONS	viii
LIST OF TABLES	ix
LIST OF SYMBOLS	x
1.0 SUMMARY	1
2.0 INTRODUCTION	3
3.0 AERODYNAMIC AND PERFORMANCE SIMULATION REQUIREMENTS	4
3.1 Properties of STOL Transport Aircraft	4
3.2 STOL Transport Landing and Takeoff Maneuvers	6
3.2.1 Nominal Landing	6
3.2.2 Nominal Takeoff	9
3.2.3 Simplified Maneuvers	11
3.3 Scaling Relationships	12
3.3.1 Power Effects	12
3.3.2 Reynolds Number	13
3.3.3 Trajectory Parameters	15
3.3.4 Frequency Response	17
4.0 EXTRACTION OF AERODYNAMIC AND STABILITY AND CONTROL DATA	20
4.1 Extraction of Aerodynamic Forces and Moments from Measured Data	20
4.2 Analysis of Aerodynamic Data	22
5.0 EXPERIMENTAL TECHNIQUES	
5.1 Motion Simulation	25
5.1.1 Constant Rate Approach	25
5.1.2 Landing Flare	29
5.1.3 Motion Simulation Errors	31
5.2 Engine Simulation Techniques	39
5.2.1 Direct Supply Engine Simulator	39
5.2.2 Ejector Engine Simulator	41
5.2.3 Air-Turbine Driven Fan Engine Simulators	44
5.2.4 Drive Air Thermodynamics	45
5.3 Model Sizing Study	46
5.3.1 Independent Scale Factors	48
5.3.2 Model Weight	50

		Page
	5.3.3 Model Scale Limitations	51
	5.3.3.1 Frequency Response	51
	5.3.3.2 Inertia Loads	52
	5.3.3.3 Reynolds Number	57
	5.3.3.4 Engine Simulator Drive Air	57
5.4	Model Size/Tunnel Size Criteria	57
	5.4.1 Floor Clearance	57
	5.4.2 Ceiling Clearance	59
	5.4.3 Blockage	62
5.5	Ground Board Boundary Layer Control	63
6.0	FACILITIES	
6.1	Technique Selection Considerations	66
	6.1.1 Wind Tunnel Techniques	66
	6.1.2 Track Techniques	68
6.2	Facility Selection	69
	6.2.1 NASA Langley V/STOL Wind Tunnel	71
	6.2.2 NASA Langley 30- by 60-foot Wind Tunnel	72
	6.2.3 NASA Ames 40- by 80-foot Wind Tunnel	73
	6.2.4 NASA Langley Vortex Research Facility	75
	6.2.5 Princeton Dynamic Model Track	77
6.3	Model Support Considerations	79
	6.3.1 Blade Strut	80
	6.3.2 Sting	82
6.4	Facility/Technique Selections	84
7.0	TECHNICAL AND COST EVALUATION	86
7.1	Dynamic Response Analysis	86
	7.1.1 Formulation of the Problem	87
	7.1.2 Blade Strut Support Frequency Response	91
	7.1.3 Sting Support Frequency Response	94
	7.1.4 Vortex Research Facility Dynamic Data	95
7.2	Model Design	98
	7.2.1 Basepoint Model	98
	7.2.2 Model Perturbations	107
	7.2.3 Model Costs	108

Page

7.3 Model Support and Actuator 110
7.3.1 V/STOL Wind Tunnel - Blade Strut Support 110
7.3.2 V/STOL Wind Tunnel - Sting Support 114
7.3.3 40- by 80-foot Wind Tunnel 118
7.3.4 Vortex Research Facility 121
7.3.5 Model Support and Actuator Costs 124
7.4 Instrumentation 126
7.4.1 Balance 126
7.4.2 Acceleration and Position Sensors 127
7.4.3 Servo Control System 128
7.4.4 Engine Simulator Sensors 129
7.4.5 Control Panel 130
7.4.6 Instrumentation Costs 130
7.5 Total Cost Summary 130
8.0 RECOMMENDED EXPERIMENTAL APPROACH 134
8.1 Discussion 134
8.2 Recommendations 137
9.0 REFERENCES 140

LIST OF ILLUSTRATIONS

		Page
	Figures	
1.	NOMINAL STOL TRANSPORT CONFIGURATION	5
2.	NOMINAL LANDING TRAJECTORY	7
3.	NOMINAL TAKEOFF TRAJECTORY	10
4.	HYPOTHETICAL AERODYNAMIC LIFT FORCE TIME HISTORY	19
5.	AERODYNAMIC LIFT FORCE SPECTRAL CONTENT	19
6.	MOTION SIMULATION TECHNIQUES FOR LANDING APPROACH	26
7.	MOTION SIMULATION TECHNIQUES FOR LANDING FLARE	30
8.	FLIGHT PATH RADIUS OF CURVATURE	33
9.	FLIGHT PATH CURVATURE ERROR	37
10.	EJECTOR ENGINE SIMULATOR INLET FLOW RATIO	42
11.	TEMPERATURE-ENTROPY DIAGRAM FOR AIR	47
12.	MODEL WEIGHT TRENDS	53
13.	MODEL SCALE LIMITATIONS	54
14.	ENGINE SIMULATOR DRIVE AIR REQUIREMENTS	58
15.	LIFT CHANGE DUE TO CEILING CLEARANCE	61
16.	DRAG CHANGE DUE TO CEILING CLEARANCE	61
17.	WALL JET BLC BLOWING REQUIREMENTS	65
18.	BLADE STRUT SUPPORT FREQUENCY RESPONSE	93
19.	STING SUPPORT FREQUENCY RESPONSE	93
20.	VORTEX RESEARCH FACILITY FREQUENCY RESPONSE	96
21.	MODEL ASSEMBLY	99
22.	MODEL ASSEMBLY	100
23.	WING ASSEMBLY	103
24.	WING ASSEMBLY	104
25.	FORWARD FLAP ASSEMBLY	105
26.	NACELLE/PYLON ASSEMBLY	106
27.	MODEL INSTALLATION-NASA LANGLEY V/STOL WIND TUNNEL (BLADE STRUT SUPPORT)	115
28.	MODEL INSTALLATION-NASA LANGLEY V/STOL WIND TUNNEL (STING SUPPORT)	116
29.	MODEL INSTALLATION-NASA AMES 40- by 80-FOOT WIND TUNNEL	119
30.	MODEL INSTALLATION-NASA LANGLEY VORTEX RESEARCH FACILITY	120

LIST OF TABLES

		Page
1.	STOL TRANSPORT GEOMETRICAL PROPERTIES	6
2.	MAXIMUM VALUES OF LANDING PARAMETERS	9
3.	MAXIMUM VALUES OF TAKEOFF PARAMETERS	11
4.	TRAJECTORY PARAMETER SCALING RELATIONSHIPS	16
5.	SCALED SIMULATION PARAMETERS	49
6.	INERTIA LOAD LIMITING PARAMETERS	56
7.	TEST TRACK FACILITIES	70
8.	WIND TUNNEL FACILITIES	70
9.	STUDIED EXPERIMENTAL SYSTEMS	85
10.	DYNAMIC SYSTEM COMPONENT PARAMETERS	92
11.	MODEL COSTS	109
12.	MODEL SUPPORT AND ACTUATOR COSTS	125
13.	INSTRUMENTATION COSTS	131
14.	TOTAL COST SUMMARY	132

LIST OF SYMBOLS

A_J	Propulsive jet area
AR	Wing aspect ratio
b	Wing span
b_H	Horizontal tail span
c	Chord length
$\bar{c}$	Wing mean aerodynamic chord
c_F	Flap chord
$\bar{c}_H$	Horizontal tail mean aerodynamic chord
c_ℓ	Sectional lift coefficient
C_L	Lift coefficient
$C_{L_{\dot{h}}}$	$\partial C_L / \partial \dot{h}$
C_{L_o}	C_L at $\alpha = 0$
C_{L_α}	$\partial C_L / \partial \alpha$
$C_{L_{(\alpha,\theta)}}$	$C_L / \partial (\dot{\alpha} + \dot{\theta})$
C_{L_∞}	C_L out of ground effect
$C_{L_{MAX}}$	Maximum lift coefficient
C_μ	Jet momentum coefficient
C_{μ_o}	Ram drag coefficient
d	Damping coefficient
D	Ground distance from flare to touchdown
e_s	Exponent of size factor
e_v	Exponent of velocity factor
f	Frequency
f_R	Required frequency response
F	Total balance force
F_g	Ideal gross thrust
F_n	Inertia force
F_s	Size factor
F_v	Velocity factor
g	Gravitational acceleration
h	Altitude, wheel-to-ground
$\dot{h}$	Sink rate
$\ddot{h}$	Vertical acceleration

h_o	Static ground height
i	$\sqrt{-1}$
I	Section moment of inertia
k	Spring rate
ℓ	2-D lift
ℓ_t	Horizontal tail arm
L	Lift force
m	mass
$\dot{m}$	mass flow rate
M_B	Bending moment
M_J	Jet Mach number
M_∞	Free-stream Mach number
n	Normal load factor
P_T	Total Pressure
P_∞	Ambient pressure
q_∞	Free-stream dynamic pressure
R	Distance from center of rotation
R_N	Reynolds number based on wing mean aerodynamic chord, $\bar{c}$
s	Arc length on surface
S	Laplace variable
S_w	Wing area
t	Time
T	Laplace transfer function
T_J	Jet temperature
T_T	Total temperature
V	Velocity
V_g	Vertical velocity of translating ground board
V_N	Normal velocity on surface
w	Weight flow rate
W	Weight
y	Vertical position of dynamic system component
$\dot{y}$	Vertical velocity of dynamic system component
$\ddot{y}$	Acceleration of dynamic system component
$\bar{y}$	Transformed y cordinate
$\dot{Z}$	Flight path vertical perturbation velocity

α	Angle of attack
$\dot{\alpha}$	α rotation rate
$\ddot{\alpha}$	α acceleration rate
γ	Flight path angle, also ratio of specific heats
Γ	Point vortex circulation
δ	Static gain
δ_F	Flap deflection angle
Δ	Dynamic gain
ΔZ	Flight path vertical perturbation distance
θ	Attitude angle
$\dot{\theta}$	θ rotation rate
$\ddot{\theta}$	θ acceleration rate
ρ	Flight path radius of curvature, also density
σ	Stress
ϕ	Inlet flow ratio
ψ_P	Potential flow stream function
ψ_R	Rotational flow stream function
ω	Fluid vorticity
Ω	Angular velocity

1.0 SUMMARY

The results of a feasibility study of techniques for the experimental investigation of transient ground effects for STOL aircraft are presented. The purpose of this study is to enable the most suitable experimental approach, in terms of facilities, model testing techniques, cost, etc., to be selected for future testing. The results of this study are generally applicable to STOL aircraft configurations employing any of the following powered lift systems:

- o Externally blown flap
- o Upper surface blown flap
- o Augmentor wing
- o Internally ducted jet flap

The simulation requirements to model the landing and takeoff maneuvers are established for a nominal STOL configuration representative of the powered lift systems listed above. Scaling relationships are developed to permit the model scale simulation requirements to be established.

Procedures for the extraction of aerodynamic forces from the measured data are discussed. Various means of expressing the aerodynamic data in forms convenient for use in performance or stability and control applications are described.

Five different techniques are presented for simulating the landing and takeoff maneuvers that depend on two different types of experimental facilities, wind tunnels and test tracks, and involve different types of model motion. Engine simulation procedures are reviewed and the conclusion is reached that in the present instance direct supply type simulators are preferable to the ejector or air-turbine driven fan simulators. The results of a preliminary sizing study to establish preferred model size and test speed trends are presented. This sizing study considers limitations due to frequency response, inertia loads, Reynolds number, and engine simulator drive air requirements. Criteria are established for model size based on the need to minimize wind tunnel wall interference while the position of the model

within the test section varies. A discussion of procedures to minimize wind tunnel ground board boundary layer simulation errors with BLC jet blowing is presented.

Candidate facilities are reviewed on the basis of on-site inspections and their ability to accommodate the motion simulation techniques. General considerations pertaining to model support provisions are analyzed. Five experimental systems are selected for further detailed study. These include three different facilities; the NASA Langley V/STOL Wind Tunnel, the NASA Ames 40- by 80-foot Wind Tunnel, and the NASA Langley Vortex Research Facility Test Track.

A technical and cost evaluation of the five experimental systems is conducted to establish the feasibility of accomplishing the experimental objectives and the cost of doing so. The technical evaluation of the systems is mainly concerned with the ability to resolve the time-varying-forces on the model as affected by the dynamic response characteristics of the model support and actuator system. The cost evaluation relies on detailed design studies of the equipment comprising the experimental systems. The three major components of the transient ground effect apparatus are: model, support and actuator, and instrumentation. Estimated costs for these components are presented.

Finally, the factors pertinent to selecting the experimental approach are reviewed and summarized. The most important considerations are:

- o Ability to comply with the simulation requirements
- o Cost of developing and installing the apparatus and model
- o Cost of conducting the experiment.

An experimental approach for the determination of STOL aircraft transient ground effects is recommended utilizing the NASA Langley Vortex Research Facility test track in a two-phase program. Prior to commencing such a program, a pilot program is suggested, utilizing existing model and instrumentation equipment as much as possible, to demonstrate the feasibility of the experimental procedure and to acquire preliminary data for correlation with analytical methods.

2.0 INTRODUCTION

The aerodynamic influence of ground proximity has been established as being potentially important in relation to STOL aircraft performance, stability, and flying qualities. Wind-tunnel investigations conducted either with fixed or moving ground planes have also established that the nature and magnitude of aerodynamic characteristics in ground proximity tend to be critically sensitive to aircraft geometry, attitude, and ground clearance, and in the case of jet-flap lift augmentation schemes, to jet disposition and inclination. There is evidence to suggest, however, that the transient nature of STOL aircraft in takeoff and landing may not be adequately predicted by such stationary model experiments. The stationary wind-tunnel model with the ground plane parallel to the mainstream can simulate neither the correct model attitude nor the dynamics associated with changing altitude.

Various procedures for correctly simulating the landing and takeoff transients for STOL aircraft model tests have been identified and in the case of reference 1, one such procedure has been implemented. The results showed moderately large and distinctive transient ground effects. However, that experiment was of limited scope and was probably affected by significant experimental error due to flow blockage and limited instrumentation transient response.

In the current study, procedures are examined for simulating transient effects of STOL aircraft landing and takeoff maneuvers and a basis is developed for selection of an experimental approach in terms of simulation requirements, experimental techniques, facilities, and costs.

3.0 AERODYNAMIC AND PERFORMANCE SIMULATION REQUIREMENTS

3.1 Properties of STOL Transport Aircraft

Four types of STOL powered lift systems have been identified as being of interest in experimental transient ground effect studies because of their effectiveness in producing the high lift required for STOL operations:

- o Externally blown flap
- o Upper surface blown flap
- o Augmentor wing
- o Internally ducted jet flap

These four types of lift systems can all be considered essentially similar in their action on the aerodynamic flow field and its interaction with the ground. The dominant feature of this flow field is a jet sheet emerging from the wing trailing edge deflected downward at a large angle.

The differences between the lift systems, as they relate to transient ground effect experimental simulation, are relatively minor. For a given level of takeoff or landing performance these differences could be expressed as variations in wing loading, thrust-to-weight ratio, etc.

A detailed examination of the relative performance of these powered lift systems was conducted by Douglas under contract to NASA Ames Research Center, and is reported in reference 2. One conclusion drawn from that work is that the variation of aircraft geometrical parameters between the different STOL concepts, designed for the same mission, is less than the variation of these parameters for a single STOL concept designed for a possible range of mission parameters such as field length, cruise speed, noise, etc. In particular the externally blown flap and the upper surface blown flap configurations were shown to be very similar, while the augmentor wing and internally ducted jet flap configurations were considered to be almost identical in terms of landing and takeoff performance. In other words, most of the values of these geometrical parameters are a consequence of the mission, not the STOL concept.

It was concluded for the degree of precision possible in the present study, that all of the STOL concepts listed above can be equally well accommodated by a common experimental capability for simulating transient ground effects. Accordingly, a single representative STOL aircraft configuration was selected to define the capabilities the experimental apparatus must fulfill. It is expected that all the identified STOL concepts could be tested equally well with this apparatus, if the configurations were designed for a common mission. Configurations developed for significantly different missions may require capabilities outside the range under consideration. Such an eventuality may dictate either additional capability for the apparatus or a relaxation of the test conditions. The conclusions and recommendations developed in the course of this study can be easily extended and modified to account for any such foreseeable configuration perturbations.

The geometrical characteristics of the STOL transport configuration selected for this study are summarized in table 1 and a three-view drawing is shown in figure 1.

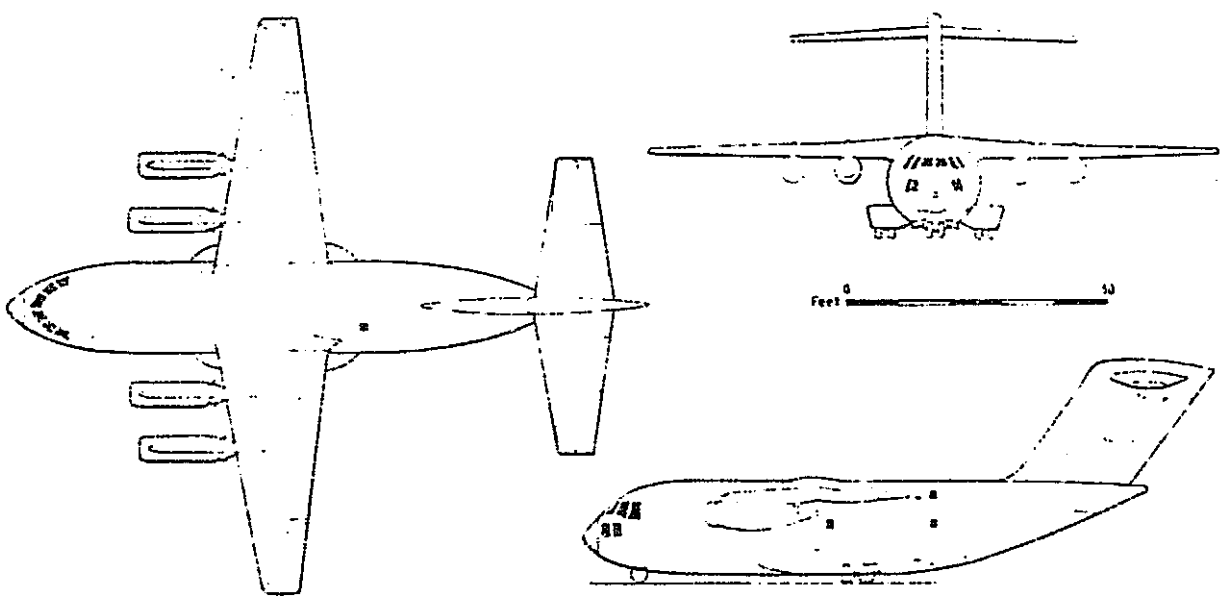

FIGURE 1. NOMINAL STOL TRANSPORT CONFIGURATION

TABLE 1. NOMINAL STOL TRANSPORT GEOMETRICAL PARAMETERS

Powered Lift System	Externally Blown Flap
Number of Engines	4
Wing Area, S_w	162 m^2 (1740 ft^2)
Wing Span, b	33.5 m (110 ft)
Wing Mean Aerodynamic Chord (MAC), $\bar{c}$	5.27 m (17.3 ft)
Wing Aspect Ratio, AR	7.0
Propulsive Jet Area, A_J	1.86 m^2 (20.0 ft^2)
Static Wing Height, h_o	0.153 b
Horizontal Tail Span, b_H	0.514 b
Horizontal Tail MAC, $\bar{c}_H$	0.687 $\bar{c}$
Horizontal Tail Length, L_H	0.563 b

3.2 STOL Transport Landing and Takeoff Maneuvers

Of the parameters that describe a landing or takeoff maneuver, many are independent of the particular configuration. Such parameters as touchdown sink rate, flight path angle, aircraft rotation rate, maximum attitude angle, etc., are specified by operational or control considerations. Other parameters (i.e., velocity, thrust to weight ratio, etc.) are governed by the mission performance requirements. Relatively few are dependent on the aircraft configuration.

3.2.1 Nominal Landing

A nominal landing trajectory for the STOL aircraft defined above is described in figure 2. The various parameters are presented as functions of height. The initial portion of the maneuver is a constant speed and descent rate approach to the flare height. The approach speed is usually defined as a certain function of the stall speed. The approach flight path angle is limited to certain levels due to operational considerations.

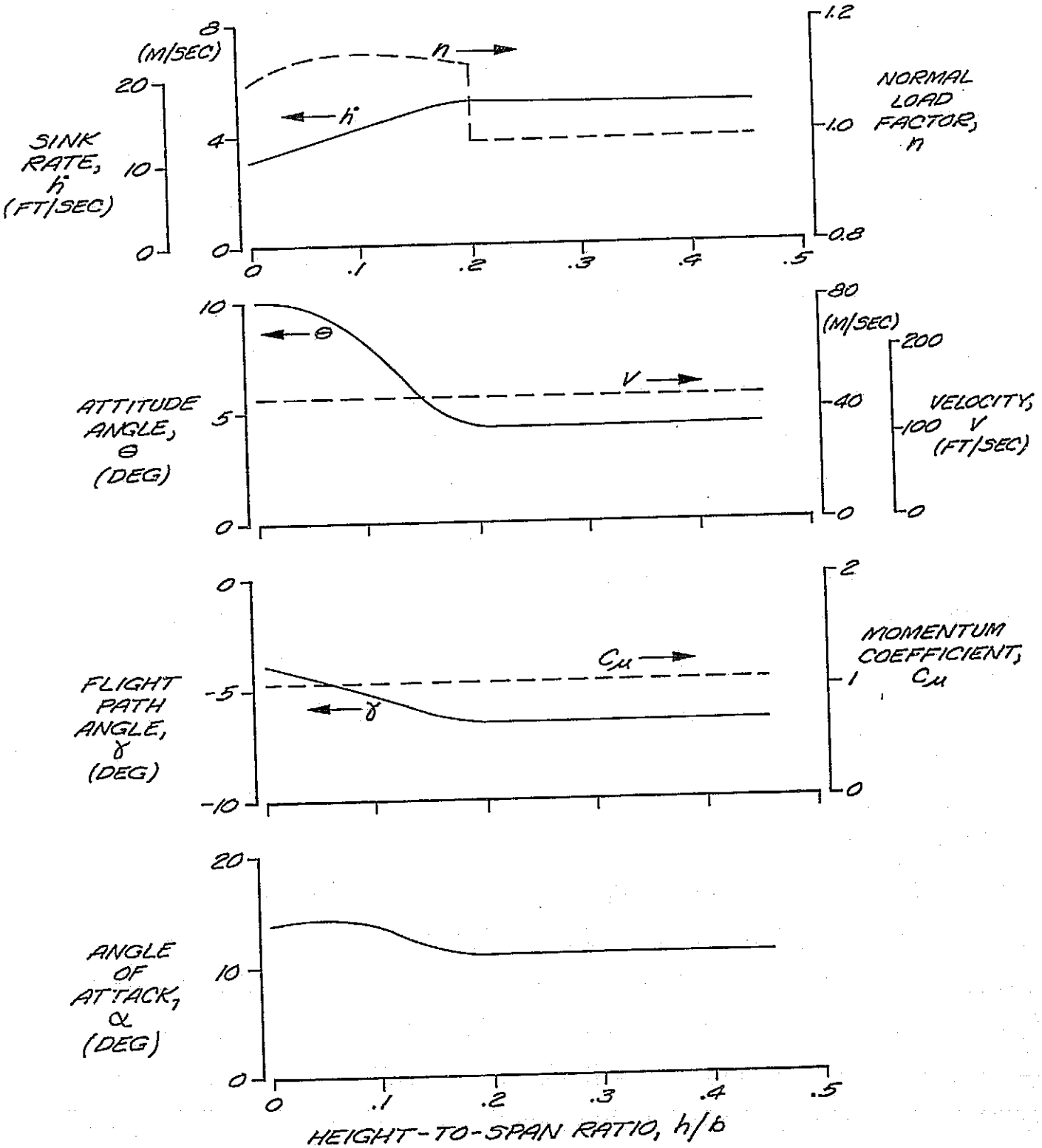

FIGURE 2. NOMINAL LANDING TRAJECTORY

At the flare height the lift of the aircraft is quickly increased through a combination of direct lift control spoiler actuation and aircraft rotation. The resulting normal acceleration is sufficient to decrease the sink rate to the required touchdown value. Throughout the maneuver the speed, thrust, and hence momentum coefficient remain very nearly constant.

A distinct characteristic of a STOL aircraft landing maneuver is the high touchdown sink rate. Performance calculations and flight simulator studies have demonstrated that a high touchdown sink rate is necessary both to reduce the air run distance as well as to improve piloting precision. The touchdown sink rate considered in the present instance of 3.1 m/sec (10 ft/sec) is typical of military STOL transport aircraft. Commercial STOL transport aircraft would tend toward lower values, but probably not less than 1.5 m/sec (5 ft/sec). By way of comparison, the maximum operational touchdown sink rate for commercial CTOL aircraft is generally considered to be 0.9 m/sec (3 ft/sec).

One consequence of the high touchdown sink rate is that the flare accelerations are not very great and that portion of the maneuver is of very short duration. Thus the airspeed remains very nearly constant and longitudinal accelerations are negligible, allowing a simpler trajectory simulation. Another consequence of this is that the trajectory simulation is made considerably more difficult by the need for very high accelerations to arrest the model sink rate close to the ground but without actually making contact.

A summary of the maximum values of the pertinent parameters for the nominal landing maneuver is provided in table 2.

TABLE 2. MAXIMUM VALUES OF LANDING PARAMETERS

V	=	45 m/sec (148 ft/sec)
$\dot{h}$	=	-5.2 m/sec (17 ft/sec)
$\ddot{h}$	=	1.4 m/sec^2 (4.6 ft/sec^2)
θ	=	10 deg
$\dot{\theta}$	=	6.8 deg/sec
$\ddot{\theta}$	=	8.0 deg/sec^2
γ	=	-6.6 deg
C_μ	=	1.06

3.2.2 Nominal Takeoff

A typical takeoff maneuver is similarly described in figure 3. This maneuver consists of a pre-lift-off rotation, which continues after lift-off to a maximum attitude angle specified by operational limits. The remaining climbout and acceleration portion of the maneuver occurs at the maximum attitude angle. Again the speed and momentum coefficient remain nearly constant throughout the maneuver. The normal acceleration of the aircraft is much greater than in the landing. The vehicle continues to accelerate at a low rate and never quite reaches an equilibrium flight path.

The range of aerodynamic conditions occuring throughout the landing and takeoff maneuvers are dissimilar and, as a consequence, the ground effects are expected to be different. The landing maneuver involves high lift and high drag conditions with the major ground effects being a change in lift. In the takeoff maneuver the lift levels are slightly lower and the drag is much less, with the result that the significant ground effect is usually felt as a change in drag. It is not possible to ascertain, in general, which maneuver is more significant, in terms of possible transient ground effects. Therefore, it is important to retain the capability of the experimental apparatus to accurately simulate both maneuvers.

A summary of the pertinent takeoff parameter maximum values is shown in table 3.

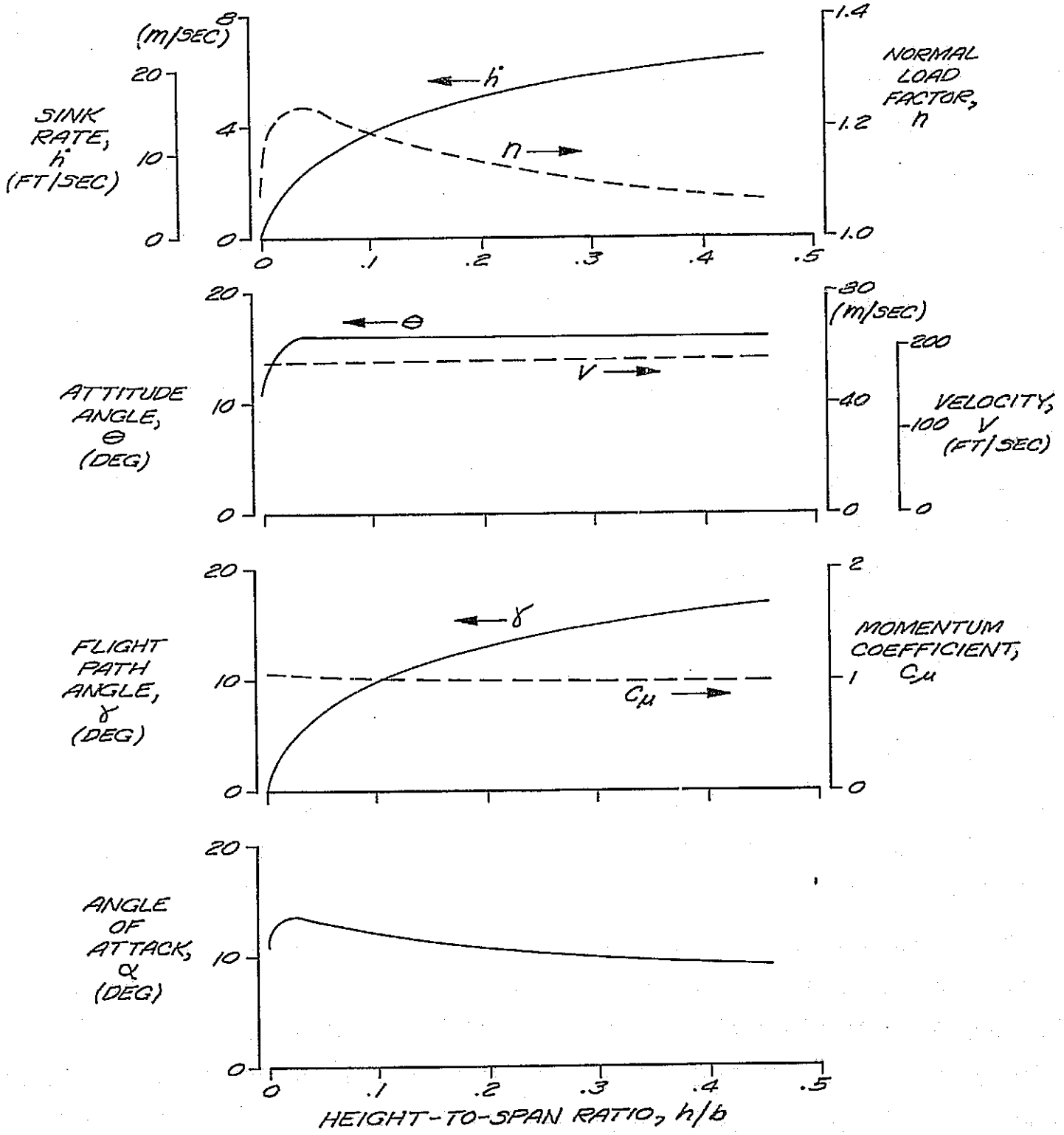

FIGURE 3. NOMINAL TAKEOFF TRAJECTORY

TABLE 3. MAXIMUM VALUES OF TAKEOFF PARAMETERS

V	=	56 m/sec (184 ft/sec)
$\dot{h}$	=	6.4 m/sec (21 ft/sec)
$\ddot{h}$	=	2.3 m/sec (7.5 ft/sec)
θ	=	16 deg
$\dot{\theta}$	=	7.4 deg/sec
$\ddot{\theta}$	=	8 deg/sec
γ	=	6.7 deg
C_μ	=	1.08

3.2.3 Simplified Maneuvers

The maneuvers described above involve rotational and translational accelerations of the aircraft, and require a complex apparatus to simulate this motion. It is of interest to examine the realism of maneuvers which are simplified from the actual flight trajectories.

The simplest simulation would involve a straight flight path with no acceleration nor rotation. This could represent the most extreme type of STOL landing maneuver with touchdown at the approach sink rate, except that in general the aircraft would experience some acceleration due to ground effect. The takeoff must always have some acceleration since the ascent rate must start from zero at lift-off. Therefore this simplified maneuver could not closely correspond to either a landing or takeoff maneuver.

A maneuver simulation involving only acceleration with no rotation does correspond to a realistic flight trajectory, if direct lift control (DLC) is employed. For current STOL transport aircraft, DLC is used to generate most of the acceleration capability in the landing flare. The utility of aircraft rotation for generating the required additional lift tends to be limited by several factors such as slow response and operational limits on maximum attitude angle. A landing maneuver with no rotation, with all the flare acceleration provided by DLC, is presently considered a viable alternative for STOL transports under study. It may therefore be possible to limit the experimental program to the study of such simplified maneuvers because of the

simplification to the experimental apparatus entailed by elimination of the need for model rotation. It appears less likely that the takeoff maneuver would be performed with no rotation. A lack of model rotation capability may then limit the ability to simulate the complete takeoff situation.

3.3 Scaling Relationships

3.3.1 Power Effects

The most prominent feature of STOL jet powered high lift systems is a jet sheet deflected downward from the wing trailing edge. The interaction of this jet sheet with the flow field generates the high lift coefficients required for STOL operation. The parameter that describes the magnitude of the jet induced forces is the jet momentum. In non-dimensional form the jet momentum coefficient is defined as

$$C_\mu = \frac{F_g}{q_\infty S_w}$$

This can be expressed in terms of jet Mach number as

$$C_\mu = \frac{\gamma P_\infty M_J^2 A_J}{\frac{1}{2} \gamma P_\infty M_\infty^2 S_w}$$

$$C_\mu = \frac{2 A_J}{S_w} \left(\frac{M_J}{M_\infty} \right)^2$$

Proper simulation of the jet and wing flow field requires that the model operate at the full scale momentum coefficient. If geometric similarity is to be maintained, the jet exit-wing area ratio, A_J/S_w, must be correct so that the jet Mach number ratio, M_J/M_∞, must therefore be maintained. The full scale jet Mach numbers for some STOL concepts are in the high subsonic range. Compressibility effects, such as strong shock waves and attendant separations have been avoided in most practical STOL aircraft, but it is likely that the jet Mach number cannot be greatly increased without running the risk of such effects. Therefore the model jet Mach number should be limited to a value equal to or less than the full scale value. This implies a similar limit on the freestream Mach number.

Another feature of jet propulsive and powered high lift systems is the engine inlet flow field. For the model scale situation, it is difficult to completely simulate the full scale inlet mass flow rate. The various types of engine simulators available for this task can offer varying degrees of inlet flow simulation ranging from zero to about 80%. As might be expected, the difficulty of accomplishing such simulation increases as the percent of complete simulation increases. The relative cost-benefit factors involved must be examined for the particular experimental requirements.

In the present instance the judgement is made that inlet flow simulation is relatively unimportant. This is based on the recognition that, for EBF configurations, and others of a similar nature, the nacelle inlets are relatively remote from the aerodynamic flow field of interest. Typically they are about two chord lengths ahead of the wing trailing edge. The perturbation velocities associated with the inlet flow can be expected to decay to insignificant levels within this distance. Furthermore the perturbations that do exist can be expected to be unaffected by the ground effect and thus not contribute to the incremental effects under study.

Significant experimental simplifications can be realized if, instead of a partially correct inlet flow, it does not exist at all. This eliminates the need to measure the inlet flow rate to correct the model forces to account for the inlet ram drag at the correct flow rate. Such inlet flow rate measurements tend to be difficult to perform with sufficient accuracy.

3.3.2 Reynolds Number

Customary aerodynamic similarity considerations for low subsonic flows require that model Reynolds number be as close as possible to the full scale value. Without going to the added complexity of a pressurized wind tunnel, this requires that the test velocity increase inversely to model size. However, the velocity is constrained by jet Mach number limitations as explained above as well as the mechanical difficulties of accomplishing proper model motion at high speeds.

Reynolds number similarity is important where viscous effects predominate. For experimental situations involving complete aircraft, the major effect of testing at too low a Reynolds number is degraded modeling of the high lift situation, especially near $C_{L_{max}}$. In some respects the present experiments may tolerate less exact Reynolds number simulation because landing and takeoff maneuvers are being simulated. As such, there is no need to match full scale $C_{L_{max}}$ values since operational rules require a certain margin from $C_{L_{max}}$. A further relaxation of Reynolds number similarity requirements can be rationalized in the present instance by recognizing that the principal flow components involved in the ground effect simulation are the trailing edge flap and jet wake regions. The wing leading edge is only important in-so-far as assuring that the flow in that region remain attached. An effective leading edge device to provide protection at a particular design point can be provided. If necessary, an unrepresentative leading edge configuration (i.e., larger than full scale slat, boundary layer blowing, etc.) can be incorporated. A further consideration, for jet powered high lift systems, is that the entrainment into the turbulent jet flow tends to provide a useful amount of boundary layer control, making such flows tolerant of low Reynolds number situations.

Most preliminary development wind tunnel testing of STOL powered lift systems has been conducted at Reynolds numbers substantially less than $1(10)^6$. This has been dictated by engine simulator drive air limitations and model size restrictions to permit low cost and convenient exploratory work. Generally, experience has shown the results to be satisfactory to Reynolds numbers as low as $0.5(10)^6$, although the bulk of both industry and NASA experience has been concentrated in the range of $0.6(10)^6$ to $0.8(10)^6$, based on wing chord. Wind tunnel tests below this level have tended to be less satisfactory due, not only to the low Reynolds number, but also due to the difficulty measuring model data at low freestream dynamic pressures.

Wind tunnel test results at these low Reynolds numbers have been acceptable because of the exploratory nature of the tests and an interest in incremental effects rather than absolute levels. There have been

relatively few instances where a specific Reynolds number survey has been conducted as part of a powered STOL model test.

Reference 3 presents results of a Reynolds number survey for an externally blown flap configuration. In that test the Reynolds number was varied over the range from $0.47(10)^6$ to $1.36(10)^6$. The principal conclusion was that "... the aerodynamic characteristics of the model were not significantly affected by changes in Reynolds number through the range tested except above the stall ..." A review of the reported data shows differences between the runs at different Reynolds numbers that might not be considered insignificant. However, these differences do not show any consistent Reynolds number effect and are generally rather irregular. Effects on lift as great as ten percent are shown, but appear as both positive and negative increments with increasing Reynolds number.

Another source of Reynolds number effects on STOL wind tunnel model aerodynamic characteristics can be found in reference 4, Figure 18, for the unpowered situation. These data show considerably better consistancy than the data of reference 3. In the linear lift curve range the effect of Reynolds number is small for values ranging from $0.53(10^6$ to $0.75(10)^6$. For the data at a Reynolds number of $0.38(10)^6$, a trend away from all the other data is just discernable.

The above considerations lead to the conclusions that conventional Reynolds number simulation requirements can be greatly relaxed for STOL model powered high lift testing. However, there still remains a minimum Reynolds number limit. The magnitude of such a limit is difficult to predict for all experimental situations, but would probably lie between $0.2(10)^6$ and $0.5(10)^6$.

The overall experimental feasibility in the present instance, is probably not strongly affected by increases in Reynolds number above the minimum level. It may be, however, that the general data quality would benefit from a Reynolds number much greater than the minimum level.

3.3.3 Trajectory Parameters

The feasibility of simulating the landing or takeoff trajectory to study transient ground effects depends strongly on the mechanical problems of providing the proper motions and accelerations. Model scale motion parameters are defined in terms of a pair of independent parameters; velocity factor,

$$F_v = \frac{\text{Model Scale Velocity}}{\text{Full Scale Velocity}}$$

and size factor,

$$F_s = \frac{\text{Model Scale Size}}{\text{Full Scale Size}}$$

The dependence of the various trajectory parameters on F_v and F_s are summarized in table 4. This table describes the parameter dependence in terms of the exponent of the F_v and F_s factors such that for a given parameter, p,

$$p = p^* F_v^{(e_v)} F_s^{(e_s)}$$

where p^* denotes the full scale parameter.

Notice that angles, such as α and γ, are unchanged with scale. Also, higher order derivatives scale as the ratio of their differentials, i.e.,

TABLE 4. TRAJECTORY PARAMETER SCALING RELATIONSHIPS

Parameter	e_v	e_s
Velocity, V	1	0
Span, b	0	1
Height, h	0	1
Time, t	-1	1
Angle of Attack, α	0	0
Flight Path Angle, γ	0	0
Sink Rate, $\dot{h}$	1	0
Rotation Rate, $\dot{\alpha}$, $\dot{\theta}$	1	-1
Vertical Acceleration, $\ddot{h}$	2	-1
Rotary Acceleration, $\ddot{\alpha}$	2	-2
Frequency Response, f	1	-1

$$\ddot{\alpha} = \frac{d\dot{\alpha}}{dt} \sim \frac{F_v^1 \, F_s^{-1}}{F_v^{-1} \, F_s^1} = F_v^2 \, F_s^{-2}$$

3.3.4 Frequency Response

A fundamental consideration in the experimental simulation of transient events is the frequency response requirement of the instrumentation measuring the time-varying forces. A structural system comprising a force balance, support structure and motion actuators can be described as a spring, mass, and damper system. The balance readout will be proportional to the displacement of the model relative to the balance ground structure. This will depend on the response of the entire structural system to the input time-varying forces. The ability to measure these input forces will require an accurate knowledge of the balance system response to the input excitation forces.

The response characteristics of a spring, mass, damper system can be most conveniently described by the ratio of output to input forces as the system is excited by a periodic, simple harmonic forcing function at discrete frequencies ranging from zero up to the highest frequency of interest. Typical response characteristics of such a system show an initial flat response at low frequencies and a monotonic decrease at high frequencies. At intermediate frequencies there may be resonance points where the output is amplified or attenuated. The flat portion of the response curve can be considered to extend up to the frequency where the output force deviates from the input by a specified tolerance. This defines the frequency response of the instrumentation system for flat response. Operation at frequencies greater than the highest for flat response can be considered, but becomes substantially more difficult. Further, operation near or beyond a resonance frequency is probably impractical.

The frequency response required to measure the input forces to the required accuracy will depend on the spectral content of the input force function. This function, or force time history can be synthesized by integrating the time derivative, dC_L/dt, which can be derived by multiplying the height

derivative, dC_L/dh, determined from steady measurements, by the descent rate, $\dot{h} = dh/dt$. The incremental effect of the transient maneuver on this force time history is not known, but is probably much smaller than the steady ground effect increment.

A hypothetical aerodynamic force time history, derived from the data of reference 5, figure 30b, for a steady descent rate is shown in figure 4. The amplitude spectrum of this time history, analyzed by a Fourier integration procedure, is presented in figure 5. The amplitude is seen to drop steadily from a high level associated with the fundamental frequency of the event, but persists into the 1-10 hertz frequency decade. Also shown in figure 5 is a curve depicting the local-to-total-power ratio. This ratio is seen to reach 98 percent at a frequency of six hertz. This represents the frequency below which 99 percent of the amplitude, which is the square root of the power ratio, is experienced. Therefore, if the force time history is to be resolved to within one percent of the correct value, fluctuating components up to a frequency of six hertz must be measured.

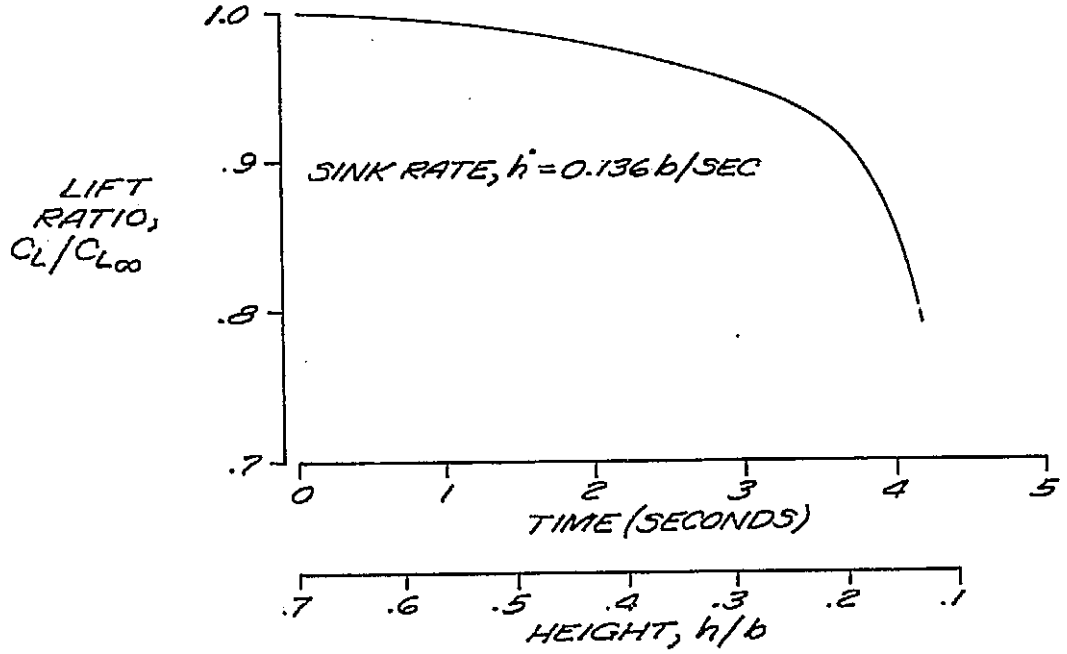

FIGURE 4. HYPOTHETICAL AERODYNAMIC TIME HISTORY

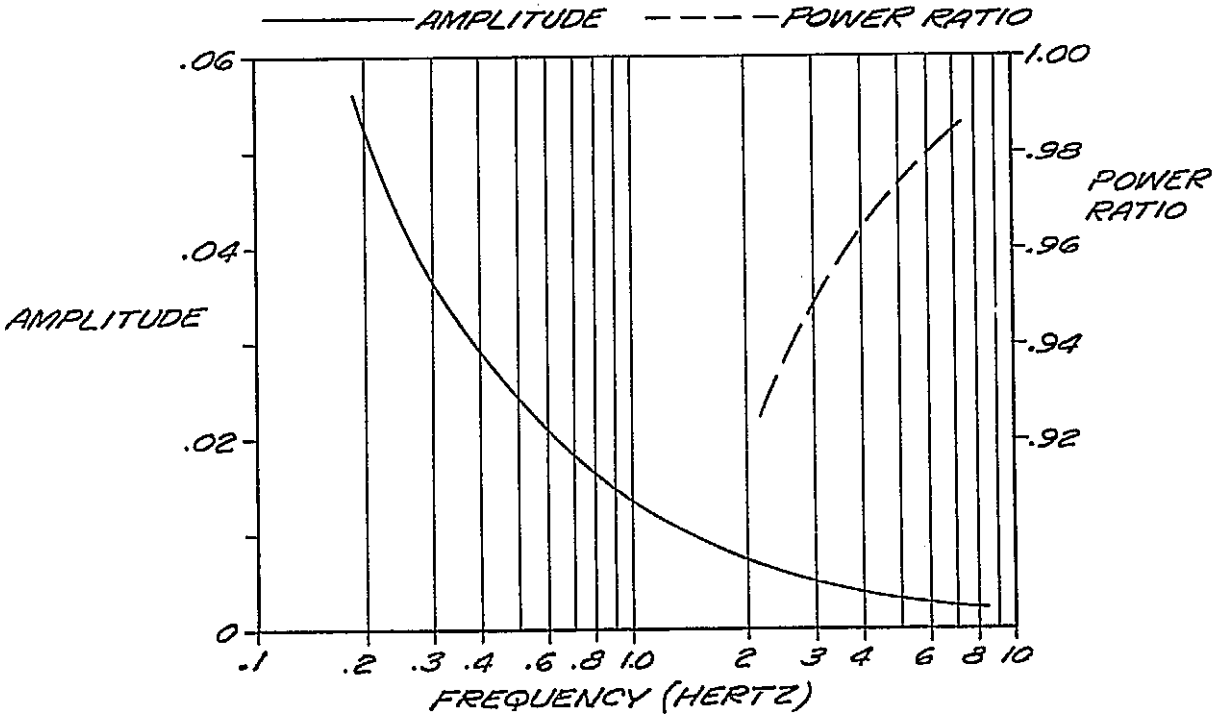

FIGURE 5. AERODYNAMIC LIFT FORCE SPECTRAL CONTENT

4.0 EXTRACTION OF AERODYNAMIC AND STABILITY AND CONTROL DATA

The process of arriving at a description of the transient ground effects from a set of experimental data depends on two different, but critically important, considerations. The first pertains to the resolution of the aerodynamic data from the measured data which may contain significantly large inertia forces due to model accelerations. The second refers to the procedure by which the aerodynamic data, essentially a time history of the forces and motion parameters, are analyzed and presented in a form convenient to the eventual user.

4.1 Extraction of Aerodynamic Forces and Moments from Measured Data

The aerodynamic forces and moments which are to be resolved from the balance data are derived from the force components measured with load sensing links within the balance. These force components include, in addition to the aerodynamic force components, inertia forces due to acceleration of the model and the support system. These inertia forces can approach the same order of magnitude as the aerodynamic forces, so they must be resolved with the same degree of precision.

The principal, or first order, inertia forces will be due to the accelerations of the simulated trajectory motion. Higher order inertia forces will undoubtedly be present due to mechanical vibration of the support and actuator system. In general, only the first order inertia forces need to be accurately determined. The higher order forces need only be known to the extent necessary to design filter systems or otherwise compensate for their effects.

The higher order inertia forces typically decay as the frequency increases except where a resonance condition is encountered. At a resonance frequency, the force may increase or decrease, depending on the dynamic properties of the system. The preferred method of accounting for these forces is through the use of filters to block the balance output above a certain frequency.

Two types of first order inertia forces will be experienced. The first is due to the starting and stopping accelerations of the apparatus. These forces will be quite large, but will not have to be resolved, since they will not be produced while aerodynamic data are being measured. The principle effect of the starting and stopping forces is to establish strength requirements for the balance elements. This tends to require oversize balance elements which may limit the balance accuracy. The starting acceleration may also excite the structure at higher frequencies unless care is taken to start the motion smoothly, with as close to simple harmonic motion as possible. The magnitude of the forces can be controlled by allowing as much distance as possible over which to perform this motion. In this regard the landing trajectory presents a simulation difficulty because high descent rates must be produced very close to the ground with small stopping distances and large inertia forces.

The other type of first order inertia force is caused by the simulated flight path acceleration of the particular maneuver studied. For both the landing and takeoff maneuvers the acceleration is directed upward, causing a downward directed inertia force. This is opposite to the lift force direction, so would generally act to reduce the total force on the balance. The vertically directed acceleration will produce inertia forces in all components of the balance, depending on the balance orientation. They must be resolved to the same degree of accuracy as that required for the aerodynamic forces, since they are directly additive.

In general, the most straightforward approach to resolving these forces will be to measure the accelerations directly with accelerometers. These may be oriented in the vertical direction, and the force components calculated, knowing the model attitude, or accelerometers may be placed adjacent to each balance element to measure the acceleration components directly. The procedure and instrumentation system for resolving these inertia forces will require experimental development. In any event, sensors and techniques to accomplish this with sufficient accuracy are readily available so this problem is not expected to limit the experimental feasibility of measuring transient ground effects.

4.2 Analysis of Aerodynamic Data

The best procedure for the analysis of the aerodynamic data will depend, not only on the nature of such data, but possibly on the eventual use of it. Ground effect data are generally important for the analysis of landing and takeoff performance and for handling quality investigations using flight simulators.

Existing analysis procedures for ground effect experimental data have been developed for the steady problem. These data are derived from wind tunnel measurements made at a constant ground height, or $\dot{h} = 0$. The ground effects are usually presented in the form of increments in lift, drag, and pitching moment coefficients, ΔC_L, ΔC_D, ΔC_M, as functions of angle of attack, α, momentum coefficient, C_μ, and ground height, h. These data are converted to three-parameter tables for use in the landing and takeoff performance computer programs.

If it develops that the principal transient effects on the ground effect increments are due to sink rate, $\dot{h}$, for example, and that the other parameters (α, q, h, etc.) have no significant effect, then it may be possible to simply extend the present technique by including a fourth parameter, $\dot{h}$, in the tabular presentation of ground effect increments.

A more general presentation may be possible if the force coefficients can be expanded in a series of linear, independent derivatives. The lift coefficient, C_L, for example, could be expressed as

$$C_L = C_{L_o} + C_{L_\alpha}\alpha + C_{L_{\dot{h}}}\dot{h} + C_{L_{(\dot{\alpha},\dot{\theta})}}\dot{\alpha} + \ldots$$

where all terms are functions of altitude, h, and momentum coefficient, C_μ. The first term in this expression, C_{L_o}, is the lift at zero angle of attack. The remaining terms are expressed in subscript notation such that

$$C_{L_\alpha} = \frac{\partial C_L}{\partial \alpha}, \quad C_{L_{\dot{h}}} = \frac{\partial C_L}{\partial \dot{h}}, \quad C_{L_{(\dot{\alpha},\dot{\theta})}} = \frac{\partial C_L}{\partial \dot{\theta}} = \frac{\partial C_L}{\partial \dot{\alpha}}$$

The lower order terms, C_{L_o} and C_{L_α}, will be evaluated from the steady, i.e., $\dot{h} = 0$, runs. It is expected that the next terms, $C_{L_{\dot{h}}}$ and to a lesser extent, $C_{L_{(\dot{\alpha}+\dot{\theta})}}$, will contain the bulk of the transient effects. This process will depend on these derivatives being nearly linear over the range of interest.

The experimental procedure to determine the $C_{L_{\dot{h}}}$ term is fairly simple. First the steady ground effects are established by runs at constant height, h. Next, a series of trajectories simulating constant sink rates, or flight path angle, are simulated. These trajectories might correspond to a range of flight path angles such as $\gamma = 2°, 4°, 6°, 8°$. The differences between the two series of runs at a certain height, h, yield the transient effects due to $\dot{h}$.

The effects of airplane rotation, that is the rates of change of angle of attack, $\dot{\alpha}$, and airplane attitude, $\dot{\theta}$, may be difficult to separate in ground effect since changes of one parameter are not independent of the other for a particular altitude, h, or sink rate, $\dot{h}$. The suggested approach is to evaluate these effects in a combined $(\dot{\alpha}+\dot{\theta})$ term. For example, runs are made at several constant altitudes, h, with one value of $\dot{\alpha}$ and at several constant descent rates, $\dot{h}$, with the same $\dot{\alpha}$. Direct correlation is then made at the corresponding altitude points and with the base case non-rotating conditions. The effects of DLC are evaluated in a similar fashion. The spoiler is deployed, in a manner analogous to the $\dot{\alpha}$ maneuver, at several constant altitudes and sink rates.

The foregoing discussion describes a procedure to extract derivatives or other local point results. An alternative approach is to examine the global transient ground effects. One possible procedure is to measure the force history throughout a complete simulated maneuver and compare that with a synthesized force history based on steady data. The differences between the two sets of data allow a qualitative evaluation of the transient effects during a complete maneuver. Time or height lag effects are evident from such a comparison.

Another possible technique is to simulate a trajectory which had been computed as an equilibrium maneuver using steady ground effect data. The forces measured during the trajectory simulation are presumably different from those used in calculating the trajectory in the first place. In order to assess the effect of these differences, the measured forces, containing the transient effects, are used to compute a revised trajectory. Presumably this revised trajectory is different in several respects from the original trajectory, such as air run distance, touchdown sink rate, etc. This difference is used as a global description of the transient ground effects.

The best analysis procedure, as mentioned earlier, will depend on the results and so cannot be established at this time. Undoubtedly the simplest procedures will be used initially and modified or extended as the results warrant.

5.0 EXPERIMENTAL TECHNIQUES

5.1 Motion Simulation

In general this study attempts to examine the feasibility of a complete simulation of the significant model motions involved in the landing and take-off maneuvers. Still, the utility of simplified trajectory motion simulations should be considered in light of potentially large cost savings or significant enchancements of technical feasibility. The first order motion of such maneuvers consists of a constant rate descent or ascent. It is logical to expect that the most significant transient effects will be due to this simple motion. The remaining trajectory parameters of significance, as discussed in section 3.2, are vertical acceleration, aircraft rotation, and configuration changes such as DLC spoiler actuation. The effect of DLC spoiler actuation in the landing maneuver is similar to aircraft rotation, that is, an increase in lift coefficient, except that it occurs at a much faster rate.

Four approaches to the experimental simulation of landing or takeoff maneuvers have been identified. These are discussed in the following sections in terms of constant rate descent, or landing approach, and in terms of the landing flare. In addition a fifth technique which is a modification of the first technique, is discussed in terms of the landing flare simulation. In most respects the takeoff maneuver is a reflection of the landing maneuver, occurring in the opposite order, except for one important difference. Landing maneuvers being considered for STOL aircraft experience relatively high descent rates at touchdown whereas the ascent rate at the lift-off point must start from zero. Thus the need to simulate high model descent rates close to the ground and subsequently to arrest that descent without damage leads to additional experimental complexity for some of the techniques.

5.1.1 Constant Rate Approach

Figure 6 depicts the four techniques for simulating the model motion of a constant rate descent landing approach.

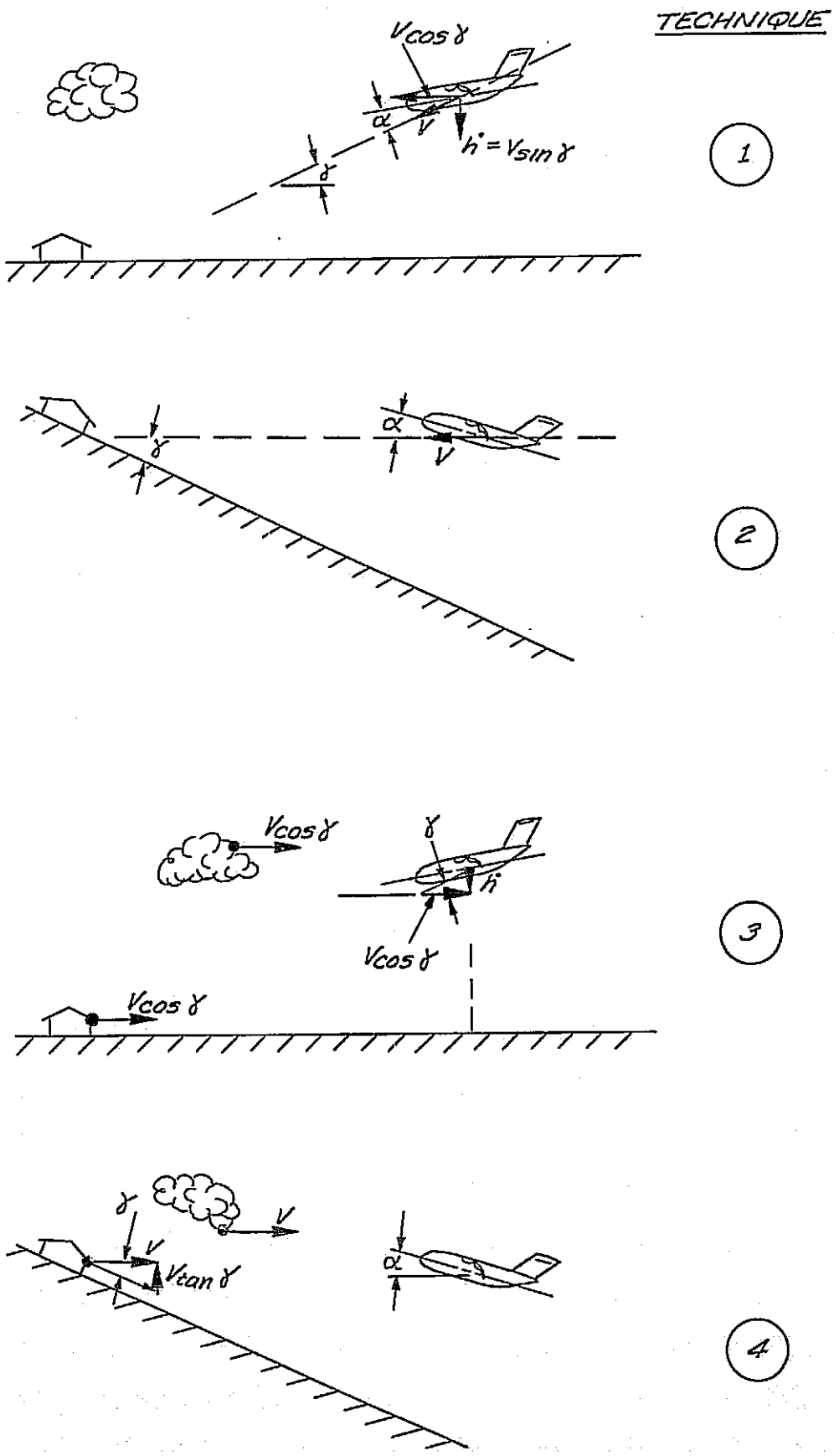

FIGURE 6. MOTION SIMULATION TECHNIQUES FOR LANDING APPROACH

Technique number one is the direct analog of the full scale flight situation. The model is moved through a stationary air mass with a combined horizontal and vertical motion. The total velocity, V, is directed along the flight path at an angle, γ, to the horizontal ground plane. The angle of attack, α, is the angle between the aircraft reference line and the flight path. The attitude of the aircraft with respect to the ground plane is given by $\theta = \alpha + \gamma$.

This technique requires the use of a track facility with a carriage having vertical motion of sufficient travel to encompass the complete height range of the flight path. The principal advantage of this technique is the ability to directly model the landing and takeoff motion without the need for any coordinate transformation. The main difficulty is that the model, air supply, sensors, signal conditioning, and data acquisition equipment must all be contained on the moving carriage which is limited in the amount of payload it can carry.

The second technique involves a rotation of the coordinate system so that the model path is horizontal. The model is moved through a stationary air mass with a single component of motion equal to the flight path velocity. The ground plane is tipped up at the flight path angle, γ, to the horizontal.

The advantage gained from this technique is that the need to provide vertical motion of the model is eliminated. Not only does this make the apparatus simpler, but it eliminates the inertia forces associated with vertical accelerations in starting and stopping the model. The principal disadvantage, as with the first technique, is that the model and equipment must be contained on a moving carriage.

Technique number three relies on the moving airstream of a wind tunnel to provide the horizontal velocity component while a traversing mechanism moves the model vertically. Exact simulation of the boundary conditions at the ground would require the ground to move at the same speed as the airstream.

This requires a moving belt ground plane or some other form of boundary layer control (BLC) to prevent the viscous boundary layer from adversely affecting the simulation at high lift conditions.

With this technique the total motion of the model is of limited extent so that instrumentation and air supply connections can easily be made to stationary equipment. In addition, higher airspeeds are generally available from wind tunnels than from moving model track systems. This permits testing at higher Reynolds numbers, although the difficulty of providing the scaled motion at higher airspeeds increases correspondingly.

Technique number four utilizes essentially the same coordinate system rotation as in technique number two, applied to the moving airstream situation of technique number three. The model remains stationary while the air mass moves with the flight path total velocity. Exact simulation of the ground requires the ground plane to be oriented at the flight path approach angle, γ, to the velocity vector, and to move toward the model at that velocity. An essential simplification to the motion simulation required by this technique is that the ground plane motion, which can be described by the vector sum of parallel and perpendicular components, be reduced to just the component perpendicular to the ground plane. The component of the ground plane motion parallel to itself is fixed at zero. A boundary layer will develop on the ground plane which may require BLC to avoid adverse interference.

The angular orientation of the ground plane and its translation rate are coupled such that the induced local angle of attack of the ground board relative to the free stream airflow is exactly zero. The only significant extraneous disturbance the translating ground board makes is due to the viscous boundary layer buildup on the board, so long as the ground board is of sufficient extent to contain the flow perturbations caused by the model.

The purpose of this unusual ground plane motion is to permit the model to remain completely stationary. The model therefore experiences no inertial forces; the only forces are aerodynamic. The principle difficulties are

associated with providing the translational motion of the ground board, especially during the starting and stopping process. The coupling between angle and translational rate of the ground board require that at rest it remain parallel to the free-stream direction. As it accelerates across the flow the orientation angle must increase to maintain

$$V_g = V \tan \gamma$$

As the board decelerates to a stop, its angle must decrease in the reverse manner. The starting process can be simplified if an open jet wind tunnel is used so that the full translational rate is achieved before the ground plane enters the airstream. This motion requirement is complicated by the fact that, in general, the full lift load of the wing will be felt as a reaction force on the ground plane, necessitating the use of powerful actuators.

5.1.2 Landing Flare

The landing flare maneuver simulation techniques are depicted in figure 7. Shown is a nominal flight path with a constant radius of curvature and a touchdown sink rate of zero.

Technique number one, again, provides a direct model of the full scale flight trajectory. The vertical motion of the model is provided by a traversing mechanism which is pre-programmed to produce the desired trajectory. For the model to maintain a constant angle of attack, it must be rotated as the flight path angle changes. An increase in angle of attack requires an additional rotation of the model. The vertical motion of the model must be completely arrested before the ground is contacted.

With technique number two, the model trajectory remains straight, and the ground surface is curved to simulate the flight path radius. Simulation of flight at a constant angle of attack requires no model rotation. A flare maneuver would require additional model rotation but a simulated flare could be performed with DLC operation which would not require a rotational drive. This procedure would eliminate the need for vertical and rotational motion mechanisms and the associated accelerations and inertia forces.

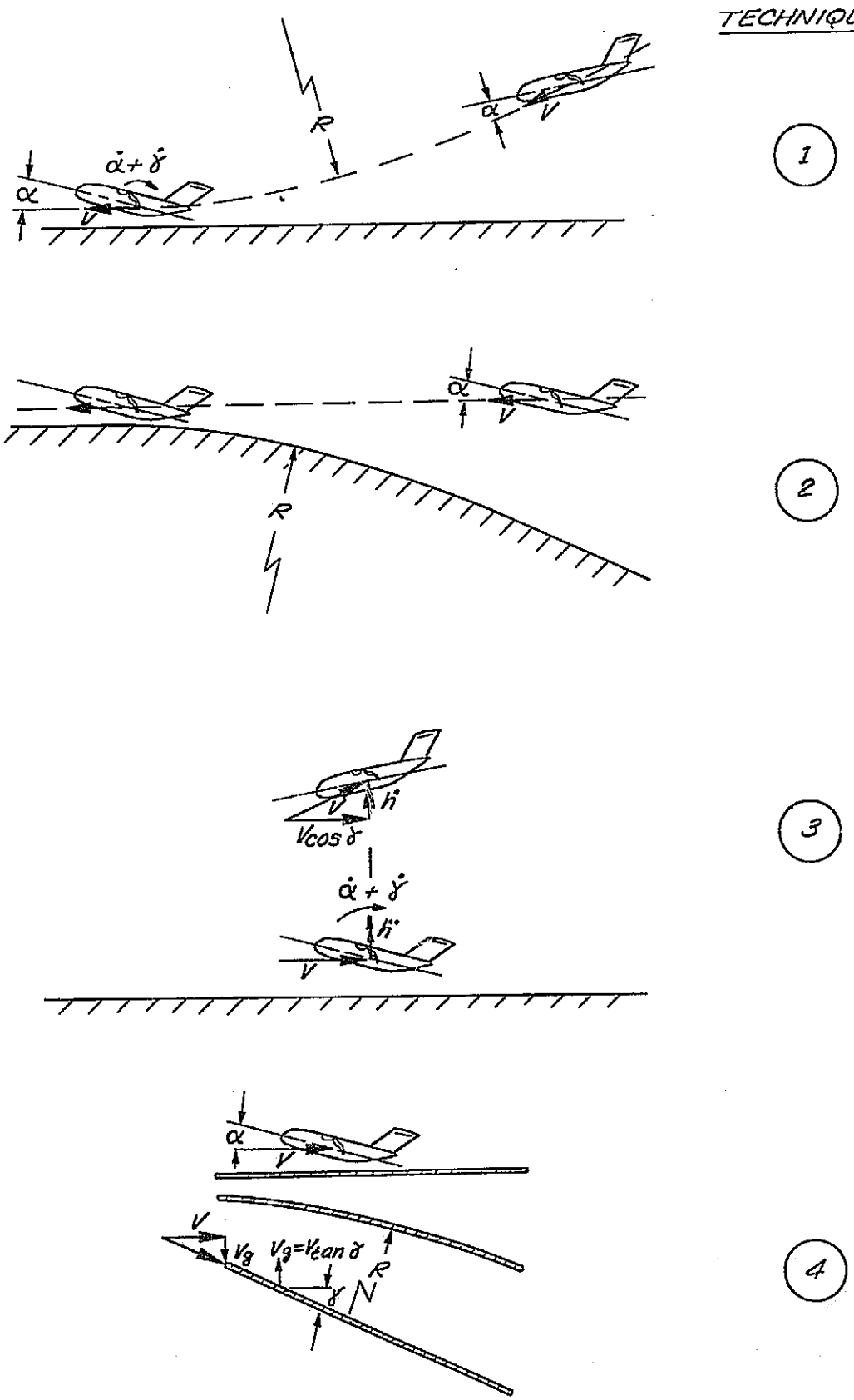

FIGURE 7. MOTION SIMULATION TECHNIQUES FOR LANDING FLARE

For technique number three the required flare simulation motions are nearly identical with technique number one. As the model descent rate is arrested by the upward directed acceleration, the model must rotate to maintain constant angle of attack.

Technique number four requires that the translating ground plane take on a curved shape as it decelerates. The required curvature would correspond to a segment of the stationary, curved surface utilized in technique number two. The ground board parameters, position, orientation, and shape would be coupled to the translation rate through a pre-programmed servo actuator system. The model could remain completely stationary except to simulate a change in angle of attack.

A modification to technique number one is possible where the exact flight path simulation is maintained, but the required vertical motion is greatly reduced. This is referred to as technique number five. The trajectory is viewed in terms of a perturbation motion from some reference line which is maintained horizontal. With technique number one, for example, the reference line is parallel to the ground. In this case the perturbation velocities correspond to the sink rates and range from 5.2 m/s (17 ft/sec) at the flare point to 3.0 m/s (10 ft/sec) at the touchdown point. The extent of the vertical motion is at least 0.5 spans. If, instead, the horizontal reference line is chosen to be parallel to the approach flight path, the initial perturbation velocity is zero and increases to a value equal to the change in sink rate or 2.1 m/s (7 ft/sec). More important, the vertical distance from the reference line is greatly reduced; about 0.05 spans, for a typical case.

5.1.3 Motion Simulation Errors

The motion simulation techniques discussed above all provide essentially correct simulation, with two possible exceptions. The first is a consequence of the viscous boundary layer development on the ground board in the wind tunnel for techniques three and four. When this boundary layer encounters the adverse pressure gradient field of the wing it develops separation tendencies which may strongly affect the flow field at high lift conditions

when close to the ground. These tendencies can be alleviated by various boundary layer control (BLC) procedures which are discussed in greater detail in a subsequent section of the report.

The second type of simulation error occurs with techniques number two and four when a curved flight path is simulated with a straight motion. Two aspects of this problem have been identified. The first is due to the free-stream onset flow condition and does not depend on the existence of a ground plane. The second aspect pertains to the orientation of the ground surface to the flight path.

The possible magnitude of these errors depends on the magnitude of the flight path curvature encountered in the simulated landing and takeoff trajectories. Figure 8 presents the flight path curvature for the trajectories of figures 2 and 3. Shown is the flight path radius of curvature, ρ/c, as a function of altitude, h/b.

The landing maneuver shows a sudden decrease in the radius at about $h/b = 0.2$, corresponding to the DLC spoiler actuation point. The radius gradually decreases further to a minimum of about $\rho/c = 280$ at a height of about $h/b = 0.1$, and increases back up to $\rho/c = 476$ at touchdown. The takeoff trajectory displays a more distinct minimum radius of about $\rho/c = 242$ at a height of $h/b = 0.04$. Above this height the radius of curvature shows a steady increase as the normal acceleration drops off.

Flight along a curved flight path through a stationary air mass is exactly equivalent to a stationary aircraft in an onset flow having a solid body type rotational motion. Such a flow has a variation in local angle of attack along the length of the configuration and has a vertical velocity gradient corresponding to a steady shear flow. For a flight path radius of curvature of $\rho/c = 240$, an aircraft element such as a chord length will have an induced angle of attack variation of

$$\Delta\alpha = \text{arc sin } c/240c = 0.24 \text{ degrees}$$

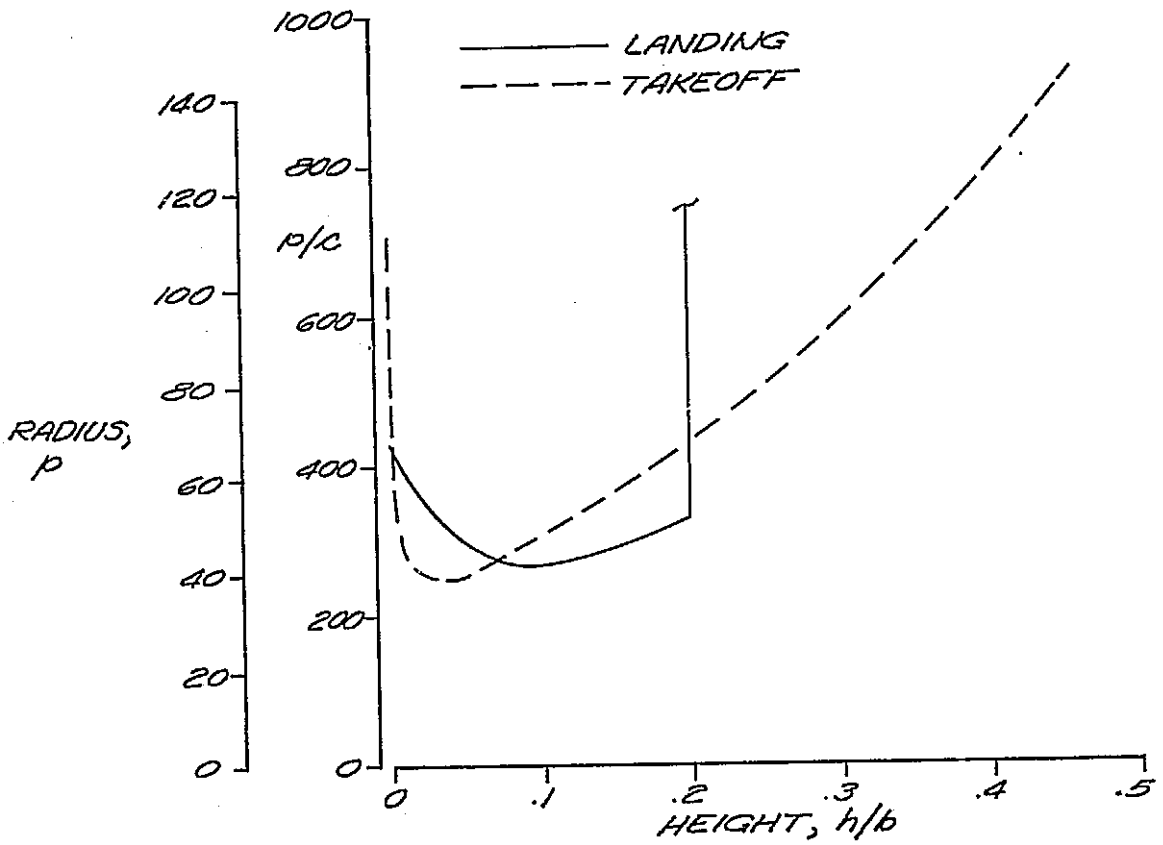

FIGURE 8. FLIGHT PATH RADIUS OF CURVATURE

Similarly, a length element corresponding to the tail arm ($\ell_t = 3.6c$) experiences an angular increment of

$$\Delta\alpha = \text{arc sin } 3.6c/240c = 0.86 \text{ degrees}$$

In general, angle increments of this magnitude acting on lifting surfaces with typical lift coefficient derivatives on the order of

$$dC_L/d_\alpha = 0.08$$

might be expected to suffer from a simulation error on the order of

$$\Delta C_L = 0.08 \times 0.24 = 0.02$$

for a wing alone or

$$\Delta C_L = 0.08 \times 0.86 = 0.07$$

for a tail surface, which may be significant in some situations.

If the magnitude of these errors can be accurately assessed and demonstrated to be insignificant, or easily corrected for, very significant experimental simplifications are possible. Most practical analytical formulations require a potential flow situation (i.e., a velocity potential can be defined). In general, rotational flows are not potential flows, but the present situation of a stationary airfoil immersed in a rotating fluid is a special "rotational" flow which can be analyzed by potential methods since the perturbation flow is irrotational.

In the stationary airfoil reference system the flowfield is described by the combination of two streamfunctions, ψ_R and ψ_P, which are the streamfunctions of the rotational and potential parts of the flows, or,

$$\psi = \psi_R + \psi_P$$

For the present potential flow problem

$$\psi_R = \frac{\omega R^2}{4}$$

where ω is the fluid vorticity, twice the angular velocity of the fluid, and R is the distance from the center of rotation. Both ψ_R and ψ_P satisfy the mass conservation condition and the fluid vorticity is given by

$$\nabla^2\psi = \nabla^2\psi_R + \nabla^2\psi_P$$

Therefore, since $\nabla^2\psi_R = \omega$, the perturbation streamfunction satisfies the Laplace equation and can be determined from potential methods. The superposition of rotating and potential flows is only possible because of the constant vorticity throughout the flowfield and invariance from streamline to streamline. The boundary condition of the potential part of the flow can be determined by considering the condition of zero normal flow along solid body boundaries,

$$\frac{\partial\psi}{\partial s} = 0$$

$$= \frac{\partial\psi_R}{\partial s} + \frac{\partial\psi_P}{\partial s}$$

or,

$$\frac{\partial\psi_P}{\partial s} = -\frac{\partial\psi_R}{\partial s}$$

Thus the potential solution boundary condition specifies a normal velocity to cancel the normal rotational flow along solid boundaries.

The Douglas Neumann 2-D potential flow program (reference 7) was modified to calculate the streamfunctions and the surface pressures for the special case. The pressures are determined using the unsteady Bernoulli equation by considering the problem in the fluid fixed reference frame. The results are shown in figure 9 for a single airfoil and for a two body configuration corresponding to the nominal STOL aircraft wing and horizontal tail arrangement.

To confirm the Neumann formulation of the problem, a simplified approach employing single point vortex to represent the airfoil was developed. A single point vortex is placed at the airfoil one-quarter chord point and

the condition of tangential flow is enforced at the three-quarter chord point. Thus for a single uncambered airfoil along a curved flight path with a constant radius, R, at an angle of attack, α, the normal velocity is

$$V_N = \Omega R \sin \alpha - \frac{\Omega c}{4}$$

where Ω is the angular velocity and c is the airfoil chord. To obtain tangential flow at the three-quarter chord point, the value of the point vortex circulation, Γ, is given by

$$\Gamma = \frac{\pi c}{\Omega R C} \left(\sin \alpha - \frac{c}{4R} \right)$$

The resultant section lift coefficient is obtained by multiplying the vortex circulation by the local flow speed so that

$$C_\ell = 2\pi \left(\sin \alpha - \frac{c}{4R} \right)$$

where

$$C_\ell = \frac{\ell}{\frac{1}{2} \rho \Omega^2 R^2 c}$$

Comparison with the Neumann solution requires the above expression to be scaled by the factor $(1 + t/c)$ to approximately account for finite section thickness.

In a similar fashion a simplified method can be formulated for a two body problem. A point vortex is placed at each airfoil's one-quarter chord point and tangential flow is specified at each three-quarter chord point. This procedure results in one equation for each airfoil in terms of the airfoil circulation values. These equations are simultaneously solved to provide the circulation representing each airfoil and hence the lift on each airfoil.

These results are presented in figure 9. The simple point vortex method is seen to agree very well with the Neumann solutions. At a flight path radius of $\rho/c = 240$, the wing-alone curve shows a lift loss of about one-half percent of the straight flight lift which is insignificant in terms of the proposed experiment. The wing-plus-tail curve, however, displays a

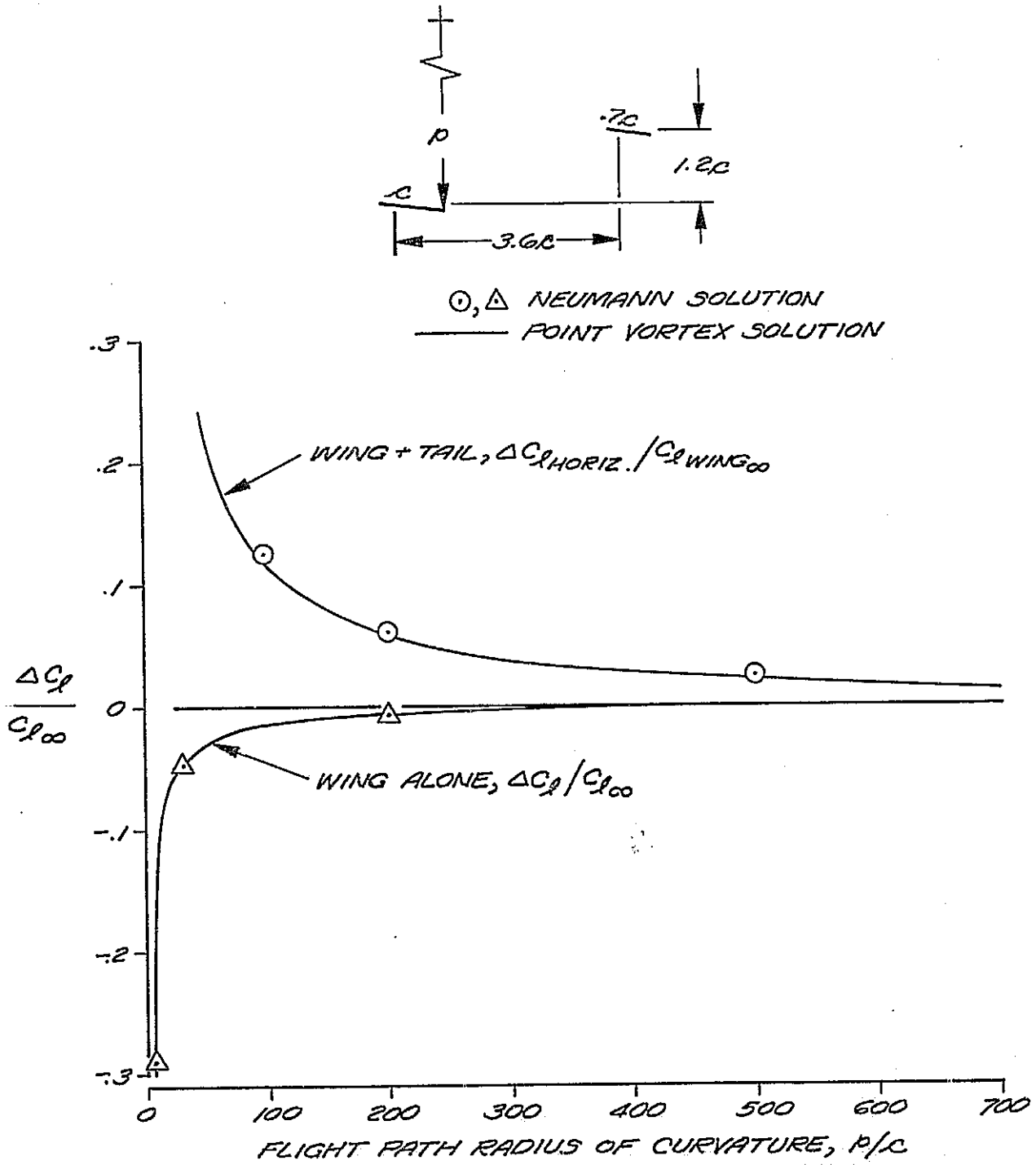

FIGURE 9. FLIGHT PATH CURVATURE ERROR

much greater effect. The tail lift increase is about five percent of the straight flight wing-lift level. The wing lift in this case has very little change and is not shown.

The other aspect of the curved flight path simulation error can be visualized as incorrect variation in the orientation of the ground along the length of the aircraft. In the correct model of the trajectory, the aircraft reference line is straight and the ground is straight. At any instant the angle between the reference line and the ground is constant. For the simulation with a curved ground surface, that angle varies along the length of the aircraft.

The magnitude of this angular error is the same as discussed above, but the effect on the aerodynamic forces is different. The analytical results presented in Part I of this study are used to estimate the incremental effect of aircraft attitude, θ, on the lift coefficient. Figure 12 of Part I presents the lift increment due to ground effect calculated by the steady and quasi-steady methods. The difference between these two curves at a height of one chord is used to estimate the derivative

$$\frac{dC_L}{d\theta} = \frac{0.037\ C_{L_\infty}}{5.71\ \text{deg}} = 0.0065\ \frac{C_{L_\infty}}{\text{deg}}$$

which, for a $\Delta\theta = 0.86$ for the tail arm, inplies a lift error of

$$\Delta C_L = 0.006\ C_{L_\infty}$$

The conclusions pertaining to the curved flight path error developed from this analysis are that ground orientation effects are insignificant compared to out-of-ground-effect onset flow distortion effects. For a wing alone condition the magnitude of the curved flight error is insignificant for a typical flight path curvature. The effects of curved flight path on the tail lift may be significant, however, it may be possible to develop a correction procedure to account for such error.

5.2 Engine Simulation Techniques

Three different types of jet engine simulators are commonly used for powered model testing; direct supply, ejectors, and air-turbine driven fans. These all use high pressure compressed air as the drive medium. Most test facilities have compressed air supply systems available for this purpose. Other fan type simulators have used both hydraulic and electric drive motors but generally are thought to be less satisfactory. Very large wind tunnel models are operated with gas turbine driven fans or complete jet engines, which appears to be the only suitable method for such large models. In the present instance the models tend to be smaller than the minimum practical for that type engine simulator.

5.2.1 Direct Supply Engine Simulator

The direct supply type jet engine simulator represents the simplest means of producing a simulated propulsive jet for small scale model testing. The entire jet mass flow is supplied as high pressure gas ducted onboard the model. No inlet flow is simulated. For podded engine nacelles the forebody is faired over with a smooth shape. The possible importance of simulating the inlet flow is discussed in Section 3.3.1.

The propulsive jet is formed from the high pressure drive in several steps. First, the supply pressure is kept to as high a level as practical to keep the supply duct size small. This simplifies the design of the balance crossover. Typical working pressure levels are as high as 14 to 21 MPa (2000 to 3000 lb/in^2). At the point where the high pressure supply line connects to the simulator plenum, a small orifice is used to drop the pressure by a throttle process to an intermediate working pressure. The intermediate pressure plenum occupies a volume within the nacelle that completely spans the maximum diameter. This plenum has as its downstream face a perforated choke plate forming the upstream end of the jet nozzle duct. The perforations act to produce a uniformly distributed array of intermediate jets which, if small enough, quickly coalesce into the main jet stream. The turbulence produced by this process is attentuated by the nozzle contraction. If desired it can be further damped by screens in the nozzle duct. The intermediate jets are kept

uniform in strength across the face of the choke plate by keeping the intermediate plenum pressure high enough to ensure that the orifices are strongly choked and that the Mach number in the plenum is low. A typical level for the intermediate plenum pressure is about 69 to 138 kPa to (100 to 200 lb/in^2) for a jet total pressure variation of from 1.5 to 2.0 atmospheres.

The ideal gross thrust and flow rate of a direct supply simulator can be conveniently expressed as

$$F_g = 1.4\, A_J\, P_\infty\, M_J^2$$

$$W = g\sqrt{\frac{1.4}{R}}\, A_J\, \frac{P_T}{\sqrt{T_T}}\, \frac{M_J}{(1 + 0.2\, M_J^2)^3}$$

The principal disadvantages of a direct supply engine simulator is that all the jet flow must be supplied to the model and that the inlet flow is not simulated. These must be weighed against several significant advantages of the system.

First, the lack of inlet flow can be considered an advantage for those situations where it is not a significant factor under study. Other types of engine simulators, with incomplete inlet mass flow, produce a ram drag which is incorrect by the ratio of inlet to total mass flow. To correct for the ram drag error the inlet mass flow rate must be measured in addition to the drive air flow rate. This requires instrumentation in the inlet, such as wall and centerbody static pressure taps, which have to be calibrated against the inlet flow rate measured by some independent means. These measurements and calibrations generally prove to be very difficult to accomplish with the required accuracy. The direct supply engine simulator obviates the need for this experimental complication.

Calibration of a direct supply engine simulator is very easily accomplished by measurement of total pressure, total temperature, and flow rate of the drive air, all of which are relatively easy to accomplish. The quality of the jet, in terms of uniformity of exit profile and turbulence level, can be

kept to a very high level by addition of smoothing screens without regard to adversely affecting the flow process, as may be the case with other types of simulators. If desired, arbitrary exit velocities profiles are easily produced using non-uniform porosity screens. The direct supply system also has potentially the lowest weight and cost of the various engine simulators.

5.2.2 Ejector Engine Simulator

An ejector engine simulator produces a limited amount of inlet flow simulation by using entrainment properties of underexpanded turbulent jets. A large array of such jets is situated completely spanning the diameter of the nacelle inlet diffuser. The drive air is supplied to the array of primary nozzles at a pressure on the order of 10 atmospheres. The entrained air supplied from the inlet is mixed with the drive air from the primary nozzles and delivered to the exit nozzle. The total exit flow rate is then the sum of the dirve air flow rate and the inlet flow rate.

The drive air pressure should be kept to the same high pressure range as for direct supply simulators, about 10 MPa to 20 MPa (1500 lb/in^2 to 3000 lb/in^2), to keep the supply line size small. For this case, because of the reduced drive air flow rate, these supply lines are somewhat smaller than for direct supply. The high pressure is throttled down to the primary nozzle pressure of about 10 to 20 atmospheres by an orifice at the entrance to the primary nozzle plenum.

The inlet rate can be expressed as an inlet flow ratio, $\phi = \dot{m}_{INLET}/\dot{m}_{TOTAL}$, which is a measure of the fraction of complete inlet flow simulation. The magnitude of this ratio depends on many design and operating factors, but the most significant dependence can be shown in terms of the mixed jet Mach number. This is essentially the exit Mach number of the simulated jet. For a given ejector design the inlet flow ratio drops steadily until eventually nearly all of the jet flow is supplied by the primary nozzles. This decrease in induction performance is associated with shock wave induced losses in the mixing process. Figure 10 shows the variation of a typical inlet flow ratio with jet Mach number, M_J. At $M_J = 0.55$, the inlet flow ratio is seen to be $\phi = 0.5$. At this condition one half the jet flow rate is supplied by the drive air from outside the model. At the jet

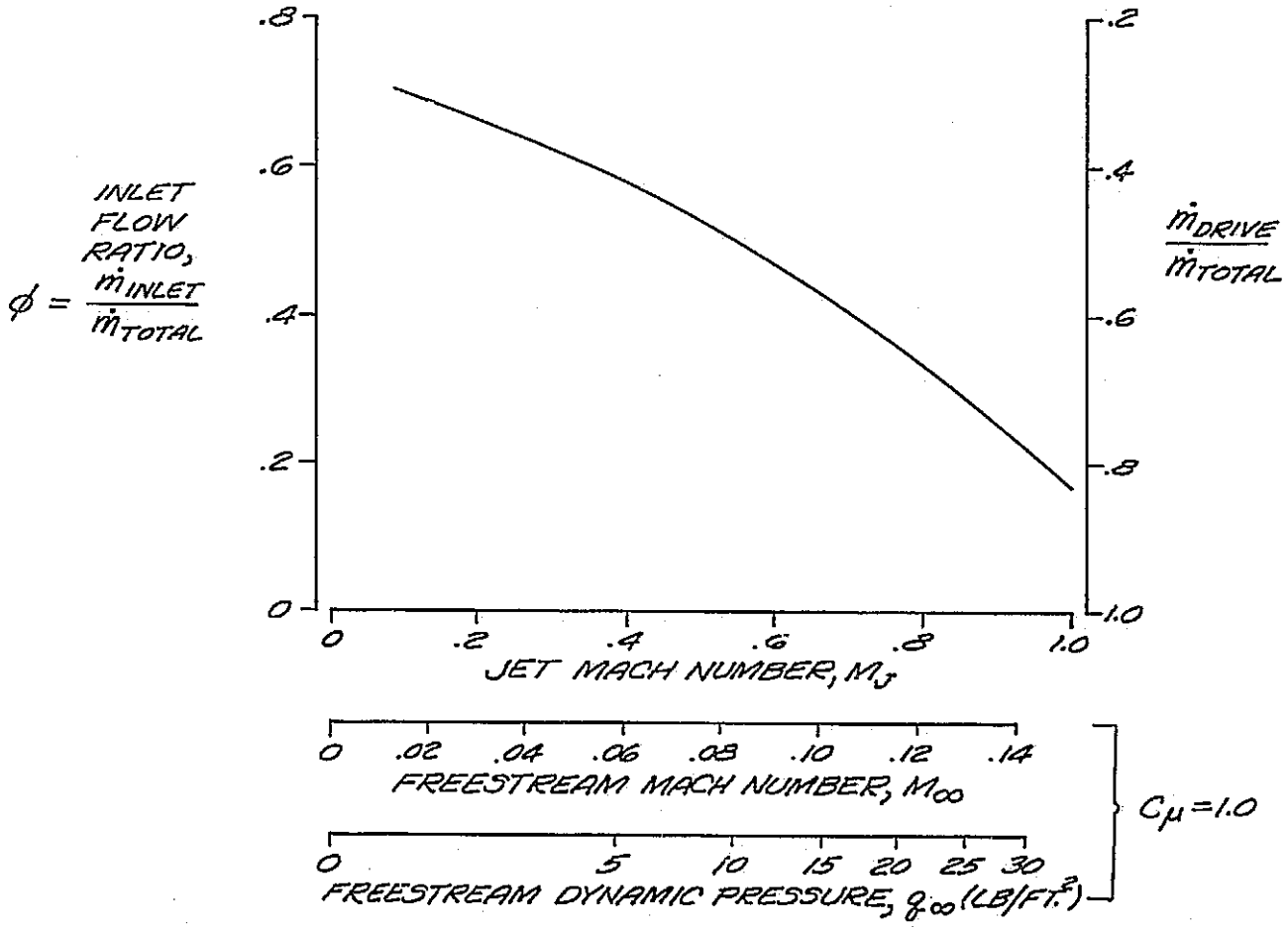

FIGURE 10. EJECTOR ENGINE SIMULATOR
INLET FLOW RATIO

Mach numbers closer to the full scale flight condition, $M_J = 0.9$ to 1.0, however, the inlet flow ratio drops to $\phi = 0.25 - 0.15$, so that the drive air required from off-board the model ranges from 75% to 85% of the total. Figure 10 also shows, on alternative scales, the freestream Mach number, and dynamic pressure for the nominal STOL aircraft geometry depicted in table 1 at a momentum coefficient of $C_\mu = 1.0$.

As mentioned in the previous section, the fact that the inlet flow is less than the correct simulation quantity requires that the inlet ram drag be corrected to account for this discrepancy. This requires additional instrumentation and calibration to permit a measurement of the actual inlet flow rate during the test. The magnitude of the inlet ram drag discrepancy can be estimated in terms of the momentum coefficient, C_μ, as follows.

The ram drag coefficient is expressed as

$$C_{\mu_o} = \frac{D_R}{q_\infty S_w} = \frac{\dot{m}_{INLET} V_\infty}{q_\infty S_w} = \frac{\phi \dot{m}_{TOTAL} V_\infty}{\frac{1}{2} \gamma P_\infty M_\infty^2 S_w}$$

and the momentum coefficient is

$$C_\mu = \frac{F_g}{q_\infty S_w} = \frac{\dot{m}_{TOTAL} V_J}{\frac{1}{2} \gamma P_\infty M_\infty^2 S_w}$$

Therefore

$$C_{\mu_o} = C_\mu \frac{\phi}{\frac{M_J}{M_\infty}\left(\frac{T_J}{T_\infty}\right)^{1/2}}$$

Most experimental situations try to arrange for the jet temperature to be close to ambient so it can be assumed

$$T_J = T_\infty$$

leading to

$$C_{\mu_o} = \phi \frac{C_\mu}{M_J/M_\infty}$$

Referring to the expression for C_μ given in Section 3.3.1,

$$C_\mu = \frac{2\ A_J}{S_w}\left(\frac{M_J}{M_\infty}\right)^2$$

permits

$$C_{\mu_o} = \phi\sqrt{C_\mu}\sqrt{\frac{2\ A_J}{S_w}}$$

and the ram drag discrepancy is

$$\Delta C_{\mu_o} = (1 - \phi)\ \sqrt{C_\mu}\sqrt{\frac{2\ A_J}{S_w}}$$

For the nominal STOL configuration being considered, and for $C_\mu = 1.0$, $\phi = 0.5$,

$$\Delta C_{\mu_o} = 0.076$$

This quantity is directly additive to the drag coefficient so it tends to be significant in terms of typical drag coefficient increments.

Ejector engine simulators are comprised of more parts and as a consequence weigh and cost more than direct supply simulators. In this instance, where the simulated jet configuration is relatively simple, the additional weight and cost are not very great. A rough estimate has been made which indicates an ejector simulator may weigh 1.5 times more than a direct supply simulator and may cost 3 times more. These factors include the effect of the reduced air supply lines capacity, but not the reduced capacity of the air supply source.

A possibly significant restriction to the general applicability of ejector simulators is found in the geometrical constraints enforced by the need to optimize the mixing chamber configuration.

5.2.3 Air-Turbine Driven Fan Engine Simulators

Air-turbine driven fan engine simulators represent the most complex means of producing the jet simulation, but also provide the closest simulation of the inlet flow. They operate in a manner very similar to full scale fan

jet engines except that the driving power is extracted from compressed air instead of the combustion of fuel. The extent of the inlet flow simulation depends on several operating factors, but typically might go as high as $\phi = 0.8$.

The operation of such simulators is strictly controlled by a characteristic map with distinct boundaries forming an operating envelope. The rotating turbine and fan assembly is highly loaded and has a limited running lifetime on the order of 100 hours. Bearing temperature and accelerations must be carefully monitored to detect anomalies and allow protective shutdowns.

This type of simulator tends to be relatively heavy and very expensive. The weight and cost factors relative to direct supply simulators are 9 and 7 , respectively. An additional restriction on the use of such simulators in this instance may be the lack of tolerance to acceleration and rotation. This problem has not been evaluated by the engine simulator manufacturer, so presently it can only be cited as a possible restriction. Nevertheless, it is anticipated that such highly loaded rotating machinery would be adversely affected by the translational accelerations on the order of 10 g's and rotation rates on the order of 100 degrees per second.

5.2.4 Drive Air Thermodynamics

Model simulation of propulsive jets can be conveniently performed with devices powered by compressed air. The compressed air should be supplied at as high a pressure as possible to minimize the supply tube and crossover size. This high pressure must then be reduced to the device working pressure, and then finally to the jet exit total pressure. The thermodynamics of this pressure dropping or expansion process are of interest as they pertain to the temperature change of the air. Usually there is a temperature drop producing air temperatures well below ambient. Operational considerations require that the jet temperature remain above a certain minimum level to avoid excess condensation or ice accumulation on model parts.

The process by which the pressure drop occurs in direct supply or ejector simulators is a throttling process characterized by flow through small orifices or through a porous medium. Since the process is essentially adiabatic and no work is performed by the flow, it takes place at constant enthalpy. For a perfect gas, a constant enthalpy implies a constant total temperature. That large temperature drops are sometimes observed in such processes must be explained by real gas effects associated with high pressures. For example, consider an air supply at 200 atmospheres and a temperature of 525°R to be expanded by the throttling process to approximately two atmospheres. Referring to the temperature/entropy diagram shown in figure 11, this corresponds to following the constant enthalpy curve of 210 BTU/lb and shows a temperature drop of nearly 70°R. In order to maintain a constant gas temperature, energy would have to be added to the gas stream to the extent of about 17 BTU per pound.

An air-turbine driven fan simulator experiences greater temperature drops in the flowing gas because of power extraction in the turbine stage. The magnitude of the drop depends on the turbine efficiency.

There is a third process by which a temperature drop can occur when using a small blowdown tank such that a large reservoir pressure change occurs as gas is consumed during a run. In this case the gas remaining in the reservoir undergoes an isentropic expansion. The resulting temperature drop is depicted in figure 11 by following a constant entropy line. The magnitude of the pressure drop is so great, in this example, as to cause liquifaction of the drive gas.

5.3 Model Sizing Study

A large array of factors must be considered when examining the feasibility of a transient ground effects experimental simulation. Perhaps more fundamental than the choice of experimental technique, is the question of the preferred scale for such an experiment, both in terms of model size and test speed. Not only are there the customary considerations of Reynolds number and Mach number conditions which set model size, test speed, air

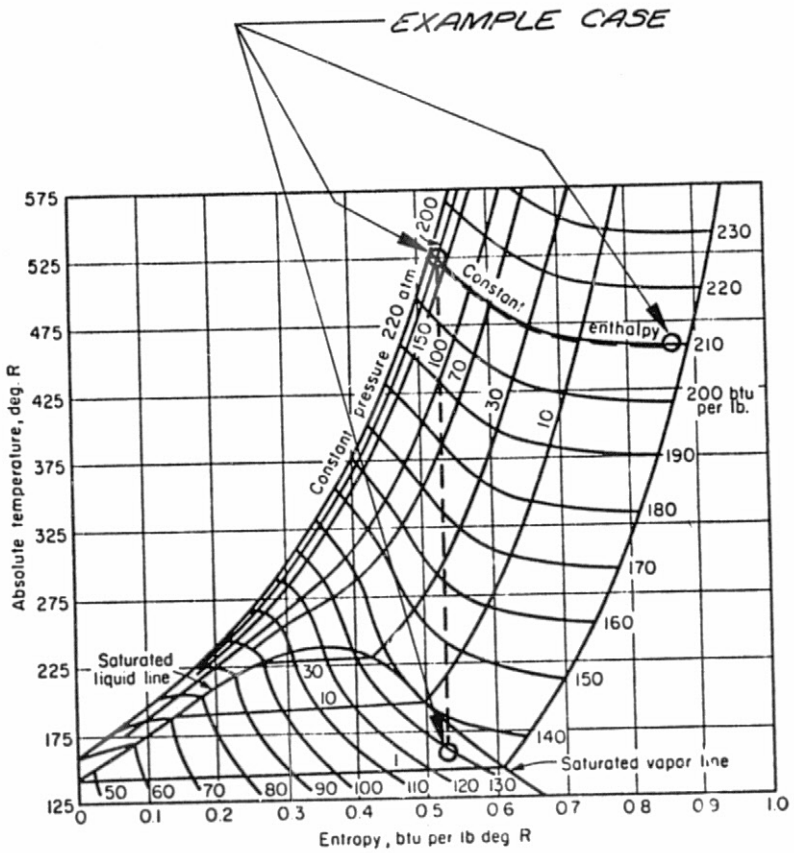

FIGURE 11. TEMPERATURE-ENTROPY DIAGRAM FOR AIR.

supply requirements, but there are the motion simulation requirements which have far-reaching implications for motion rates and power requirements of the apparatus, model strength for inertia forces, instrumentation frequency response, etc.

In an attempt to arrive at a rational procedure for selecting the preferred scale factors, a general sizing study was instituted to examine the various trends and limitations involved. The results of this sizing study are expressed in terms of model weight, W, as a function of velocity factor, F_V, and size factor, F_S.

5.3.1 Independent Scale Factors

The first step in the sizing study is to select a practical range of values for the velocity factor, F_V, and the size factor, F_S. The values selected for the factors F_V and F_S are

$$F_V = 0.2,\ 0.6,\ \text{and}\ 1.0$$
$$F_S = 0.05,\ 0.10,\ \text{and}\ 0.20$$

The maximum value of F_V was dictated by the Mach number simulation considerations discussed in Section 3.3.1. There is no specific lower limit for this parameter. The value chosen was based on consideration of minimum controllable airspeeds in typical wind tunnels, minimum desired Reynolds number, and the difficulty of accurate force and pressure measurements at low dynamic pressures.

The maximum value for the size factor, F_S, was based on the largest model that might be accommodated by the 40 x 80 foot wind tunnel, keeping in mind the space required for the transient ground effect maneuver. The minimum value of this parameter was chosen to correspond approximately to the smallest STOL model used at Douglas. This size is dictated mainly by the cost and convenience of manufacture for the high lift system components.

Table 5 summarizes some of the trajectory parameters for the nominal landing and takeoff and illustrates their variation with the scale factors F_V and F_S. These have been scaled as indicated by the factors summarized in table 4.

TABLE 5. SCALED SIMULATION PARAMETERS

Full Scale Quantities
b = 33.5 m (110 ft)
V = 56 m/sec (184 ft/sec)
$\dot{h}$ = ±5.2 m/sec (±17 ft/sec)
$\ddot{h}$ = 2.3 m/sec^2 (7.5 ft/sec^2)
θ = 0 – 16 deg
$\dot{\theta}$ = 7.4 deg/sec
$\ddot{\theta}$ = 8.0 deg/sec^2
γ = 6.7 deg
q = 1.93 kPa (40.3 lb/ft^2)
R_N = 20.3 (10)^6
f = 6.0 h_z

F_s / Γ_v	0.05	0.10	0.20
1.0	b = 1.7 (5.5) V = 56 (184) $\dot{h}$ = ±5.2 (±17) $\ddot{h}$ = 46 (150) θ = 0 → 16 $\dot{\theta}$ = 148 $\ddot{\theta}$ = 3200 γ = ±6.7 q = 1.93 (40.3) R_N = 1.0 (10)^6 f = 120	b = 3.4 (11) V = 56 (184) $\dot{h}$ = ±5.2 (±17) $\ddot{h}$ = 23 (75) θ = 0 → 16 $\dot{\theta}$ = 74 $\ddot{\theta}$ = 800 γ = ±6.7 q = 1.93 (40 3) R_N = 2.0 (10)^6 f = 60	b = 6.7 (22) V = 56 (184) $\dot{h}$ = ±5.2 (±17) $\ddot{h}$ = 11 (38) θ = 0 → 16 $\dot{\theta}$ = 37 $\ddot{\theta}$ = 200 γ = ±6.7 q = 1.93 (40.3) R_N = 4.1 (10)^6 f = 30
0.6	b = 1.7 (5.5) V = 34 (110) $\dot{h}$ = ±3.1 (10) $\ddot{h}$ = 16 (54) θ = 0 → 16 $\dot{\theta}$ = 89 $\ddot{\theta}$ = 1152 γ = ±6.7 q = 0.69 (14) R_N = 0.61 (10)^6 f = 72	b = 3.4 (11) V = 34 (110) $\dot{h}$ = ±3.1 (10) $\ddot{h}$ = 8.2 (27) θ = 0 → 16 $\dot{\theta}$ = 44 $\ddot{\theta}$ = 288 γ = ±6.7 q = 0.69 (14) R_N = 1.2 (10)^6 f = 36	b = 6.7 (22) V = 34 (110) $\dot{h}$ = ±3.1 (10) $\ddot{h}$ = 4.1 (14) θ = 0 → 16 $\dot{\theta}$ = 22 $\ddot{\theta}$ = 72 γ = ±6.7 q = 0.69 (14) R_N = 2.4 (10)^6 f = 18
0.2	b = 1.7 (5.5) V = 11 (37) $\dot{h}$ = ±1.0 (3.4) $\ddot{h}$ = 1.8 (6.0) θ = 0 → 16 $\dot{\theta}$ = 30 $\ddot{\theta}$ = 128 γ = ±6.7 q = 0.077 (1.6) R_N = 0.20 (10)^6 f = 24	b = 3.4 (11) V = 11 (37) $\dot{h}$ = ±3.1 (10) $\ddot{h}$ = 0.91 (3.0) θ = 0 → 16 $\dot{\theta}$ = 15 $\ddot{\theta}$ = 32 γ = ±6.7 q = 0.077 (1.6) R_N = 0.41 (10)^6 f = 12	b = 6.7 (22) V = 11 (37) $\dot{h}$ = ±3.1 (10) $\ddot{h}$ = 0.46 (1.5) θ = 0 → 16 $\dot{\theta}$ = 7.4 $\ddot{\theta}$ = 8.0 γ = ±6.7 q = 0.077 (1.6) R_N = 0.81 (10)^6 f = 6

5.3.2 Model Weight

The next step in the sizing study is to establish the model weight level and trends. A basepoint is established for the condition

$$F_v = 1.0$$
$$F_s = 0.05$$

This is chosen because it corresponds the closest to the model test experience of Douglas.

The preliminary weight estimate for this basepoint design is based on model construction techniques carefully chosen to minimize weight. This is important to permit high frequency response and to minimize power requirements for the motion actuators. The backlog of experience at Douglas in the design and construction of powered STOL models and lightweight flutter models permits a high degree of confidence in the present instance.

The entire metric mass of the model and balance is estimated to be 80 pounds. By way of comparison, it is estimated that an existing STOL model of similar size and load capability which weighs 300 pounds can be modified, by removal of nonessential on-board components such as engine air distribution manifold and extra strut mounting provisions, to a weight of about 120 pounds.

The weight trends used to extrapolate the weight of the models for the other points in the scaling matrix are determined from general scaling rules for beams. Experience has confirmed that the complete model weight variations closely correspond to the wing weight variations which depend on beam bending moment considerations. The bending stress of a beam is given by

$$\sigma = \frac{M_B}{I/d}$$

The bending moment, M_B, is given in terms of the aerodynamic load, $C_L\, q\, S_w$, and moment arm, ℓ,

$$M_B = C_L\, q\, S_w\, \ell$$

The section moment of inertia is defined in terms of the spar depth, d, and the spar cap area, A,

$$I = Ad^2$$

and the weight, W, is given by

$$W = \rho A \ell$$

The weight variation for a constant bending stress is given by

$$W = \frac{C_L \, q \, S_w \, \ell \rho}{\sigma d/\ell} \sim \frac{F_v^2 F_s^2 F_s}{F_s/F_s} \sim F_v^2 F_s^3$$

Figure 12 shows the extrapolated weights over the range of F_v and F_s.

5.3.3 Model Scale Limitations

Given the model weight trends of figure 12 the final step is to analyze the limitations which exist so as to establish preferred scale factor (F_v and F_s) trends. The limitations, to be discussed in the following subsections, are expressed as the limiting weight to satisfy the particular criterion. The various limit lines are shown in figure 13 superimposed on the data of figure 12.

5.3.3.1 Frequency Response

One of the most significant limitations to the experimental feasibility is the ability of the instrumentation to respond to the transient forces, or the frequency response. The response in question is that of the balance readout to the input aerodynamic and inertia force time history. This readout is proportional to the relative displacements of the metric and non-metric components of the balance, but depends on the motion of the entire dynamic system comprised of the model, balance, strut, actuator, and supporing framework.

A complete dynamic analysis of the system is beyond the scope of this initial sizing study. A simplified model of the balance dynamic system is used to establish the frequency response trends over the range of velocity and size factors. This system consists of the model metric mass supported on a spring representing the balance strain gage elements. The limiting frequency

response, f, is taken to be one-half the undamped natural frequency of the system given by

$$f = 0.5 \sqrt{\frac{k}{W/g}}$$

The factor of one-half is selected to limit the operation to a frequency sufficiently below the resonance condition.

This limit is expressed as the limiting weight to satisfy the required frequency response, f_R. As shown in Section .3.3, this has the scaling properties

$$f_R \sim F_v^1 F_s^{-1}$$

The spring rate, k, scales as

$$k \sim F_v^2 F_s^1$$

The limiting weight, therefore, varies as

$$W \sim \frac{k}{f_R^2} \sim \frac{F_v^2 F_s^1}{F_v^2 F_2^{-2}} \sim F_v^0 F_s^3$$

This limit is shown in figure 13 superimposed on the data of figure 12. It is seen to be independent of velocity and to vary with model size at the same rate as the model weight. Therefore, a preferred model size cannot be inferred from it, but a limit to maximum F_v is implied.

5.3.3.2 Inertia Loads

Starting and stopping accelerations of the model impose inertia loads on the balance. The balance must be sized to withstand these loads, even though they may be associated with parts of the test where aerodynamic data may not be needed. The greatest accelerations are most likely to be due to stopping the model close to the ground with high sink rates after a descent. There will be a desire to keep the stopping distance as small as practical because of the anticipated interesting aerodynamic effects at those conditions. Starting and stopping the model far from the ground can presumably be done over a longer distance.

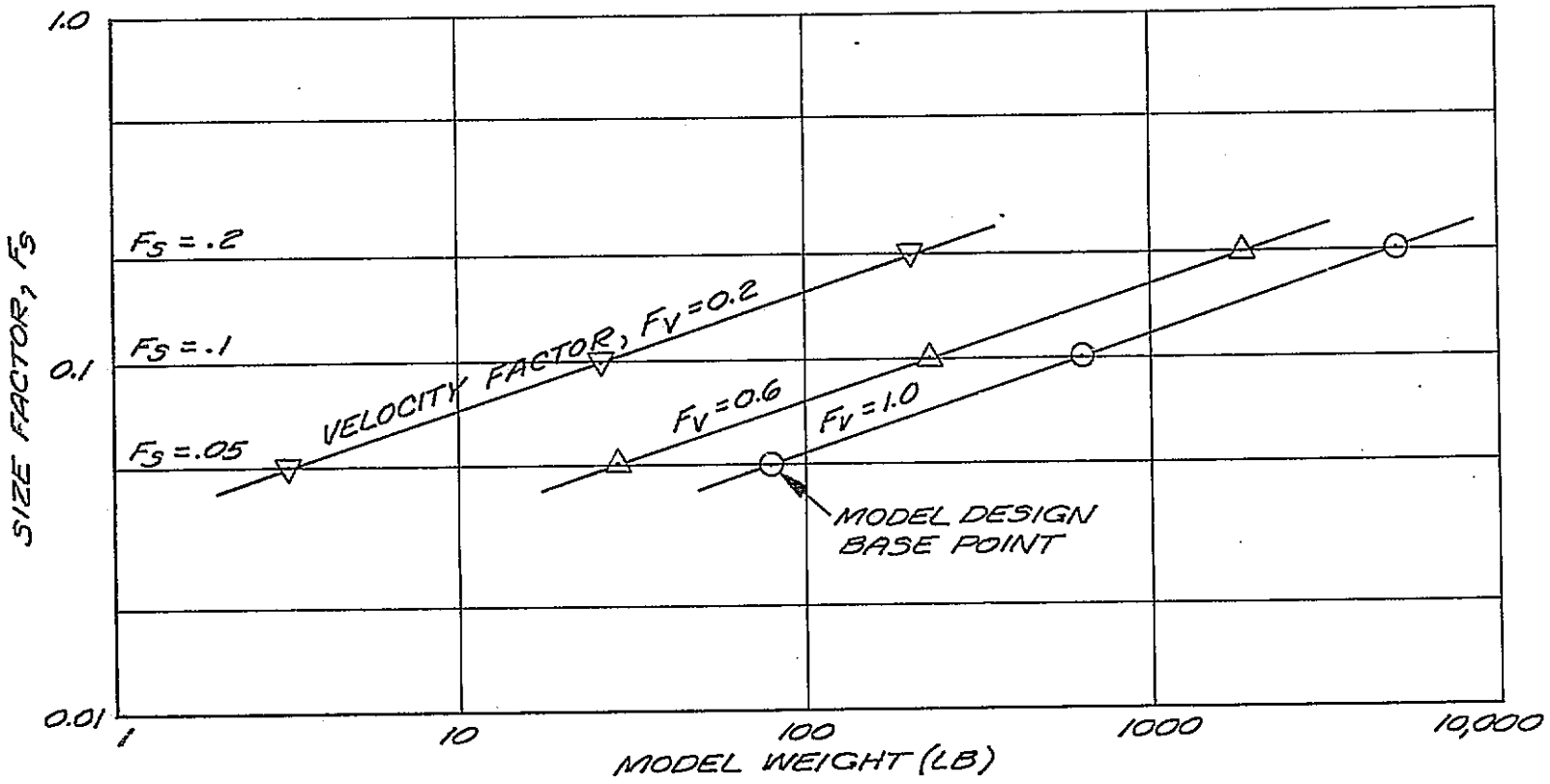

FIGURE 12. MODEL WEIGHT TRENDS

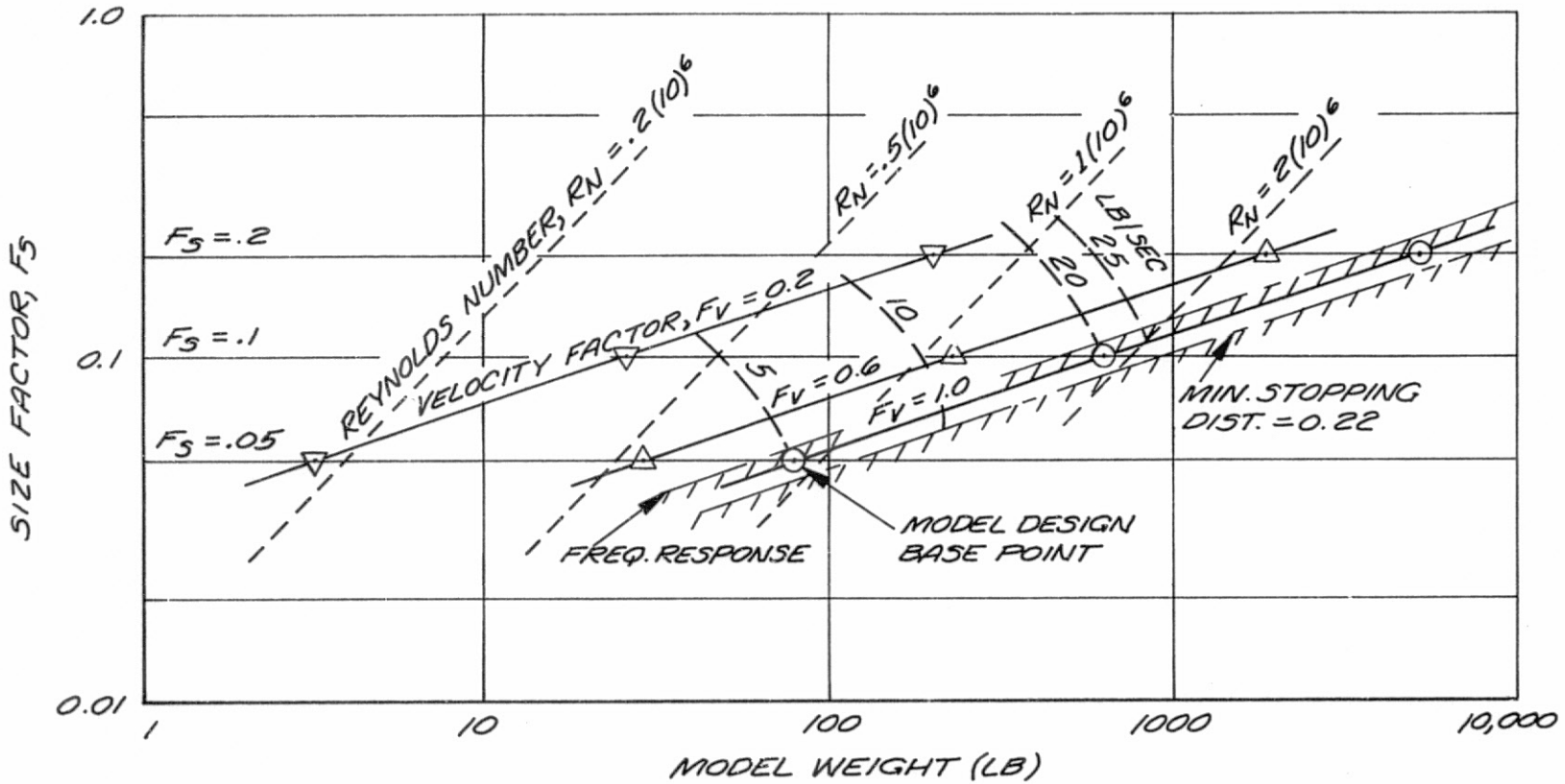

FIGURE 13. MODEL SCALE LIMITATIONS

The limiting weight criterion depends on the desired resolution of the aerodynamic forces and the maximum resolution capability of the balance. For the purpose of this discussion, the desired aerodynamic force resolution is specified as

$$\Delta L/L = 0.01 \quad (C_L = 5, \ \Delta C_L = 0.05)$$

The balance resolution is specified in terms of the fraction of the total balance force, F, required to resolve that aerodynamic force increment. Balance technology is available to reliably resolve one-half of one percent of the full scale load. This gives

$$\Delta L/F = 0.005$$

The sketch below depicts the descent stopping condition where the acceleration is directed upward. The forces consist of the lift, L, and the inertia force, F_n. The acceleration is defined in terms of load factor, so that

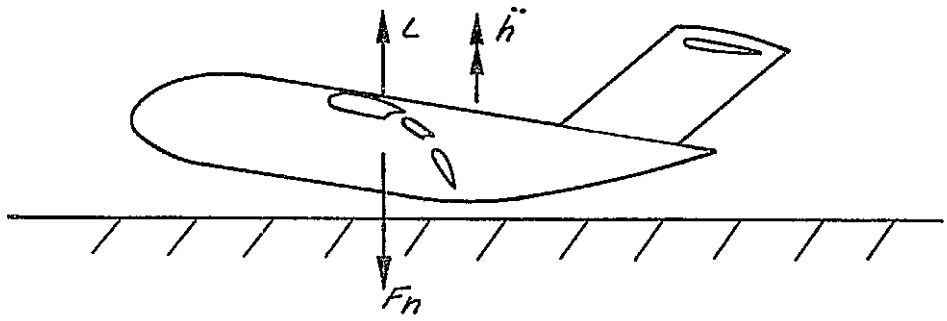

$$F_n = \frac{W}{g}\ddot{h} = Wn$$

The inertia force resulting from the acceleration is directed opposite to the lift so

$$F = F_n - L = Wn - L$$

and

$$\frac{\Delta L}{F} = \frac{(\Delta L/L)L}{Wn - L} = \frac{(\Delta L/L)}{(W/L)n-1}$$

$$\frac{W}{L} n = \frac{\Delta L/L}{\Delta L/F} + 1$$

substituting $\Delta L/L = 0.01$ and $\Delta L/F = 0.005$, gives

$$W = 3 \frac{L}{n}$$

This limiting weight, shown in figure 13, scales as

$$W \sim \frac{L}{n} \sim \frac{F_v^2 \; F_s^2}{F_v^2 \; F_s^{-1}} \sim F_v^0 \; F_s^3$$

and displays the same trend as the frequency response limit. It is independent of velocity factor and varies with size at the same rate as the model weight. Therefore the inertia load consideration does not act as a size limit but it does limit the maximum velocity.

The magnitude of the acceleration needed to impose a certain stopping distance is given by

$$n = \frac{\dot{h}^2}{2g \; \Delta h}$$

which shows that, for a stopping distance equal to a constant fraction of the model scale, the load varies with size such that a smaller model experiences greater acceleration than a larger model. Typical values for the example that the limit line of figure 13 was calculated for are summarized in table 6.

TABLE 6. INERTIA LOAD LIMITING PARAMETERS

$F_v = 1.0$, $\Delta h = 0.2c$, $\dot{h} = 4.6$ m/sec (15 ft/sec), $C_L = 5$				
F_s	L, kN (lb)	n	W, kN (lb)	L/W
0.05	3.9 (880)	20	0.58 (130)	6.7
0.1	16 (3500)	10	4.6 (1040)	3.4
0.2	62 (14000)	5.0	37 (8300)	1.7

In practice, other factors may come into play which limit the acceleration to values less than some of those shown above. In that case the effect on the force resolution capability of the balance will is less stringent, but greater distance is required to bring the model to rest.

5.3.3.3 Reynolds Number

Lines of constant Reynolds number are shown in figure 13. As discussed in section 3.3.2, the fact that a lower limit to this parameter exists is generally accepted, but the magnitude of it is somewhat controversial. A lower limit of between 0.2 $(10)^6$ and 0.5 $(10)^6$ is usually adhered to.

5.3.3.4 Engine Simulator Drive Air

The engine simulator drive air requirements are presented superimposed on figure 13 as well as in figure 14 for the range of F_V and F_S considered. The flow rates are calculated using the relationship given in Section 5.2.1 for a direct supply type engine simulator. For application to an ejector engine simulator the values given must be factored down by the ratio $\dot{m}_{DRIVE}/\dot{m}_{TOTAL}$ as shown in figure 10.

In some instances, the air supply system of a particular facility may impose an additional limit on a test situation. Reynolds number lines superimposed on figure 14 shown that if the flow is limited to a certain maximum, the maximum Reynolds number will occur at the maximum velocity factor.

5.4 Model Size/Tunnel Size Criteria

The importance of wind tunnel wall interference effects in establishing model size requirements is especially significant in the present case because of the motion required to simulate the flight trajectory. As the height of the model above the ground varies during a run, the position of the model with respect to all the other boundaries, and hence their interference effects, also changes. Thus, in addition to the magnitude of the interference, the change of interference for a range of model positions must also be considered.

5.4.1 Floor Clearance

The range of model position required to accommodate a ground effect experimental program depends on the maximum height needed to ensure the out-of-ground-effect condition. This height, in general, will depend on the

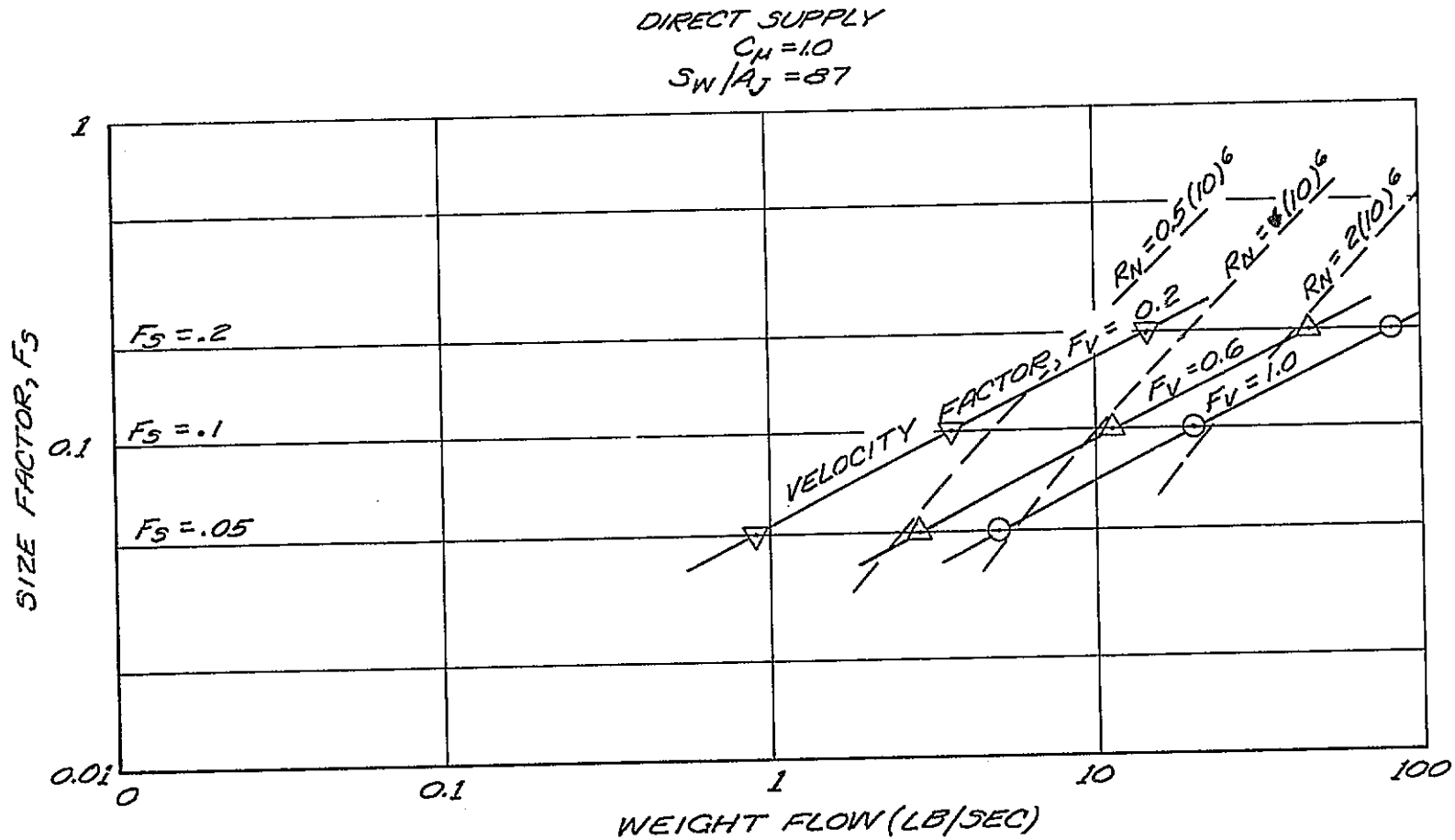

FIGURE 14. ENGINE SIMULATOR DRIVE AIR REQUIREMENTS

configuration, the lift, and power levels. Existing experimental data (reference 5, figure 30) indicate that for a STOL transport configuration similar to those considered here, the apparent outer limit to ground effects extends from about 0.6 to 0.8 wing spans above the ground. Furthermore, this behavior does not depend strongly on the thrust level up to a momentum coefficient of $C_\mu = 3.0$, which is greater than the maximum considered in this study. The data of this reference are thought to be reliable, especially since the experiment used a moving belt ground plane simulation.

Based on these data, as well as similar trends from analytical results, an outer limit to ground effects of one span height appears to be conservative and is selected for use in this study.

5.4.2 Ceiling Clearance

Accurate estimation of wind tunnel wall interference factors tends to be rather involved, especially for powered, high lift configurations. In principal, such factors can be estimated for a range of model positions in a wind tunnel, and applied continuously throughout a simulated trajectory. It is felt, however, that because of the possibly critical nature of the experiment in attempting to resolve small force increments due to transient effects, it is appropriate to keep to an insignificant level both the interference effects and the change in interference due to model position changes.

It was recognized early in the analytical ground effect studies that classical linear theory does not provide a sufficiently accurate description of the induced effects of the ground plane. Linear theory does not include a streamwise perturbation component which proves to be significant in ground effect. The nonlinear effects are discussed in Part I of this report and examples are presented to illustrate their magnitude for 2-D unpowered and jet flap configurations. The newly developed nonlinear analytical method is utilized in the present instance to assess the interference effects of the ceiling and to develop a ceiling clearance criterion to meet the needs of the transient ground effect experimental program. This approach recognizes the relative unimportance of the wind tunnel side walls in producing changes of

boundary interference with vertical position of the model. The resulting size criterion results in moderately small models for which the sidewalls become relatively insignificant.

The available analytical methods for 3-D configurations do not include power effects. The method of Heyson (reference 8), a quasi-non-linear theory which includes a jet wake deformation effect, is frequently used for wind tunnel boundary interference calculations for powered STOL configurations. This method has illustrated the importance of modeling the jet wake for those instances where its trajectory approaches the wind tunnel boundaries. However, for the question of ceiling clearance the jet wake becomes less significant. Since this method was not available for the present study, it was not employed in determining the model size criterion. The effect of a 2-D jet wake is considered relative to the 2-D unpowered condition to indicate possible power effect trends.

Initially, calculations were made using the Douglas Nonplanar Lifting Systems Program (NPLSP) and the Douglas 2-D Jet-Flap Potential Flow Program. Subsequently, additional calculations were made with the Douglas 3-D Lifting Neumann Program to help explain what appeared to be unusual ceiling clearance effects calculated by NPLSP. Figure 15 presents the lift change due to ceiling clearance. The NPSLP curve shows a lift increase close to the ceiling which quickly drops, becoming a small lift loss at heights above $h/c = 5.5$ and then asymptotically approaching the free air value. In an attempt to substantiate this behavior, three Neumann runs were made which showed a surprising difference from the NPSLP data with a much more gradual decay in the lift increase.

This apparent discrepancy was eventually determined to be due to the thickness of the wing used in the Neumann solution. The NPLSP program does not include thickness, but is correct within that constraint. These results illustrate the sensitivity of the ground effects results to details that are insignificant for out-of-ground-effect conditions.

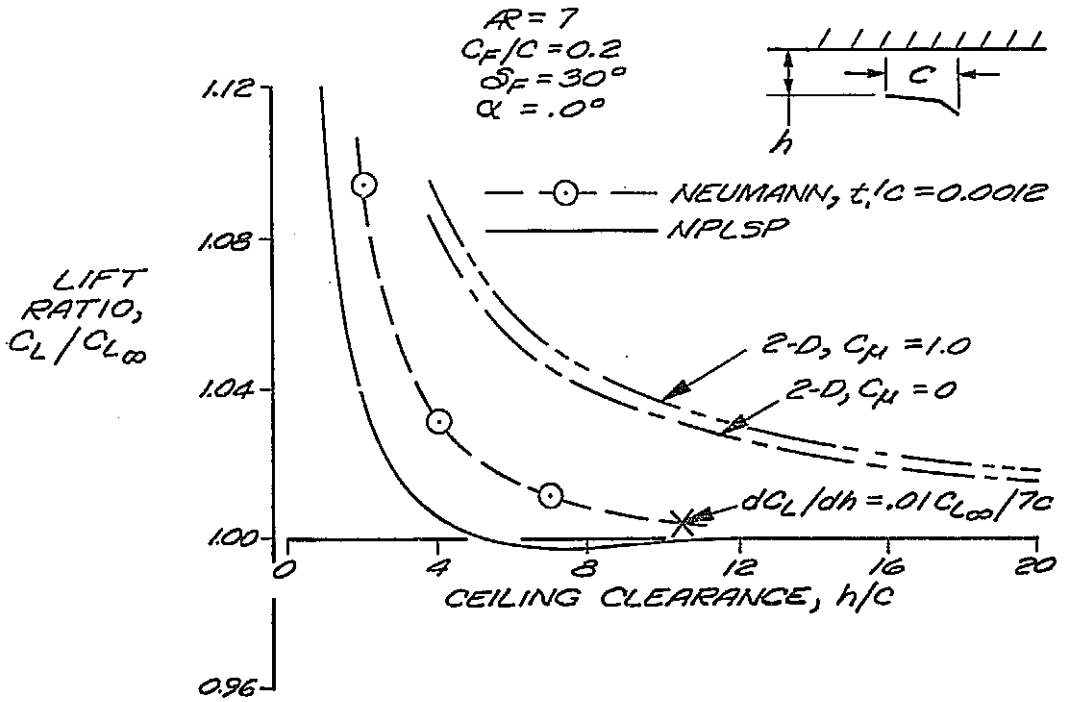

FIGURE 15. LIFT CHANGE DUE TO CEILING CLEARANCE

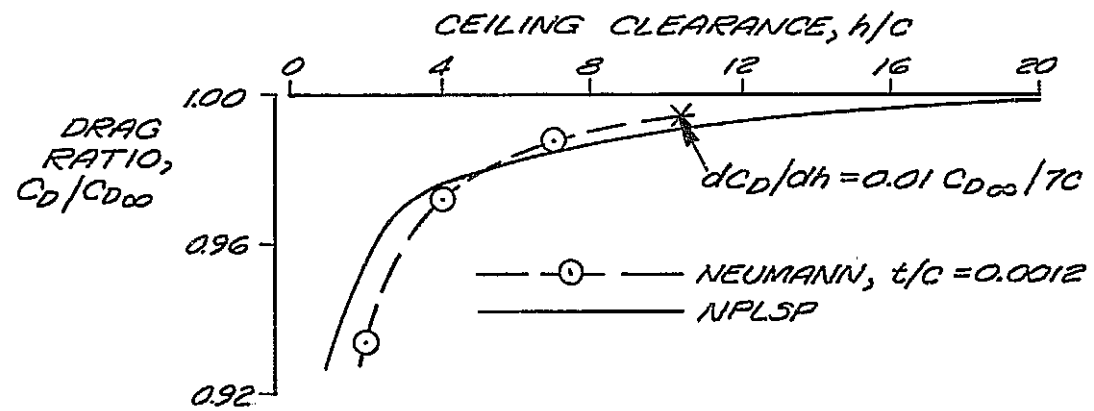

FIGURE 16. DRAG CHANGE DUE TO CEILING CLEARANCE

For the Neumann solution the level of lift interference drops to one percent at $h/c = 7$ or $h/b = 1.0$. The point where the rate of change of lift with height is one percent per span (7 chords) occurs at $h/c = 10.5$, or $h/b = 1.5$.

The curves showing the 2-D results, with and without jet blowing, illustrate that the effect of the jet-flap on ceiling interference is small and consistent, even though the lift levels are greatly different. These results provide further confidence in applying the unpowered 3-D results to the powered STOL model condition.

The effect of ceiling clearance on the drag coefficient is illustrated in figure 16. The NPLSP results are seen to be in much better agreement with the Neumann solutions. Evidently the ceiling clearance effects on drag are less affected by airfoil thickness. The magnitude of the effect on the drag is very similar to the effect on lift, but of opposite sign. The drag interference level drops to about one percent at $h/c = 7$ ($h/b = 1.0$) and the point where the rate of change of drag with height equals one percent per span occurs at $h/c = 10.5$ ($h/b = 1.5$).

Based on the foregoing analysis, two slightly different ceiling clearance criteria are established. For test conditions where the model motion is on the order of one span, as in techniques one and three, the minimum clearance is specified as 1.5 wing spans. For tests where the model motion is appreciably less than one span, as in techniques two, four, or five, the minimum clearance is reduced slightly to one wing span.

5.4.3 Blockage

The model size criteria developed in the previous two sections result in model sizes somewhat smaller than typical for powered STOL wind tunnel testing. That, plus the relatively wide wind tunnel test sections being considered act to reduce the magnitude of the wind tunnel blockage corrections to a level that, while not insignificant, is small and easily accounted for.

5.5 Ground Board Boundary Layer Control

The ground effect simulation error found in wind tunnels with fixed ground boards is a consequence of the viscous boundary layer development on the ground board. Experience has shown that this can be accommodated with no serious error when the model is relatively far from the ground or relatively lightly loaded. As the model approaches the ground closely or the lifting elements become more highly loaded, the ground boundary layer interferes significantly with the model flow field. This interference is caused by separation of the ground board boundary layer due to adverse pressure gradients induced by the model.

The most realistic means of simulating a free flight ground plane flow condition in a wind tunnel is with the use of a moving belt ground plane in conjunction with a boundary removal system upstream of the belt. This is the arrangement used in the NASA Langley V/STOL wind tunnel. Immediately upstream of the moving belt, a perforated floor plate is provided through which the floor boundary layer is removed into a large suction duct beneath the floor. After the boundary layer has been removed from the floor by the suction, the moving belt is used to maintain that condition for some distance underneath the model. In principle the moving belt can operate at speeds less than or greater than the wind tunnel test speed to simulate the effects of atmospheric wind induced ground boundary layers.

While the moving belt arrangement may represent an aerodynamic ideal for ground plane simulation, it also represents a complex mechanical system, especially for large wind tunnels or model installations involving floor mounted struts. These factors dictate the need for alternate experimental ground plane simulations means.

Since the ground effect simulation error of fixed ground boards is principally due to boundary layer separation, means of preventing such errors depend on conventional boundary layer separation control techniques. The magnitude of the adverse pressure gradients induced by powered STOL configurations on the ground plane boundary layer tends to be rather severe at typical power settings. Thus relatively powerful, active BLC systems are

required to prevent separation. Distributed suction or wall jet blowing techniques are most frequently considered for this application. Distributed suction has a potential advantage in requiring less power and providing less extraneous disturbance for a given degree of BLC, but wall jet blowing systems have important operational advantages in terms of ease of adjustment, small supply duct size, wide tolerance to a range of flow conditions, etc.

At least two thorough studies (references 9 and 10) have identified wall jet blowing BLC techniques as the preferred procedure for powered STOL ground effect wind tunnel testing. The first of these included a design study for the installation of a wall jet BLC system in the NASA 40- by 80-foot wind tunnel. This study examined procedures for carefully tailoring the blowing requirements to a specific model configuration and test condition to conserve blowing air and to minimize possible extraneous disturbances to the flow. Reference 10, on the other hand, took more of an empirical approach in developing a wind tunnel installation. As a result it demonstrates the ability of the technique to perform properly for a relatively wide range of conditions. Figure 17, reproduced from reference 10 shows the effect of wall jet momentum coefficient, $C_{\mu_{slot}}$, on the lift of a three-dimensional jet-flap wing for several flap momentum coefficients, $C_{\mu_{flap}}$, and two wall jet locations. Both wall jet locations exhibit the same behavior and shows the lift rising to a constant value as $C_{\mu_{slot}}$ is increased. The value of $C_{\mu_{slot}}$ at which the lift becomes constant increases as the $C_{\mu_{flap}}$ increases. For $C_{\mu_{flap}} = 1.0$, the wall jet requires about $C_{\mu_{slot}} = 1.0$, or about the same flow rate as the wing flap.

The asymptotic behavior of the model forces with $C_{\mu_{slot}}$ allows the wall jet to be overblown without serious effect except that excessive flow rate may be required. More sophisticated procedures for detecting the proper wall jet condition are possible by considering wall surface pressure distributions or total pressure profiles at selected locations.

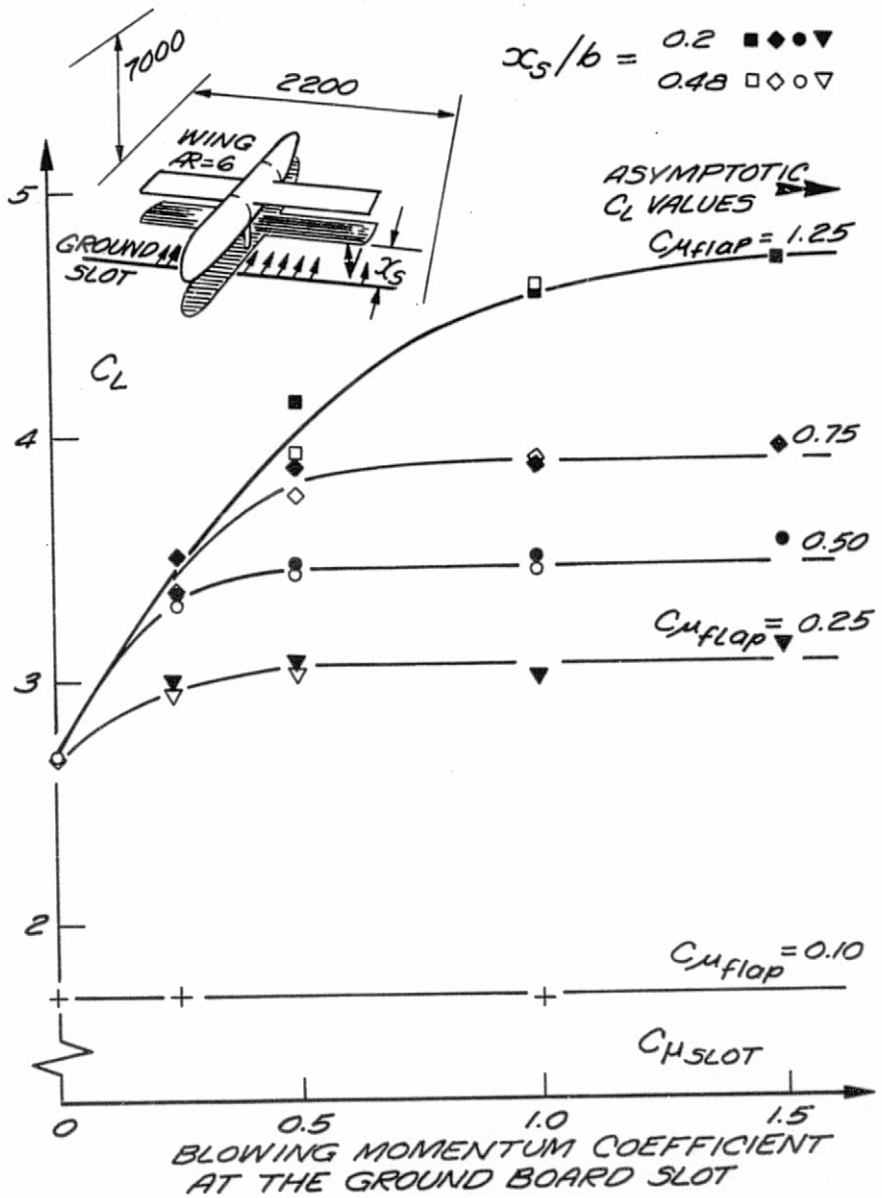

FIGURE 17. WALL JET BLC BLOWING REQUIREMENTS

6.0 FACILITIES

6.1 Technique Selection Considerations

The motion simulation techniques described in Section 5.1 involve two distinctly different types of experimental facilities; wind tunnels and test tracks. General considerations pertaining to these techniques are discussed below in terms of these two types of facilities. Based on these considerations five experimental system employing various facility/technique combinations are selected for detailed evaluation.

6.1.1 Wind Tunnel Techniques

The principal distinguishing feature of wind tunnel facilities is the high test velocities available. That, in conjunction with the potentially large model sizes for some of the wind tunnels, permits high Reynolds numbers to be achieved. The limited model motions required for these techniques allow the use of stationary equipment to power and control the model and acquire the data. In addition, the model mount and traversing equipment installation can generally be designed for maximum stiffness without regard to a specific weight limitation.

Of the two techniques utilizing wind tunnels, technique number three offers the more accurate simulation of the transient maneuver. However it imposes large inertia forces on the model. The largest inertia forces occur when the measurement of the aerodynamic forces are not required, such as during the starting and stopping of the motion. These forces do not have to be measured, but they do establish the maximum load capacity of the balance. The lesser inertial forces experienced during the simulated trajectory must be separately measured, such as with accelerometers, to resolve the aerodynamic forces. This tends to limit the accuracy of the aerodynamic measurements.

Technique number four maintains the model stationary, except for rotation in some instances. This eliminates the large translatory accelerations, and thus the need to size the balance for the higher loads and to separately measure the accelerations. For those situations where the model is rotated, there are still some inertia force components, but they are small.

The equipment to produce the translatory motion of the ground board is considerably more complex than the equivalent equipment for moving the model for all but the simplest type of experiment. The basic boundary condition requires that the translation speed, V_g, be coupled to the simulated flight path angle, γ, and velocity, V, by,

$$V_g = V \tan \gamma$$

This requires different motions from the various actuators and therefore different controllers. If, in addition, the ground plane curvature is to be controlled to simulate the flare, the actuator and control systems become even more complex. The forces on the translating ground board without the presence of the model are very small, consisting only of the skin friction forces and a small thickness drag. However, with the lifting model in place, the entire lift force of the model is felt as a reaction on the ground board. This aggravates the actuator system requirements.

Both of the wind tunnel techniques suffer from incorrect simulation of the viscous boundary layer on the ground plane. As discussed in Section 3.5 this simulation error can be tolerated at moderate ground heights or lift levels. For some of the anticipated operating conditions of a STOL model, however, it is almost certain that BLC will be required to prevent flow breakdown. The facility arrangement of technique number three can accommodate BLC installations much more easily than the translating ground board. Any of the available BLC procedures, moving belt, suction, of wall jet blowing, can be applied. The limitations imposed by the translating ground board would limit the choice of BLC to wall jet blowing. This may be a satisfactory method, in any event, but inclusion of this capability within the translating ground board will represent a significant complication.

The difficulties that technique number four is intended to alleviate are principally the inertia forces due to the forced accelerations. The impact these accelerations have on the feasibility of technique number three depend principally on the ratio of model lift to weight. With the high values of L/W possible for the present model designs the high accelerations required can be accommodated with current balance technology. In addition to

the influence of the inertia force in sizing the balance capacity, the requirement for a high natural frequency drives the balance design to very stiff load links. This also implies a high load capacity. Thus it may be that a balance sized for just the aerodynamic forces, with no inertia forces, would be too flexible to achieve the required frequency response.

All these considerations suggest that technique number three is the clear choice of the wind tunnel methods. Technique number four is considerably more complex with seemingly no overriding advantages. It may offer a slight advantage for the case of a simple simulation where neither acceleration nor rotation is to be modeled using an open jet wind tunnel. This would allow the ground board orientation angle to be fixed. However, it cannot offer the flexibility and accuracy of simulation of technique number three.

6.1.2 Track Techniques

Motion simulation techniques using track facilities require a moving carriage traveling through a stationary air mass. The moving carriage tends to be the limiting factor in all such facilities. The maximum speed is strongly limited by acceleration capability and the available track length. The acceleration capability is, in turn, limited by the drive power available which is dependent on the strength of the track itself since it limits the maximum weight of the carriage and hence the payload available for model and equipment. Because of these factors, existing track facilities have significantly less velocity capacity than wind tunnels and generally have strongly limited payload capabilities.

The principal effect of the limited speed capability of the track facilities is to limit the Reynolds number. As discussed in Section 3.3.2, low Reynolds number considerations tend to place a lower limit on the acceptable test speed which may be a deciding factor for track facilities.

The payload capacity is significant in two important respects. First, the high frequency response required to measure the transient event depends on a support structure that is very stiff and well damped. This implies a heavy structure. Secondly, these techniques require that the model, the

model support and actuation system, the engine simulator drive air supply, and the data acquisition equipment must be self-contained on the moving carriage. As a consequence track facilities are generally more limited in applicability to the transient ground effect problem than wind tunnels tend to be.

On the other hand, track facilities have the best potential for exact motion simulation of the landing and takeoff maneuvers. The air mass is stationary with respect to the ground so no incorrect boundary layer development can occur. The motion simulation of technique number one (or technique five) is a direct analog of the full scale flight situation and correctly performs the curved flight path.

The accuracy of the simulation when not producing the flight path perturbation motions, as in technique number two, is more limited, but acceptable under some conditions as discussed in section 5.1.3. This method appears to offer the potentially lowest cost approach of all the techniques.

6.2 Facility Selection

At the start of this study several facilities had been identified as being of potential use for the transient ground effect experiment. These facilities are:

- NASA Langley V/STOL Wind Tunnel
- NASA Langley 30- by 60-foot Wind Tunnel
- NASA Ames 40- by 80-foot Wind Tunnel
- Princeton Dynamic Model Track (PDMT)
- NASA Langley Vortex Research Facility (VRF)

In the course of this study, on-site inspections were made of all the NASA facilities. The PDMT had previously been examined as part of an earlier study, and telephone conversations with personnel at that facility were made to ascertain the current status and possible improvements to the facility. A summary of pertinent characteristics of the track facilities is presented in table 7, and for the wind tunnel facilities, in table 8. These characteristics are discussed below.

TABLE 7. TEST TRACK FACILITIES

FACILITY	Princeton Dynamic Model Track (PDMT)	NASA Langley Vortex Research Facility
SPEED	V = 12 m/sec (40 ft/sec) F_V = 0.22	V = 30 m/sec (100 ft/sec) F_V = 0.54
MODEL SIZE	b = 2.1 m (7.0 ft) F_S = 0.064	b = 1.8 m (5.8 ft) F_S = 0.053
REYNOLDS NUMBER	$R_N = 0.28\ (10)^6$	$R_N = 0.58\ (10)^6$
ENGINE SIMULATOR AIR SUPPLY	None	Nitrogen Blowdown
DATA ACQUISITION	Telemetry (21 Channels)	Analog Tape (14 Channels)
CARRIAGE PAYLOAD	136 Kg (300 lb)	454 kg (1000 lb)

TABLE 8. WIND TUNNEL FACILITIES

FACILITY	LANGLEY V/STOL	LANGLEY 30 x 60	AMES 40 x 80
SPEED	V = 104 m/sec (340 ft/sec) F_V = 1.8	V = 46 m/sec (150 ft/sec) F_V = 0.82	V = 91 m/sec (300 ft/sec) F_V = 1.6
MODEL SIZE	b = 1.8 m (5.8 ft) F_S = 0.053	b = 3.7 m (12 ft) F_S = 0.11	b = 3.7 m (12.1 ft) F_S = 0.11
REYNOLDS NUMBER (based on F_V = 1.0)	$R_N = 1.1\ (10)^6$	$R_N = 1.8\ (10)^6$	$R_N = 2.2\ (10)^6$
ENGINE SIMULATOR AIR SUPPLY	w = 67 N/sec (15 lb/sec) @ 14 MPa (2000 lb/in^2)	w = 80 N/sec (18 lb/sec)* @ 2.4 MPa (350 lb/in^2)	w = 172 N/sec (25 lb/sec)* @ 21 MPa (3000 lb/in^2)
DATA ACQUISITION	100 Analog Ch.	45 Analog Ch.	120 Analog Ch.
TEST SECTION	Open or Closed	Open	Closed
BROUND BOARD BLC	Suction + Moving Belt	None	Wall Jet Blowing*

*DENOTES FUTURE CAPABILITY

6.2.1 NASA Langley V/STOL Wind Tunnel

The NASA Langley V/STOL Wind Tunnel is a relatively new facility. The test section size is 4.4 m (14.5 ft) high, 6.6 m (21.75 ft) wide, and 15.2 m (50.0 ft) long. It is a continuous flow closed circuit facility with the propeller drive at atmospheric pressure. The test section operates below atmospheric pressure. The test section is designed so that the walls can be entirely removed and the ceiling raised 3.0 m (10 ft), for operation as an open jet wind tunnel over a fixed floor. The test section floor is comprised of two bays in which any of several carts can be installed. A floor boundary layer removal system is located immediately upstream of the first bay. This system operates by drawing off the floor boundary layer air through a perforated plate into a large suction manifold under the test section floor. For ground effect testing the suction system is used to remove the floor boundary layer, and a moving belt cart, installed in the first bay, is used to maintain the zero boundary layer thickness condition. The model is supported from a sting mount and positioning drive installed in a cart in the second bay.

The speed range available from the wind tunnel is 3-104 m/sec (10-340 ft/sec). This corresponds to a velocity factor range $0.05 \leq F_V \leq 1.8$. The boundary layer removal suction system is only capable of providing complete removal to a speed of 30 m/sec (100 ft/sec). In addition, the maximum speed of the moving belt is 30 m/sec. Operation at greater velocities with situations needing ground board BLC would require upgrading of the existing system or installation of an additional BLC system. The system of carts comprising the test section floor would conveniently accommodate a wall jet blowing BLC arrangement.

The model size criterion developed in Section 5.4 leads to a model span of b = 1.8 m (5.8 ft) or a size factor of $F_S = 0.0527$. At the velocity corresponding to $F_V = 1.0$, the Reynolds number is $R_N = 1.07\ (10)^6$, based on the wing MAC.

The auxiliary air supply can provide flow rates up to 67 N/sec (15 lb/sec). The supply pressure can be as high as 28 MPa (4000 lb/in^2), but more commonly is supplied at 12 MPa (1800 lb/in^2).

The data acquisition equipment includes a Sigma 3 system with one hundred analog channels. Additional equipment is available for real time readout, video monitoring, etc.

6.2.2 NASA Langley 30- by 60-foot Wind Tunnel

This wind tunnel (reference 11) has been in use for many years for studying the aerodynamics of complete airplanes and large scale models. More recently it has been used for free flight powered model testing. The facility is presently out of commission while it is being rehabilitated. It is scheduled to be back in operation early in 1976. The speed range will be continuously variable from zero to 46 m/sec (150 ft/sec) which corresponds to $0 \leq F_v \leq 0.81$. The test section size of 9.1 m (30 ft) by 18.3 m (60 ft) permits a model size of b = 3.7 m (12.0 ft). This allows a maximum Reynolds number of $R_N = 1.80\ (10)^6$. A new auxiliary air supply system will be installed capable of a supply rate of 80 N/sec (18 lb/sec) at a pressure of 2.4 MPa (350 lb/in^2). This low a pressure might present difficulties in ducting the engine simulator drive air into the model.

The test section is an open jet with an elliptic throat. An external balance chamber is located directly under the test section. A fixed ground board has been installed at the bottom edge of the jet. This remains in position for all testing to prevent interference of the flow with the top of the balance chamber, which would otherwise shed a large wake into the diffuser entrance. There are no BLC provisions for the ground plane, nor are there plans to provide any.

The balance chamber is largely filled with balance frames and equipment which would preclude installation of transient ground effect test apparatus. The area just upstream of the balance chamber is completely occupied by a newly constructed control room that contains all the data acquisition equipment, and so this area is also unavailable for such an installation. The only available space that could accommodate the apparatus is just downstream of the balance chamber near the trailing edge of the ground board. The flow quality is thought to be poor at this point.

This facility was judged to be unsuitable for the proposed experiments, principally because of the lack of a convenient location for the installation of the required apparatus.

6.2.3 NASA Ames 40- by 80-foot Wind Tunnel

The 40- by 80-foot wind tunnel is a continuous flow, closed circuit tunnel with a closed, solid wall test section. The test section cross-sectional shape is square with semi-circular ends making up a 24.4 m (80 ft) width with a 12.2 m (40 ft) height. The test section length is 24.4 m (80 ft). The center portion of the test section is occupied by the external balance turntable with a diameter 10.4 m (34 ft). The test section ceiling includes a folding door arrangement that provides access through an opening 23.0 m (78.5 ft) wide and 14.9 m (49 ft) long.

The speed range available from the tunnel is from zero to 91 m/sec (300 ft/sec), or $0 \leq F_V \leq 1.62$. Applying the model size criterion of Section 5.4 to the test model height of 12.2 m (40 ft) results in a model size of $b = 4.9$ m (16 ft), or $F_S = 0.145$. However, the drive air required for a model of that size, using direct supply engine simulators at a momentum coefficient of $C_\mu = 1.0$ and a velocity factor, $F_V = 1.0$, would exceed the available flow rate of the planned auxiliary air supply system. This system will provide air flow at up to 25 lb/sec at a pressure of about 21 MPa (3000 lb/in^2). Figure 14 shows that for the conditions mentioned above the maximum size model that can be powered with 172 N/sec (25 lb/sec) of air flow is a size factor of $F_S = 0.11$. This amounts to a model span of $b = 3.7$ m (12.1 ft).

The use of ejector engine simulators would permit a somewhat larger size model for the same C_μ, depending on the magnitude of the inlet flow ratio, ϕ. For the jet Mach numbers implied by $F_V = 1.0$, the magnitude of the inlet flow ratio is likely to be less than $\phi = 0.25$. This would allow a model size as large as $F_S = 0.127$, or $b = 4.3$ m (14 ft). It is just as likely, however, that the extra flow augmentation of ejector simulators, in this case, would be used to increase the test range of C_μ. The value of $C_\mu = 1.0$ cited refers to a nominal value from a particular flight trajectory.

Undoubtedly the test would encompass values larger than $C_\mu = 1.0$. In any event, direct supply engine simulators have been assumed for the purpose of consistency in this study. It is unlikely that a model size difference of less than two feet in span would have a significant effect on the experimental feasibility, except possibly for the model cost.

The Reynolds number capability in the facility implied by $F_V = 1.0$ and $F_S = 0.11$ is $R_N = 2.24\ (10)^6$.

The area under the balance turntable is occupied by the balance chamber. The large amount of equipment within the balance chamber precludes the installation of transient ground effect simulation apparatus in that location. The test section ceiling does not permit a practical installation because of the existence of the access doors, not to mention the extra height and resulting structural flexibility of the apparatus. Such an apparatus could be installed just upstream or downstream of the balance chamber with equal ease. The upstream location is thought to provide slightly better flow quality, but, more significantly, it would interface more conveniently with a planned tunnel floor BLC system (reference 9). The accessibility to this area for installation of the transient ground effect apparatus is very good. The reinforced concrete structure of the balance chamber could serve as an important part of the system installation.

The data acquisition system of the 40- by 80-foot wind tunnel has recently been extensively upgraded, as reported in reference 12. The new system has a high speed data acquisition system capable of providing signal conditioning and conversion to digital signals for 60 analog channels and a dynamic recording system for analog signal recording and playback of 56 channels. In addition, a dynamic analysis system can operate on-line to gather data from all or any two of 32 signal sources and perform any one of a number of time series analyses in real time. In particular, it can perform histograms, autocorrelation, cross-correlation, impulse response, characteristics functions, Fourier transforms, autospectrums, cross spectrums, and transfer functions. The system also includes a wide variety of readout

devices such as digital displays, cathode ray tubes, X-Y plotters, printers, etc. The tunnel has an extensive video monitor and recording system as well.

This facility is well suited for the proposed transient ground effect experiments. The test velocity and size parameters will allow high Reynolds numbers and have a potential for very good quality data. The data acquisition system is more than adequate. The planned wall jet blowing BLC system will be sufficient to control the adverse interference effects of the test section floor boundary layer and has sufficient adjustment range to accommodate the proposed model location for this problem. The proposed location for the model support and traversing apparatus is convenient for installation and the system could remain in place as a permanent installation without interferring with the other functions of the facility.

6.2.4 NASA Langley Vortex Research Facility

This facility is a high speed aerodynamic track converted from a previously existing ship towing tank (reference 13). The tank has been drained and a new overhead dual-rail and carriage system installed. The facility was developed principally for the study of aircraft vortex wakes. The overall length of the track is 549 m (1800 ft). Most of this length is required for starting and stopping the carriage. A 91 m (300 ft) long test section is situated approximately in the middle of the track length. The test section is fully enclosed with a width of 5.5 m (18 ft) and a height of 4.3 m (14 ft). The model support strut comes through a narrow slot in the test section ceiling and is sealed with baffle plates.

The carriage consists of a streamlined body enclosing a frame supported by four pneumatic wheels. The front part of the frame is converted from an Oldsmobile Toronado engine-transmission-front-wheel-drive assembly. Lateral restraint is provided by four pneumatic wheels bearing on the sides of the rails.

The velocity capability of the facility is limited to 30 m/sec (100 ft/sec), corresponding to $F_V = 0.54$. Applying the size criteria of

section 5.4 for a model with limited vertical motion (i.e. $\Delta h/b = 1.0$) and allowing additional floor clearance to accommodate necessary ground plane equipment results in a model size approximately the same as in the V/STOL wind tunnel. For the purpose of this study the model selected for the Vortex Research Facility has a span of b = 1.8 m (5.8 ft), or $F_S = 0.0527$. The resulting Reynolds number is $R_N = 0.58\ (10)^6$.

The maximum operating weight of the complete carriage system is 1.1 kN (5000 lb). The equipment onboard the carriage includes engine and speed controls, safety systems, high pressure nitrogen bottles and controls for engine simulators, and a 14 channel analog data acquisition system and FM tape recorder. As used for the vortex wake studies, the carriage system includes an arrangement of trailers extending behind the main model to support a trailing model used to study wake penetration. These trailers are not needed for the proposed transient ground effect experiment. The maximum weight of the carriage system is dictated by its starting and stopping acceleration capability, not the bearing weight of the main wheels. Therefore, the additional payload capacity of the carriage would be increased by the weight of the trailers, 860 pounds, which results in a total additional payload capacity to nearly 1000 pounds. This would be available to accommodate additional equipment needed to fulfill the simulation requirements of the experiment such as vertical traverse and pitch motion actuators, extra drive gas for the engine simulators, additional data acquisition and recording capacity, etc.

The present engine simulator drive gas supply consists of two high pressure nitrogen bottles containing about 4.5 N (20 lb) of gas each. The required flow rate for the velocity and size factors using direct supply engine simulators at a $C_\mu = 1.0$ is w = 0.58 N/sec (2.6 lb/sec). The duration of the data run will depend on the trajectory parameters being simulated but in any case will be less than two seconds. Allowing a fifty percent margin for starting, the total gas consumed will be less than 1.8 N (8 lb) or twenty percent of the total quantity on board. An analysis of the isentropic temperature drop due to such a quantity consumed indicates it is less than 50°F and thus not likely to cause any significant experimental problems.

The on-site inspection of the facility revealed that the carriage system is very stiff. Measurements of the vertical spring rate were determined by measuring the static deflections with two heavy persons on the carriage. The initial impression of the dynamic properties of the carriage was very favorable. Additional dynamic information was sought which would more completely describe the carriage response. Plans were made to acquire three types of dynamic response data. The first would involve mounting an array of accelerometers on the model strut base plate to record the natural motions during typical data runs. The second required exciting the carriage with a shaker at various orientations over a range of frequencies encompassing the natural frequencies of the system. The third type of measurement consisted of measuring the static deflections in the vertical direction for a range of loads of up to 225 N (1000 lb) applied to each of the four wheels.

The results of these studies suggest that the NASA Langley Vortex Research Facility is potentially very useful for transient ground effect studies. An especially attractive aspect of this facility is that with a relatively small investment an initial study of transient ground effects can be initiated using technique number two. If the initial results warrant it, the study can later be expanded to include complete motion simulation of technique number five.

6.2.5 Princeton Dynamic Model Track

The Princeton Dynamic Model Track (PDMT) was originally developed as a facility to study the motion of V/STOL aircraft models. In that capacity it uses dynamically scaled (mass and inertia) powered models. The apparatus is operated, using position and force sensors, to follow the motion of the model with as little restraint as possible. The desired test data consist of time histories of the model motion under certain constraints. This type of operation has been referred to as "dynamic" testing. Another mode of operation the facility is capable of is called "static" testing. In this case the model is driven through a particular motion and the forces and moments on the model are recorded. This is the type of operation required in the present instance.

The PDMT, which is briefly described in reference 6, consists of a 229 m (750 ft) long monorail track on which a servo-controlled power carriage rides. The track is enclosed in a test section building of 9.1- by 9.1-m (30- by 30-ft) cross-section. The maximum velocity of the carriage is 12.2 m/sec (40 ft/sec) which can be maintained over a central 91 m (300 ft) long segment of the track. This corresponds to a velocity factor of $F_V = 0.22$. The monorail track is about 4.6 m (15 ft) above the ground and the servo-driven vertical traverse mechanism is attached to the side of the carriage with a total motion capability of seven feet. The model is supported by a strut extending to the side of the carriage. The model size criterion of Section 5.4 cannot be applied in this instance because the model is not enclosed in a well defined test section. The 9.1 m square building includes the track and carriage. The maximum model span that can be accommodated by this facility is b = 2.4 m (8 ft). However, this size would result in minimal clearance from the track support structure. For initial study purposes a model span was selected that is equal to the vertical motion of the traverse mechanism, or b = 2.1 m (7 ft), $F_S = 0.064$. This results in a maximum Reynolds number $R_N = 0.28\ (10)^6$. As discussed in Section 3.3.2, the minimum acceptable value of Reynolds number cannot be determined with certainty for this experimental situation. However, a value this low is considered close to the minimum acceptable level.

The maximum weight of the carriage is approximately 450 N (2000 lb). With the vertical traverse mechanism, model pitch mechanism, and model with balance installed, the additional payload capacity of the carriage is about 67 m (300 lb). The existing data acquisition system consists of a telemetry unit on the carriage with up to 42 channels available. However, the existing system is insufficient to acquire all the transient data with sufficient bandwidth. The most convenient means of acquiring the data would be with a tape recorder system, however it would have to compete with the engine simulator drive gas tankage for the available payload. A lighter, but more costly, approach would be to replace the existing telemetry system with a modern one having greater capacity.

The carriage drive wheels are arranged in a tandem or bicycle configuration on the monorail track. The weight of the model and traversing

mechanism on its extended arm causes a rolling moment about the track which must be counterbalanced by the extra equipment onboard the carriage. As the forces on the model, such as aerodynamic lift and inertial reactions due to vertical acceleration, change during a test, an active control is used to change the moment arm of the counterbalance mass to keep the roll motions small. This rolling motion tendency is also restrained by a slider on the carriage bearing on a channel section slightly below the track.

The roll freedom that does exist has the effect of producing a relatively low vertical stiffness at the model. The entire system has a roll resonance frequency of two Hertz. The effective vertical stiffness of the model is about 443 N/m (50 lb/in) which is so low as to make it difficult to ascertain the model position with sufficient accuracy. The effect of this motion, as well as other flexibilities of the lightweight strut support, on the ability to discern the transient aerodynamic forces from the inertia forces cannot be determined with certainty without preliminary experimental trials.

Because of these dynamic properties of the carriage and model support system, as well as the payload and Reynolds number limitations, it is concluded that the PDMT is poorly suited for the proposed transient ground effect experiments.

6.3 Model Support Considerations

The design requirements for a model support system to accomplish the transient ground effect experimental tasks are dominated by two aspects of the problem. The first is the need for sufficiently high frequency response to resolve the transient forces. The second is the requirement to provide the motion needed to simulate the maneuver. This second factor influences the first requirement through the inertia forces caused by the accelerations of the motion.

One of the most evident initial findings in this study is that typical wind tunnel external platform balance systems are unsuited for this application. The massive frames of the load transfer linkages preclude the measurement of transient forces. The only feasible means of measuring the

transient forces is with a multiple component strain gauge balance internal to the model itself. Thus an internal strain gauge balance can be identified as an integral part of the support system.

The forces measured by such a system are derived from the relative displacement of the metric and non-metric sides of the balance. The model with its aerodynamic forces are integral with the metric side and the model support system, which transmits the various acceleration and excitation forces, is connected to the non-metric side. The relative displacement of the metric and non-metric components depends on their dynamic response to the various transient forces and motions. The ability to accurately measure the required forces requires that the dynamic response of the support system be well behaved, if not perfectly linear, to the desired resolution level up to the highest frequency of interest. This implies a system that is stiff, i.e., has a high spring rate, is of low mass, and is well damped. Therefore, it is generally required that the structural members be as short and direct as possible, to reduce deflections, and that they be light. Structural damping is more difficult to influence except by using bolted or riveted joints in preference to welded joints. Beyond that, active damping systems can be considered but may require extensive development.

The other aspect of the support system problem is the need to provide the trajectory motion. The principal motion is linear and at rates of up to 5.2 m/sec (17 ft/sec). In addition the accelerations are moderately high, possibly as great as 10 g's during starting and stopping. These combined requirements effectively preclude any other actuator system but hydraulic. Even so, the motion rates are so great as to approach the state-of-the-art in hydraulic actuators. The use of mechanical devices such as levers or gears to amplify the motion and permit lower actuator rates is not feasible because of the aforementioned stiffness requirements.

6.3.1 Blade Strut Support

The most satisfactory model support from a mechanical point of view is a centerline blade connected directly to both ends of the balance cage within the fuselage. This arrangement offers the greatest economy of structural

material with the best potential for high stiffness and low mass. Such an arrangement is relatively good from an aerodynamic point of view as well.

A strut emerging from the bottom of the model produces very little interference with the model flow field for conditions of lateral symmetry. The only significant direct effect on the model is a small wake running along the fuselage afterbody. There is possibly a greater effect due to the test section floor boundary layer, but means of controlling this are available if necessary, such as with additional wall jet BLC blowing near the strut. For aerodynamic flow fields involving lateral asymmetry such as steady sideslip, engine out, etc., more interference is likely, but can be alleviated by reducing the chord length of the blade and increasing the thickness at the expense of increased afterbody and floor boundary layer interference. A bottom strut arrangement is incompatible with a moving belt floor BLC system unless the belt is split to go around the strut.

A blade strut emerging from the top of the model is likely to have a greater aerodynamic interference with the wing flow field, for both lateral symmetry and lateral asymmetry. Also the wake will be running past the empennage. As with the bottom strut, the magnitude of this interference will depend on the thickness and chord of the strut, as well as means taken to alleviate the interference. In this case the floor will be completely clear for any BLC provisions desired.

Mechanical considerations pertaining to the choice of bottom or top strut location depend on the simulation technique. Wind tunnel installations using technique number three, for example, will have model positions ranging from one wing span length above the floor to zero height above the floor. The model sizing criterion of Section 5.4 calls for a minimum ceiling clearance of 1.5 wing spans, therefore the model-to-ceiling distance would vary from 1.5 to 2.5 wing spans while the model-to-floor distance would vary from one wing span to zero. In this case, a bottom strut is favored. For a track facility using technique number five, the required vertical motion of the model is greatly reduced. That, in addition to the problem of strut interference with the ground board, dictates a top strut installation.

The remaining mechanical considerations of the model support system pertain to the provisions for pitch rotation of the model. Proper trajectory simulation requires that the model rotate about the aircraft center of gravity. The most direct means of producing such rotation is with the pivot point at the desired center of rotation. In general, however, remote center drive schemes can also be used. The sketch below shows one possible remote center drive using a circular segment track riding on rollers. The utility of such

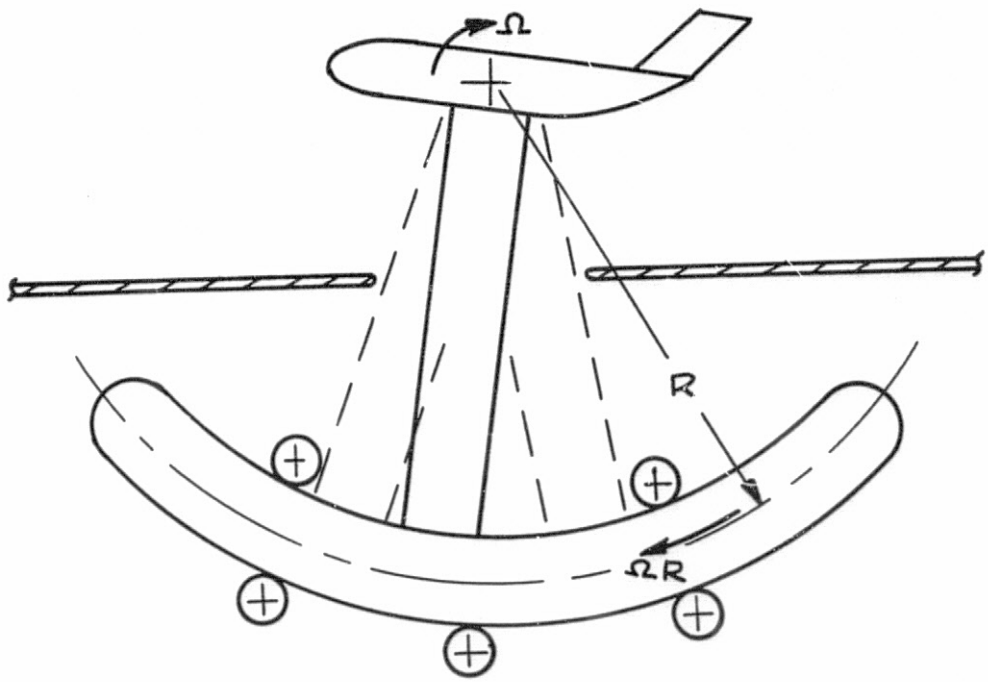

schemes is limited in the present instance by the fact that the motions required to produce a given rotation rate increase in proportion to the radial distance from the center of rotation. For the rates required by the simulation trajectories under study, these motions quickly become excessive.

6.3.2 Sting Support

A sting support system offers a possible alternative to the blade strut

support for those situations mentioned in the previous section where the blade strut may produce excessive interference, namely asymmetrical flow conditions such as steady side-slip, engine out, etc. This type of support system is considerably more difficult to design with the same stiffness and motion requirements as the blade strut.

Conventional sting support struts are too flexible for this application. The aerodynamic interference criteria of conventional stings have to be relaxed to allow a thicker and shorter sting. Therefore there is increased interference with the fuselage afterbody and empennage. The required pitch motion cannot be accomplished with a remote center drive because of the excessive motion rates of the mechanism, as discussed in the previous section. The pitch pivot location must be located near the fuselage afterbody cutout to allow a reasonably small sting base cavity. This is still rather far from the aircraft center-of-gravity so some vertical motion perturbation will be required to approximate center-of-gravity rotation. The aerodynamic interference of the sting with the empennage is greatest at high model pitch angles. The ability to relieve the interference by bending the sting tends to be limited by the need to approach the ground closely. This may limit the available pitch angle range or necessitate different sting elbows for different angle ranges.

6.4 Facility/Technique Selections

A review of the considerations cited in the previous sections leads to the conclusion that several of the potential facility/technique combinations are feasible from a technical point of view. Their relative technical feasibility will depend on consideration of additional factors such as desired accuracy of trajectory simulation, importance of high Reynolds number, etc. In addition to the technical feasibility, cost/benefit factors must be considered. These are examined in the following sections of this study. The experimental systems selected for further study are described below.

The facilities selected are:

- o NASA Langley V/STOL Wind Tunnel
- o NASA Ames 40- by 80-foot Wind Tunnel
- o NASA Langley Vortex Research Facility

The wind tunnel facilities are examined using motion simulation technique number three. The track facility is examined with two different motion simulation techniques; number five and number two (respectively, with and without vertical model motion). The principal model support system is the blade strut. For the wind tunnel installations it emerges from the bottom of the model and for the track it emerges from the top of the model. In addition, a sting support system is examined for the V/STOL wind tunnel installation.

Table 9 summarizes pertinent features of these selected experimental systems.

TABLE 9. STUDIED EXPERIMENTAL SYSTEMS

	EXPERIMENTAL SYSTEMS				
	A	B	C	D	E
Facility	NASA Langley V/STOL Wind Tunnel		NASA Ames 40x80 W.T.	NASA Langley Vortex Research Facility	
Technique	3	3	3	5	2
Support System	Blade	Sting	Blade	Blade	Blade
Velocity Factor, F_V	1.0	1.0	1.0	0.54	0.54
Velocity, V m/sec (ft/sec)	56(184)	56(184)	56(184)	30(100)	30(100)
Size Factor, F_V	0.0527	0.0527	0.11	0.0527	0.0527
Model Span, b, m (ft)	1.8(5.8)	1.8(5.8)	3.7(12.1)	1.8(5.8)	1.8(5,8)
Model MAC, $\bar{c}$, m (ft)	0.27(0.91)	0.27(0.91)	0.58(1.9)	0.27(0.91)	0.27(0.91)
Dynamic Pressure, q, kPa (lb/ft^2)	1.93(40.3)	1.93(40.3)	1.93(40.3)	0.57(11.9)	0.57(11.9)
Reynolds number, R_N	$1.07(10)^6$	$1.07(10)^6$	$2.24(10)^6$	$0.58(10)^6$	$0.58(10)^6$
Lift (C_L=5),L,kN,(lb)	4.33(973)	4.33(973)	18.9(4240)	1.28(288)	1.28(288)
Model Weight,W,kN(lb)	0.31(69)	0.31(69)	3.23(727)	0.18(40)	0.18(40)
Sink Rate,$\dot{h}$, m/sec (ft/sec)	5.2(17)	5.2(17)	5.2(17)	1.9(6.3)	0
Rotation Rate,$\dot{\theta}$, deg/sec	140	140	67	76	0
Stopping Distance, $\Delta h/b$ (6 "g" acceleration)	0.13	0.13	0.06	0.02	0
Required Frequency Response, f_R, Hz	114	114	56	61	61

7.0 TECHNICAL AND COST EVALUATION

The detailed evaluation of the selected experimental systems consists of determining the feasibility of accomplishing the experimental objectives and the cost of doing so. The experimental objectives consist of performing the simulated motion and resolving the resulting forces. The greatest technical risk concerns the resolution of the forces. This is most strongly affected by the dynamic response of the support system. The motion simulation, on the other hand, involves relatively little technical risk. It most strongly affects the costs of the experimental systems.

The technical evaluation is concerned principally with the dynamic response characteristics of the model support systems. An analysis of the characteristics is presented in the next section.

Following that is the cost evaluation. This requires a relatively detailed description of the equipment. The three major components of the transient ground effect apparatus are: model, support and actuator, and instrumentation. Design studies of these components were conducted in sufficient depth to permit reasonably accurate cost estimates to be made. The results of these design studies and cost estimates are presented following the dynamic response analysis.

7.1 Dynamic Response Analysis

A useful index of the dynamic characteristics of a system is the frequency response - the variation with frequency of the response amplitude when the input is a sinusoidal function having constant amplitude. Graphical representations of the frequency response are commonly given in the form of either vector plots (Nyquist Diagram) or as plots of the dynamic gain (Bode Diagram). The latter clearly shows regions of flat response and resonance, and has been used in this report.

In performing the analysis, only motion in the vertical direction has been considered and the various support components have been idealized as mass-spring-damper systems. In general, the model support and actuator

C. 2

systems have been treated with three-degrees of freedom. That is, three independent coordinates are involved in the definition of the system. The results may be obtained in several ways and require the simultaneous solution of three differential equations. An approach using Laplace transforms was selected as most convenient.

7.1.1 Formulation of the Problem

The basic mathematical model for the dynamic analysis is based on a three-component mass-spring-damper system as shown in the sketch. Each mass

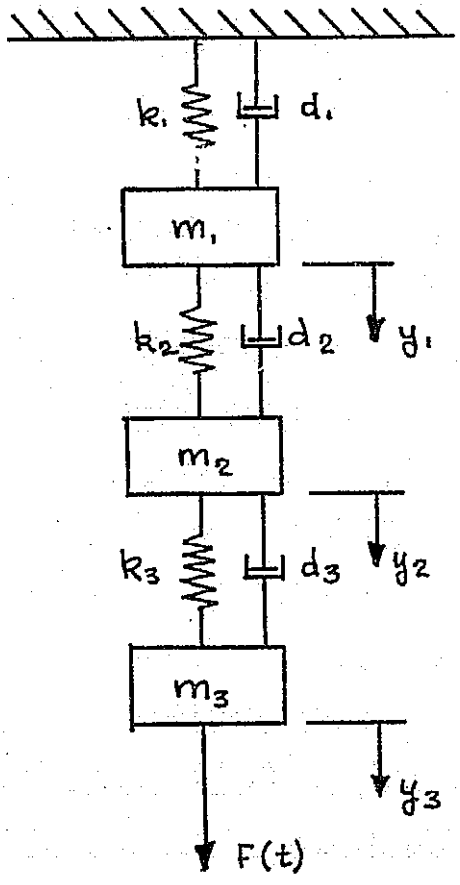

is free to move only in the vertical direction, y. Attached to each mass is a spring whose restitutive force is proportional to the displacement and a viscous damper whose force is proportional and opposed to the velocity. The input force function, F(t), is shown acting on element m_3.

The correspondence between this idealized model and the physical systems is as follows:

Blade-Strut Support System:

m_3	mass of the model and metric part of the balance
k_3	stiffness of the balance beams
d_3	damping of the balance beams
m_2	mass of the balance housing and vertical actuator rod
k_2	stiffness of the actuator rod and hydraulic fluid
d_2	damping of the actuator
m_1, k_1, d_1	correspond to the actuator cylinder and base and, owing to the relatively large stiffness of the member, is ignored in the analysis.

Sting Support System:

m_3	mass of the model and metric part of the balance
k_3	stiffness of the balance beams
d_3	damping of the balance beams
m_2	mass of the balance housing and part of the sting
k_2	stiffness of the pitch actuator and sting
d_2	damping of the pitch actuator and sting
m_1	mass of the vertical actuator rod and sting
k_1	stiffness of the actuator rod and hydraulic fluid
d_1	damping of the vertical actuator

Vortex Research Facility

m_3	mass of the model and metric part of the balance
k_3	stiffness of the balance beams
d_3	damping of the balance beams
m_2	mass of the balance housing and vertical actuator rod
k_2	stiffness of the actuator rod and hydraulic fluid
d_2	damping of the vertical actuator
m_1	mass of the vertical actuator and carriage
k_1	stiffness of the carriage tires
d_1	damping of the carriage tires

Note: For experimental system E, there is no vertical motion and the second component is not included in the analysis.

Component number three always represents the model. The difference $(y_3 - y_2)$ is proportional to the output of the balance and is the principal quantity of interest. The forcing function corresponds to the aerodynamic loads in the test situation and to the sinusoidal function in the frequency analysis.

The differential equations of motion for the system are

$$m_1\ddot{y}_1 + (d_1 + d_2)\dot{y}_1 - d_2\dot{y}_2 + (k_1 + k_2)y_1 - k_2y_2 = 0$$

$$m_2\ddot{y}_2 - d_2\dot{y}_1 + (d_2 + d_3)\dot{y}_2 - d_3\dot{y}_3 - k_2y_1 + (k_2 + k_3)y_2 - k_3y_3 = 0$$

$$m_3\ddot{y}_3 + d_3\dot{y}_3 + d_3\dot{y}_3 = k_3y_3 + k_3y_3 = F(t)$$

This is a set of linear second-order differential equations with constant coefficients. The resulting motion of the system consists of two parts. The first represents a free motion in the natural rhythm of the system and dies out in time on account of the damping terms. This part is referred to as the transient. The second part represents motion in rhythm with the exciting force, F(t), and provides the response characteristics of the system. The response is described by the magnification or gain of the motion and the phase difference between the output and the input. The total gain is expressed as the product of two terms, the static gain and the dynamic gain. The static gain is simply the displacement resulting from the application of a constant force of unit magnitude and can usually be determined by inspection. The dynamic gain is a function of the frequency of the forcing function and represents the dynamic characteristics of the system. The procedure used to obtain these quantities is briefly described in the following paragraph.

Owing to the presence of the forcing function, the equations are non-homogeneous and it is convenient to use Laplace transforms to obtain a

solution. The transfer function is defined as the ratio of the Laplace transforms of the output and the input:

$$T(S) = \frac{\bar{y}_{output}}{\bar{y}_{input}}$$

The total gain of the system is the ratio of the output to the input and is defined

$$\frac{y_{output}}{y_{input}} = T(i\omega) = \delta \cdot \Delta e^{-i\phi}$$

where δ is the static gain given by

$$\delta = \lim_{S \to 0} T(S),$$

Δ is the dynamic gain, and ϕ is the phase angle by which the output lags the input.

For the three component system being considered, the Laplace transform of the equations of motion may be written

$$\bar{y}_1 = T_1 \bar{y}_2$$

$$\bar{y}_2 = T_2 \bar{y}_3$$

$$\bar{y}_3 = F(S)\, T_3$$

The output of the balance is

$$(\bar{y}_3 - \bar{y}_2) = F(S)\,(T_3 - T_3 T_2) = F(S)\, T_{32}$$

The dynamic gain for the five experimental systems is presented in the following sections. The results have been obtained using a generalized control systems computer program and are given in the form of the gain in decibels versus the exciting frequency in hertz.

These results are for the idealized models of the actual support systems. The analysis treats the components as stationary when in fact they are moving. A more exact analysis may require consideration of an additional forcing function representing this applied motion. Nevertheless, the present analysis contains the essential features of the system and the results are considered to be indicative of the response that can be expected. Additionally, the values of the parameters m, k, and d used in obtaining the dynamic gain are important factors. Values for the mass and spring constants are estimated reasonably well based on the designs presented for the systems. However, magnitude of the damping factor is difficult to estimate. The values used in the analysis are based on typical values for similar mechanical systems. Values of damping ratio (damping coefficient/ critical damping coefficient) of 0.05 are used for the main structural elements and 0.02 for the balance strain gage beams. There is a possibility of improving the response characteristics by altering the damping factors with tuned damping systems. Estimation of the possible gains in system performance, however, is beyond the scope of this study.

7.1.2 Blade Strut Support Frequency Response

The dynamic response characteristics of the blade strut support, and actuator systems installed in the V/STOL Wind Tunnel and the 40- by 80-foot Wind Tunnel are very similar except for a displacement in frequency to account for their different sizes. The parameters used in the analysis are summarized in table 10. The results are shown in figure 18. The required frequency for the two systems is 114 hertz and 56 hertz, respectively.

The response curve for the V/STOL Wind Tunnel system displays a strong resonance at about 300 hertz which corresponds to the natural frequency of the balance. At 114 hertz the dynamic gain is just starting to deviate upward from the zero level. Below this frequency the dynamic gain remains flat at zero except for a deviation occurring between 13 hertz and 26 hertz. The response shows a small amplification and attenuation which is due to resonance of the hydraulic actuator.

TABLE 10. DYNAMIC SYSTEM COMPONENT PARAMETERS

Component	Mass, m	Spring Rate, k	Damping Coef., d	Damping Ratio
	kilogram $\left(\frac{\text{lb-sec}^2}{\text{in}}\right)$	$\frac{\text{newton}}{\text{metre}}$ $\left(\frac{\text{lb}}{\text{in}}\right)$	$\frac{\text{newton-sec}}{\text{metre}}$ $\left(\frac{\text{lb-sec}}{\text{in}}\right)$	
V/STOL Wind Tunnel - Blade Strut Support				
1	--	--	--	--
2	499 (2.85)	$7.0\text{x}10^6$ ($4.0\text{x}10^4$)	$5.95\text{x}10^3$ (34)	0.05
3	36 (0.207)	$1.1\text{x}10^8$ ($6.2\text{x}10^5$)	$2.45\text{x}10^3$ (14)	0.02
40- by 80-foot Wind Tunnel - Blade Strut Support				
1	--	--	--	--
2	3630 (20.7)	$1.75\text{x}10^6$ ($1.0\text{x}10^5$)	$2.52\text{x}10^4$ (144)	0.05
3	331 (1.89)	$2.28\text{x}10^8$ ($1.3\text{x}10^6$)	$1.10\text{x}10^4$ (63)	0.02
V/STOL Wind Tunnel - Sting Support				
1	1270 (7.25)	$1.96\text{x}10^7$ ($1.12\text{x}10^5$)	$1.58\text{x}10^5$ (90)	0.05
2	91 (0.518)	$2.84\text{x}10^5$ (1620)	$5.08\text{x}10^2$ (2.9)	0.05
3	36 (0.207)	$1.09\text{x}10^8$ ($6.2\text{x}10^5$)	$2.45\text{x}10^3$ (14)	0.02
Vortex Research Facility - Blade Strut Support				
1	1410 (8.03)	$7.29\text{x}10^5$ (4170)	3210 (18.3)	0.05
2	106 (0.604)	$7.30\text{x}10^6$ ($4.17\text{x}10^4$)	1840 (10.5)	0.033
3	13.6 (0.078)	$1.21\text{x}10^7$ ($6.9\text{x}10^4$)	508 (2.9)	0.02

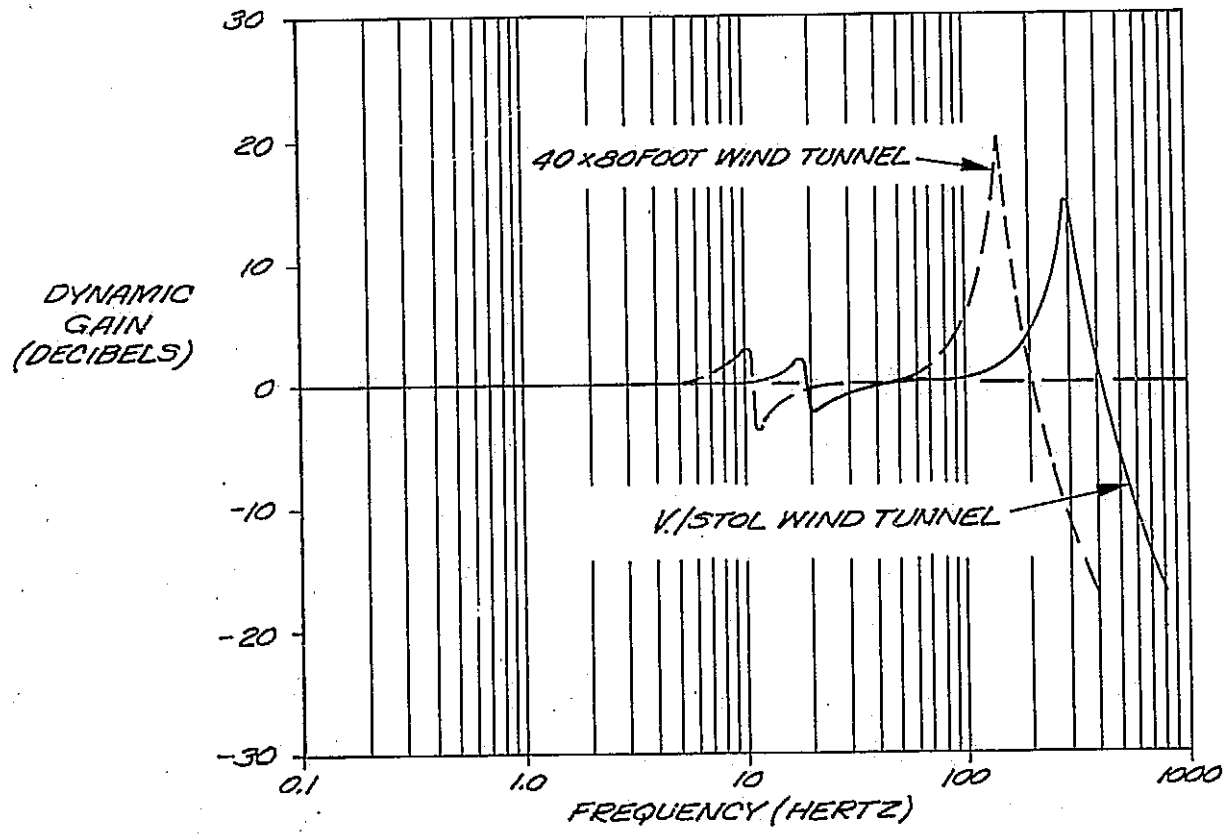

FIGURE 18. BLADE STRUT SUPPORT FREQUENCY RESPONSE

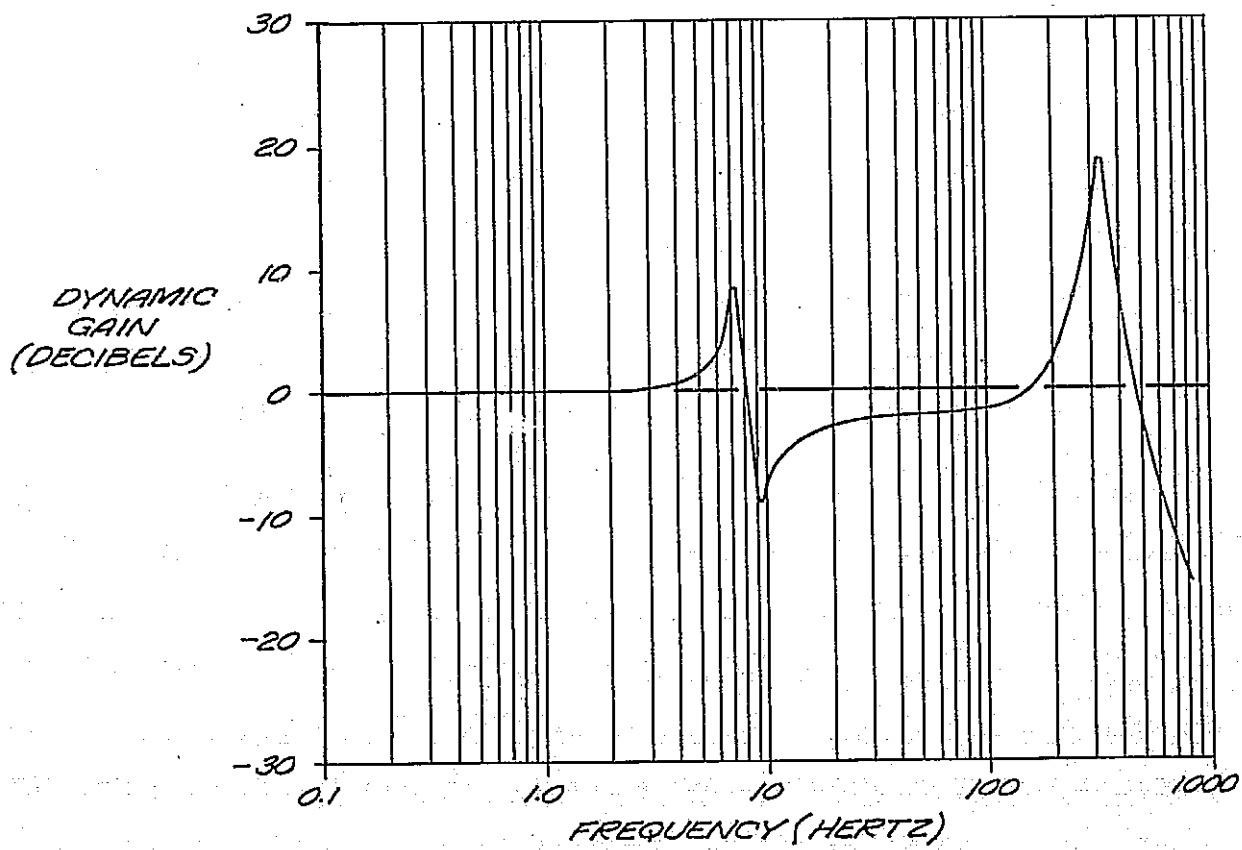

FIGURE 19. STING SUPPORT FREQUENCY RESPONSE

This behavior is not considered to represent a significant problem for signals with spectral content above or below this frequency. For frequencies near this point, the real physical system may exhibit increased damping which will limit the deviation. Since the deviation is nearly symmetrical, it tends to be self-canceling for an input signal having a nearly constant spectral content across that frequency range.

The results for the 40- by 80-foot Wind Tunnel show very similar trends but the balance resonance occurs at 140 hertz, still well above the required frequency of 56 hertz, and the hydraulic actuator resonance occurs between 8 hertz and 16 hertz.

The behavior of these blade strut support and actuator systems appear to be satisfactory for the transient ground effect experiment. The small deviation that does occur at frequencies within the range of interest can probably be tolerated without serious error. It may be possible to apply tuned damper systems at a discrete frequency to reduce the deviation somewhat.

7.1.3 Sting Support Frequency Response

The values of the parameters used in the analysis of the sting support and actuator system are also presented in table 10. The frequency response results are shown in figure 19. A similar resonance at the balance natural frequency of 300 hertz is seen, as in the blade strut case, but the resonance associated with the hydraulic actuator produces a much greater deviation from the flat response level. The frequency range for the deviation extends from 3 hertz to 16 hertz and reaches levels of $\pm$ 10 decibels. Also, the response curve above 16 hertz shows a nearly constant attenuation up to the highest frequency of interest.

The effect of this dynamic behavior on the transient ground effect experiment is difficult to establish at this point. The higher frequency attenuation can probably be accounted for in the data processing, but the impact of the hydraulic actuator resonance on the experiment will probably require a more thorough analysis to ascertain.

7.1.4 Vortex Research Facility Frequency Response

Of all the proposed experimental facilities, the Vortex Research Facility is closest to the condition required for the transient ground effect experiments. It therefore has the potential for direct measurement of some of the dynamic system parameters. This was recognized during the on-site inspection of the facility and plans were made for such measurements.

Three types of measurements were discussed with the facility staff. The first involved mounting an array of accelerometers on the model strut base plate to record the natural motions during typical data runs. The second involved exciting the carriage with a shaker at various orientations over a range of frequencies encompassing the natural frequencies of the system. The third type of measurement would be to record the static deflections in the vertical direction for a range of loads applied to each of the four wheels of the carriage up to a maximum load of 225 N (1000 lb). This information is sufficient to accurately define the natural frequency, stiffness, and damping characteristics of the carriage. While at the facility a single point measure of the stiffness was made by loading the carriage with two persons. This value is incorporated in the analysis.

The results of the analysis are presented in figure 20 for both experimental systems, a vertically stationary model, and an installation including a vertical hydraulic actuator. The required maximum frequency response is 61 hertz as scaled by the factor shown in Table 4. The curves for both systems display a balance natural frequency of 160 hertz. The stationary installation curve shows an almost flat response out to about 50 hertz where the gain starts to deviate upward slightly. A very slight deviation is apparent at the carriage resonance point at about 4 hertz but it is of such a small level to be insignificant.

The response for the moving model installation is dramatically different. Three resonance conditions are evident that correspond to the natural frequencies of the three components. The lowest resonance, occuring at the carriage natural frequency, has a relatively large deviation, about

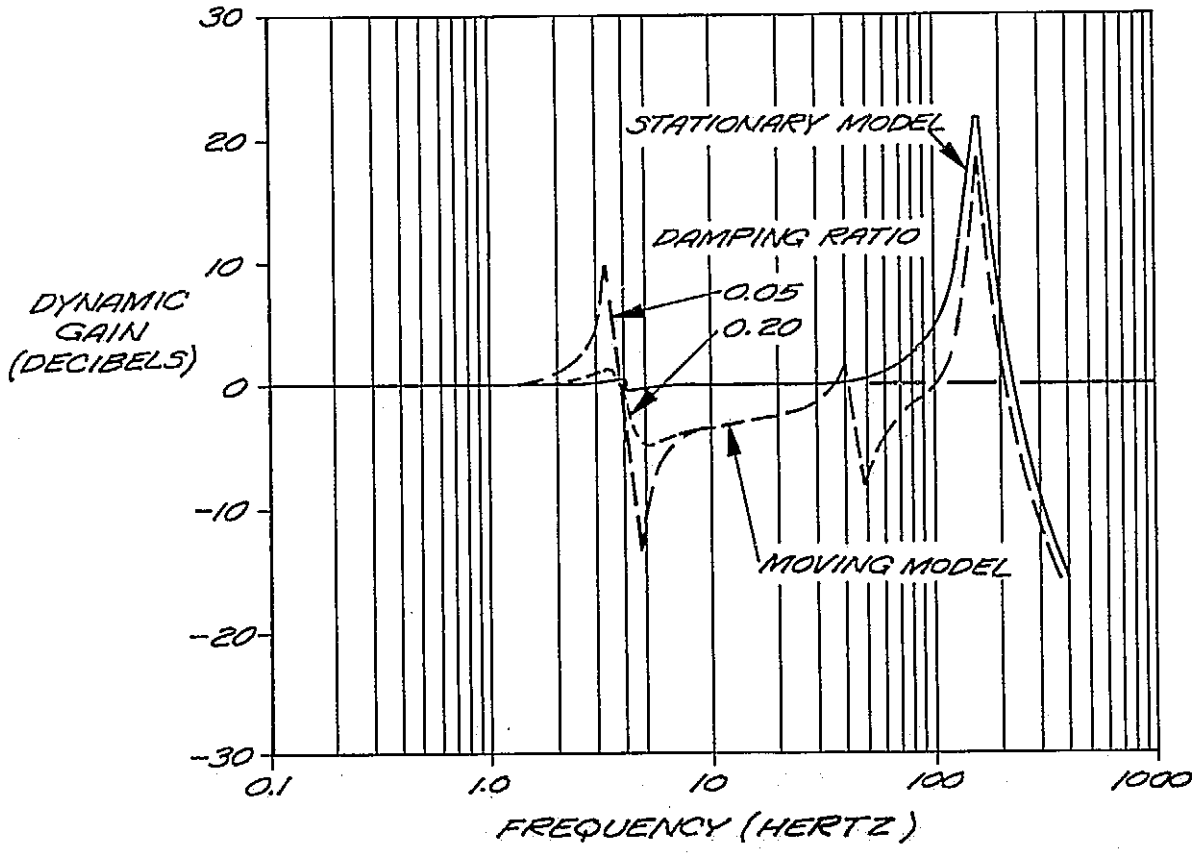

FIGURE 20. VORTEX RESEARCH FACILITY FREQUENCY RESPONSE

± ten decibels, over the frequency range from three hertz to six hertz. The hydraulic actuator resonance occurs at about 40 hertz which is close enough to the upper frequency limit that its effect can be considered minimal. Between these two conditions the response displays an attenuation of several decibels.

The Vortex Research Facility carriage is an unusual dynamic system in that it is supported by rubber pneumatic wheels. The damping properties may not be well represented by the damping ratio of 0.05. Therefore another curve is shown with the damping ratio increased to 0.20. This result shows a strong improvement in the deviation of the dynamic gain at the carriage natural frequency.

The implications of this analysis for the success of the proposed transient ground effect experiment are clear for the stationary model installation. There should be no dynamic problems with the model support system. The other installation may present a greater problem. Since the equipment is largely existing, however, direct measurements of the dynamic properties can be made to permit a careful dynamic analysis. In addition, the relatively low masses of the dynamic components make them especially susceptible to successful applications of active, or tuned, damping systems.

7.2 Model Design Study

7.2.1 Basepoint Model

The design study for the model centered on a basepoint design for the V/STOL wind tunnel. The model perturbations required to satisfy the other test conditions are small enough that the same basic design can be used with appropriate allowances for the effects of increased size or decreased aerodynamic loads. The characteristics of the various other models were derived from the general scaling laws summarized in table 4.

The aerodynamic philosophy of this model design is influenced strongly by the need for low model mass and emphasizes the simulation of only those conditions that are of significance to the possible transient ground effects. This is felt principally as configuration simplifications. As discussed in Section 3.3.1, the effects of engine inlet flow are judged to be relatively insignificant, allowing the use of direct supply engine simulators. Configuration details such as wing spanwise twist and thickness distributions, which pertain to the cruise performance, are not modeled, allowing the wing box to be fabricated with straight development lines from root to tip. Configuration flexibility is sacrificed somewhat. The flap and slat positions are fixed at either a single takeoff or a single landing position.

The model fuselage (figures 21 and 22) structure is built around two strong bulkheads that attach to the two ends of the metric balance core. Plates are bolted between the bulkheads to form a strong box to which the wing is attached. The wing loads are thus transmitted to the balance with as direct a load path as possible. Stringers run fore-and-aft to additional lightweight bulkheads. The fuselage external surface is formed from fiberglass shells which fit over and attach to these bulkheads and stringers. Removable panels are provided in the center region for access to the balance and drive air cross-over. The main landing gear fairings are formed of rigid foam with a thin fiberglass skin, and are bonded to the fuselage skin. The wheels are attached with simple spring-loaded telescoping struts to permit accidental ground contact without damage.

The upper end of the blade strut terminates in the pitch pivot trunnions on the non-metric balance case. These incorporate rotaty glands to transmit

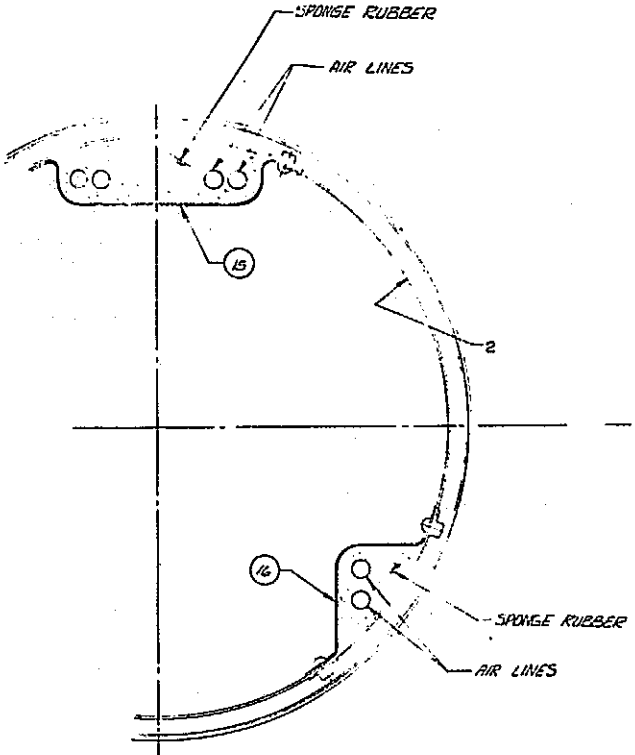

A-A

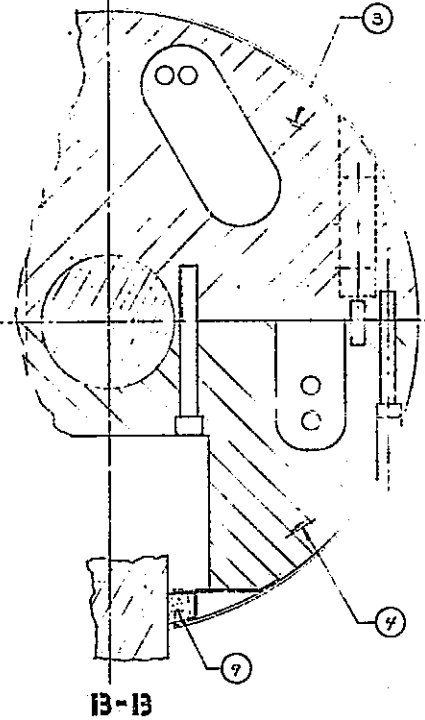

B-B

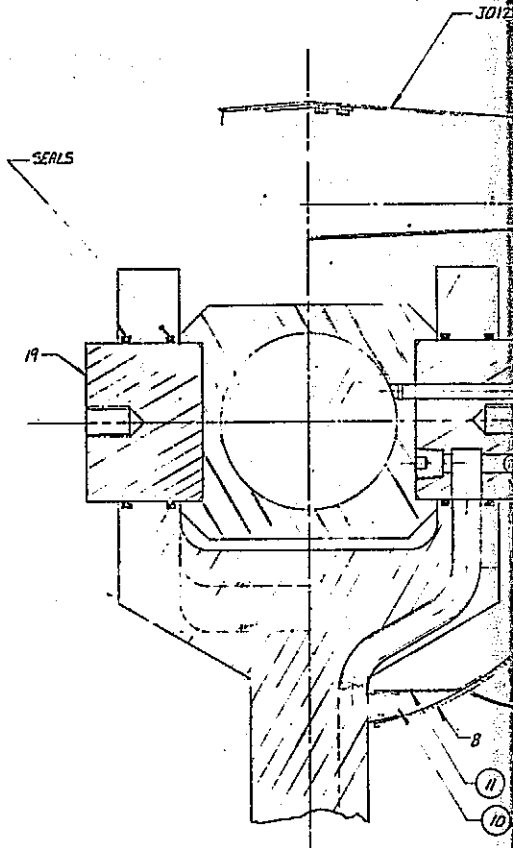

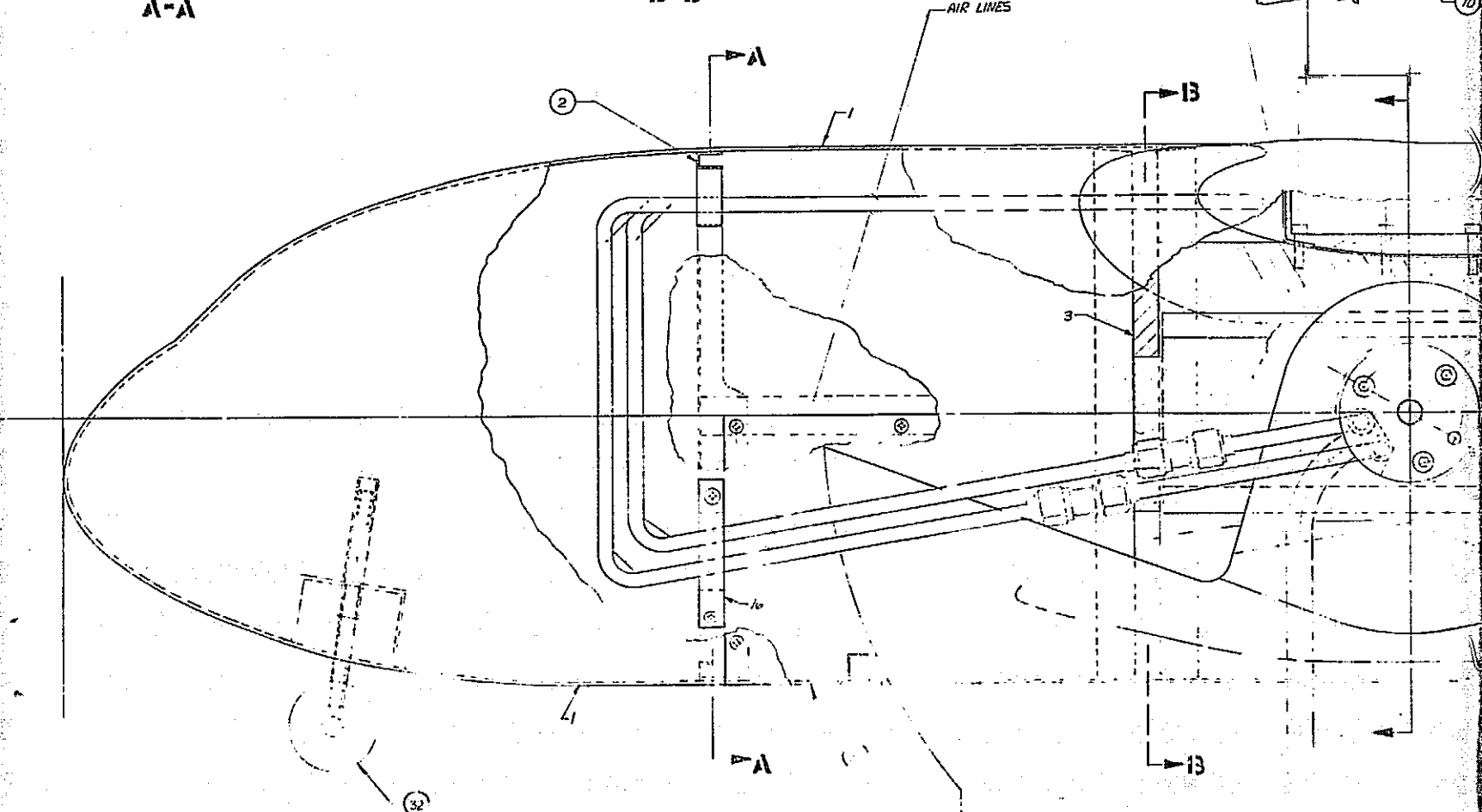

FOLDOUT FRAME

ORIGINAL PAGE IS
OF POOR QUALITY

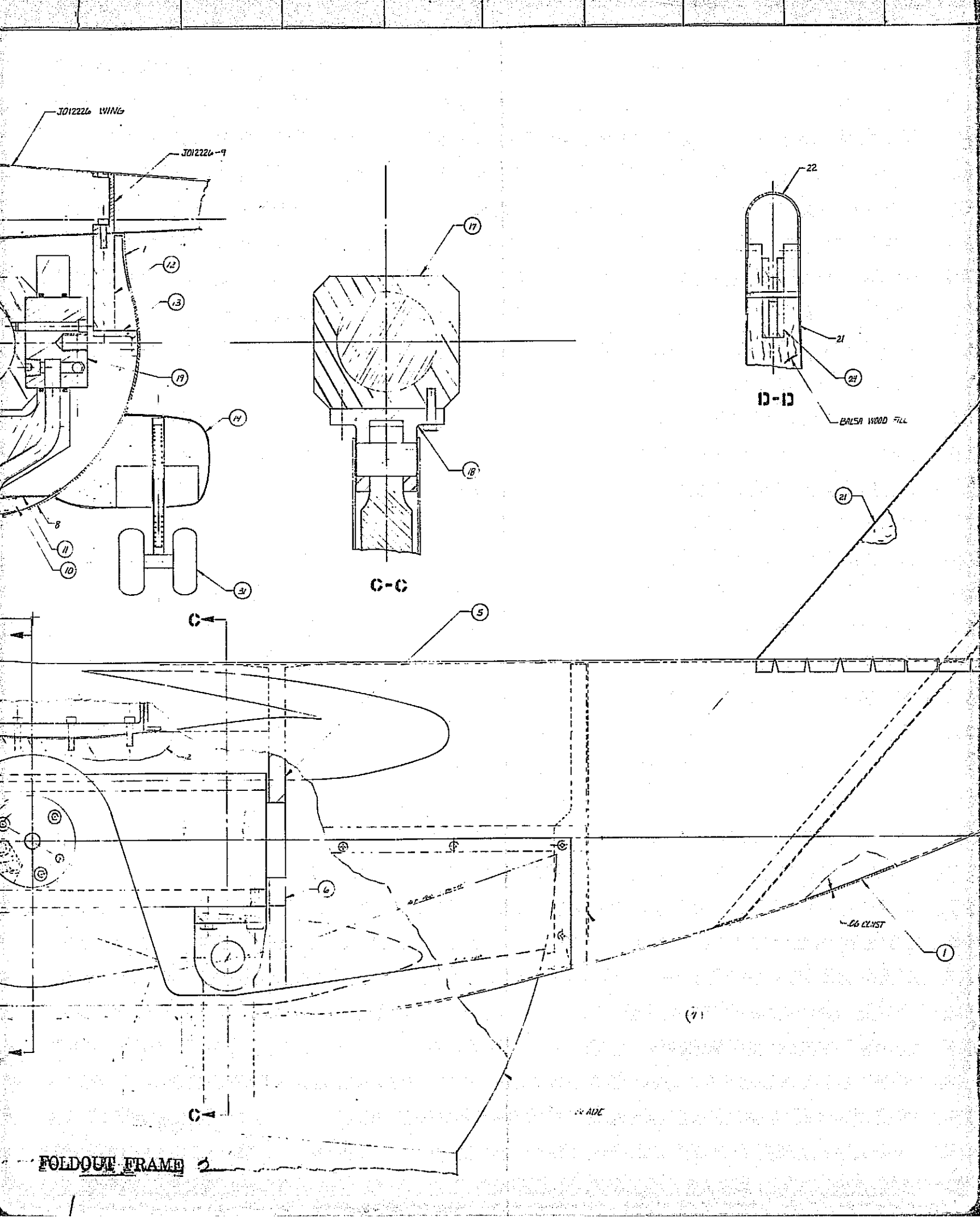

FOLDOUT FRAME 2

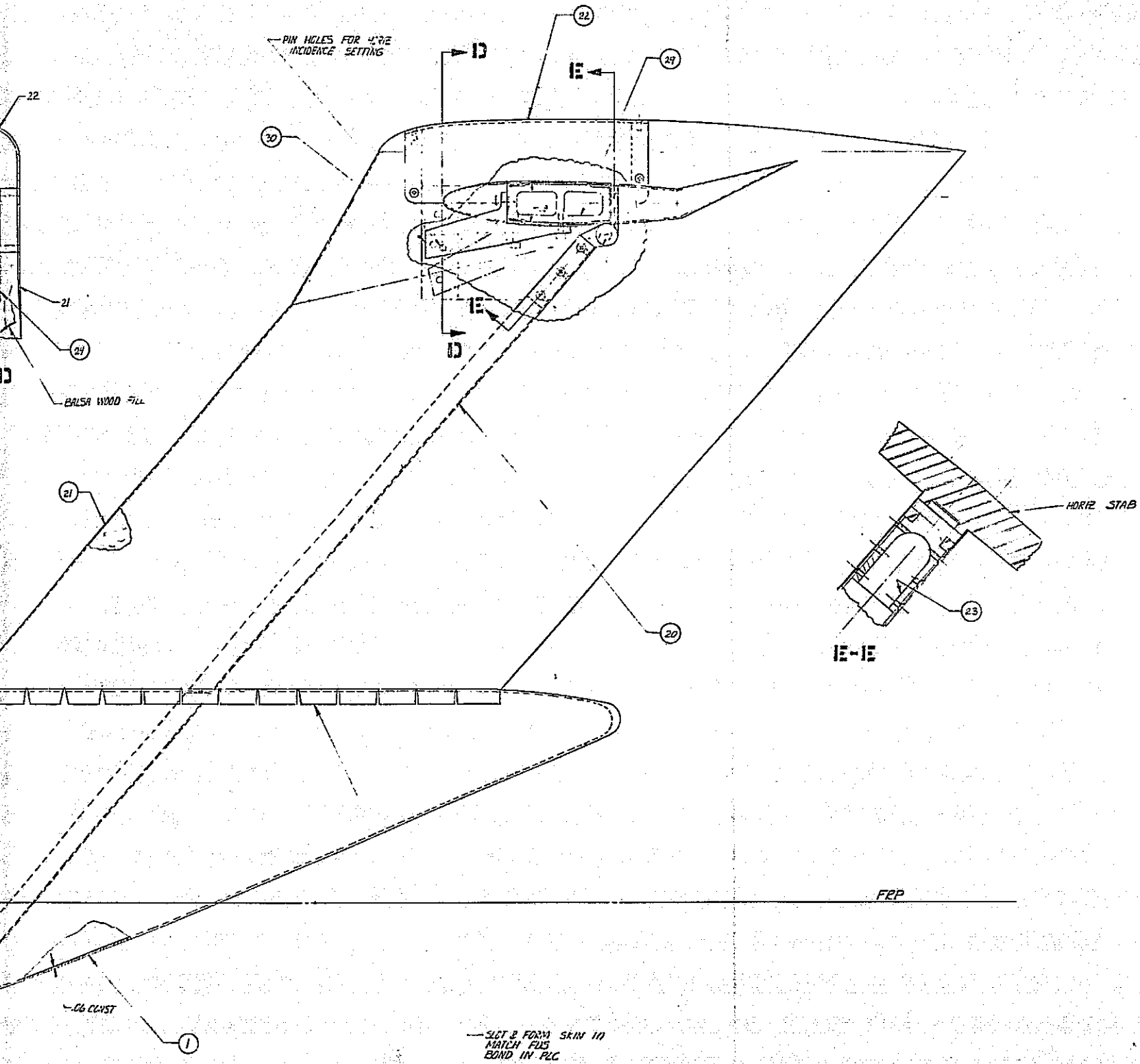

FIGURE 21. MODEL ASSEMBLY-ELEVATION VIEW

MODEL ASSY- STOL T. AIRCRAFT GROUND EFFECTS	DWG. [illegible]
	DATE [illegible]
	SCALE 1/2
DOUGLAS AIRCRAFT COMPANY LONG BEACH, CALIFORNIA	J012222

FOLDOUT FRAME

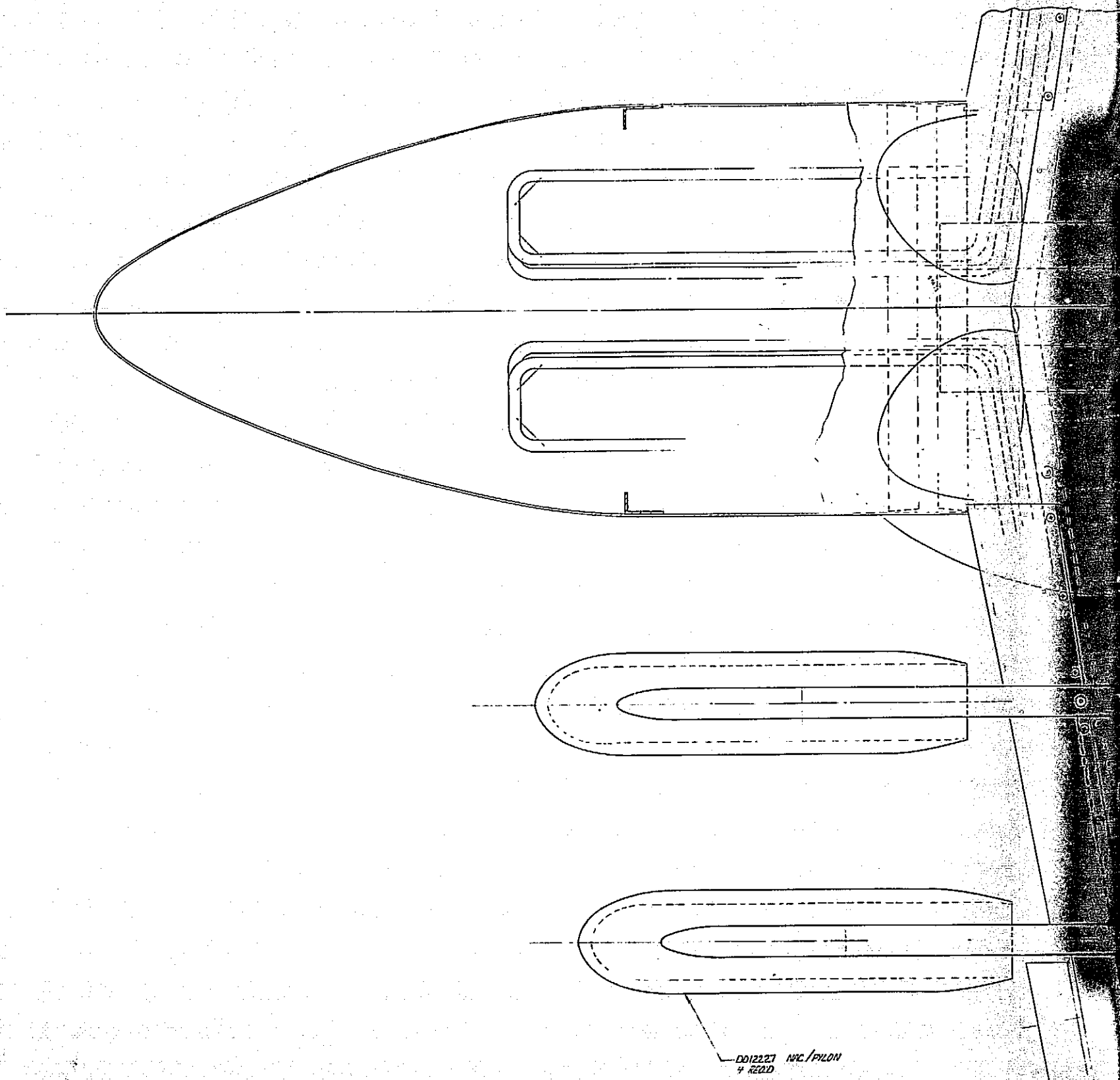

FOLDOUT FRAME

ORIGINAL PAGE IS
OF POOR QUALITY

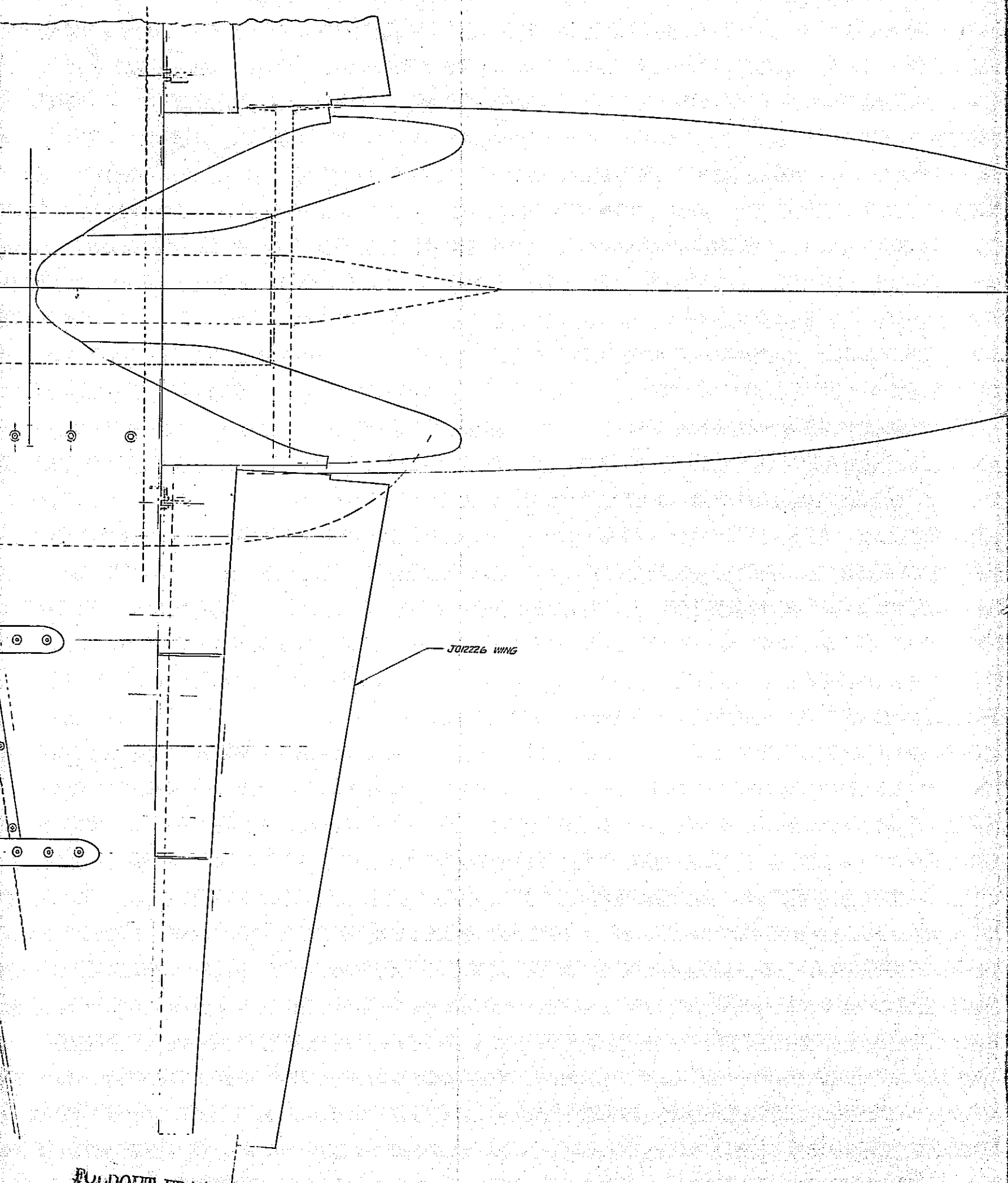

FOLDOUT FRAME 2

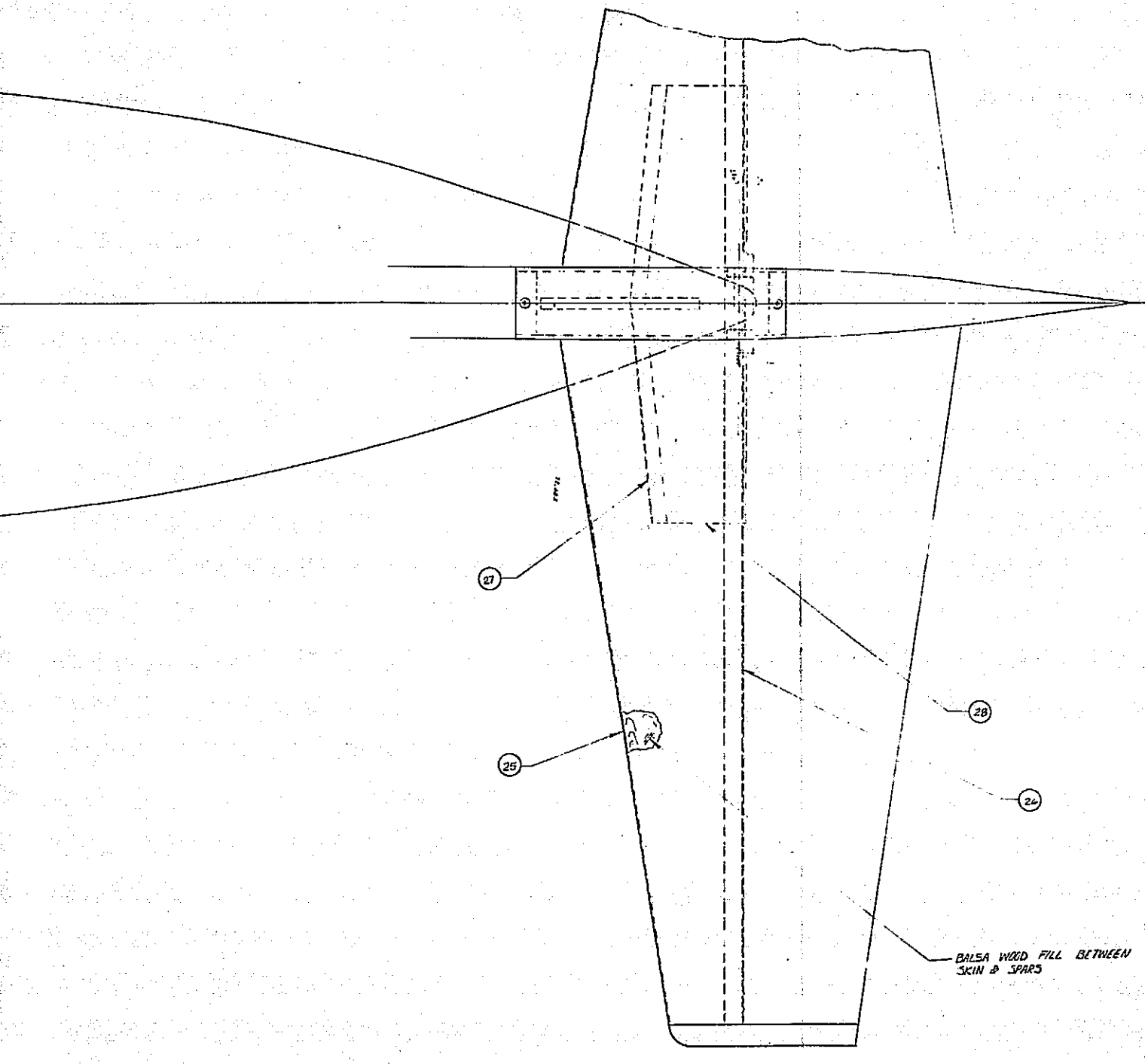

FIGURE 22. MODEL ASSEMBLY-PLAN VIEW

FOLDOUT FRAME 2

DOUGLAS | SIZE A | CODE IDENT. NO. 88277 | J012222 | SHEET

10555S

the engine simulator drive air. The fairing on the upper end of the strut is made with constant cross-section radial development lines to maintain a constant clearance gap with the fuselage cut-out as it rotates in pitch. The gap is sealed with soft foam. The strut chord is equal to 2 $\bar{c}$ and has thickness/chord ratio of ten percent.

In addition to the drive air lines, the strut encloses instrumentation leads, the pitch actuator, and the pitch actuator hydraulic lines. The pitch actuator rod connects to the bottom of the balance cage.

The engine simulator drive air balance cross-over system is comprised of four separate thin wall steel tubing parts connected to the pitch trunnion glands. Each tube is routed forward into the fuselage nose, up and back to the wing box, and out the wing in the leading edge to the pylon where it is secured with a clamp. This arrangement works very satisfactorily with the small diameter tubing permitted by the high pressure drive air being considered. The tubes pass through stabilizing restraints made of soft foam in the forward fuselage bulkhead.

The vertical tail structure consists of leading and trailing halves made of formed aluminum skin filled with a balsa wood core. These halves are attached to a banjo spar which forms the aft fuselage bulkhead. The tip of the spar has a fitting to receive the horizontal tail. The vertical tail also includes provisions for setting the horizontal tail incidence over a range of values.

The wing (figures 23 and 24) utilizes a stressed skin and rib type construction. The main wing box has front and rear spars formed from sheet aluminum. The rear spar is straight and continuous across the entire span. Aluminum ribs are spaced at the fuselage attachment, the pylon, and the flap bracket stations. The space between the spars and ribs is filled with soft balsa wood to stabilize the skin. The wing skin is formed of aluminum and riveted and bonded to the spars and ribs. The wing skin and spar thickness is tapered by chemical milling.

The leading edge segments inboard of the pylons are formed of aluminum sheet, spot welded to end ribs, and attached to the front spar with screws and nutplates. These segments are removable for access to the drive air lines. The leading edge outboard of the pylons is formed of aluminum sheet and riveted and bonded to the front spar. The leading edge slat is supported by brackets attached to the leading edge lower surface. The slat is machined from solid aluminum. The wing leading edge skin is tapered by chemical milling.

The wing flap segments are supported by brackets attached to the wing box ribs. Two sets of brackets are provided; one for a takeoff rigging, and one for a landing rigging. The forward flap segment (figure 25) consists of a core with the skin bonded and spot welded to it. The core is machined from solid aluminum to a rib and spar configuration with a solid trailing edge. The skin is formed to wrap around the leading edge and is tapered in thickness by chemcial milling. The aft flap is machined from solid aluminum.

The spoiler assembly is designed for two position operation. The spoilers are deployed upward for the initial part of the simulated landing trajectory at about half of full deflection. At a certain point in the run they are quickly retracted to the minimum deflection position. This is accomplished with a simple "mouse trap" mechanism. The spoiler panels are spring loaded to return to their final position. Before the run they are cocked and held in deployed position by a series of cams on a pull rod. The pull rod is spring loaded to release the cams and permit the spoilers to retract.

The nacelles (figure 26) are attached to the wing structure with pylons that go over and under the wing and are screwed to the wing main ribs. The pylons interrupt the wing leading edge and butt up to the front spar. The drive air line is routed from the leading edge region into the pylon to the engine simulator. The drive air line is brazed to a boss on the engine simulator which forms a small orifice that acts to drop the supply pressure from about 100 atmospheres to 10 atmospheres. The engine simulator consists of the high pressure plenum, the chocked baffle plate, the nozzle duct and

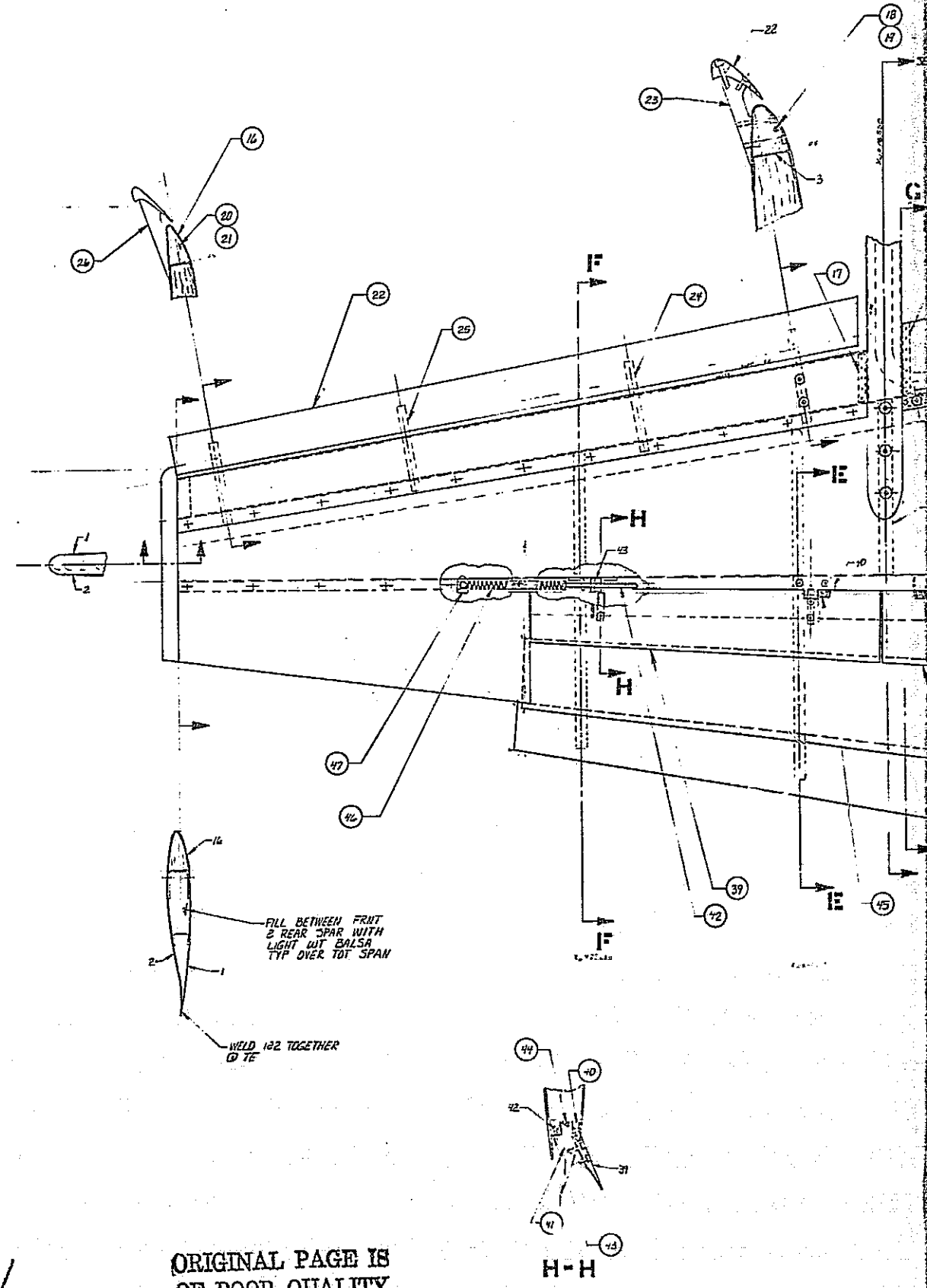

FOLDOUT FRAME /

ORIGINAL PAGE IS OF POOR QUALITY

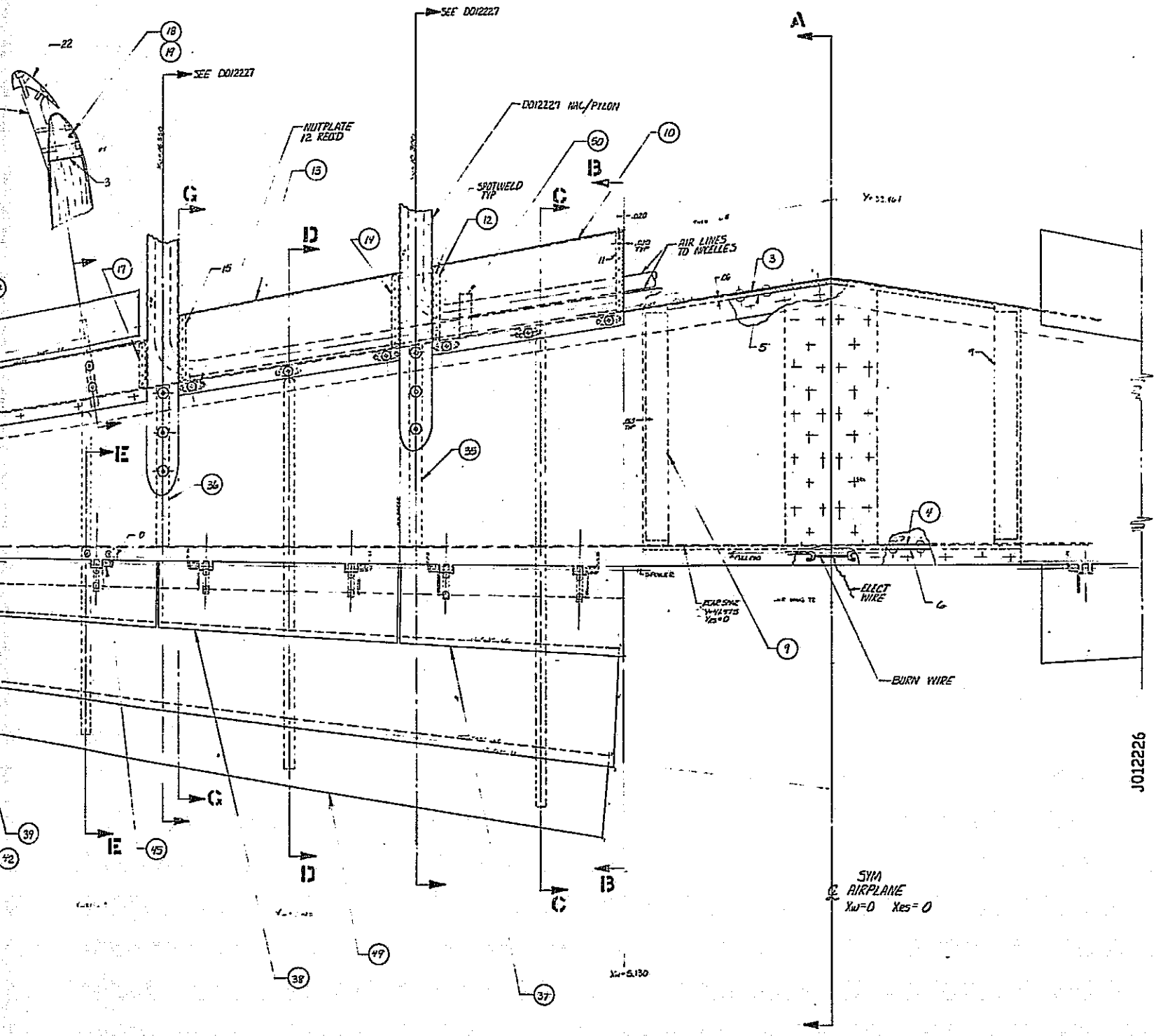

FIGURE 23. WING ASSEMBLY-PLAN VIEW

FOLDOUT FRAME 2

WING ASSY-STOL TRANSIENT GROUND EFFECTS MODEL

DOUGLAS AIRCRAFT COMPANY LONG BEACH, CALIFORNIA

J012226

JUN 13 1975

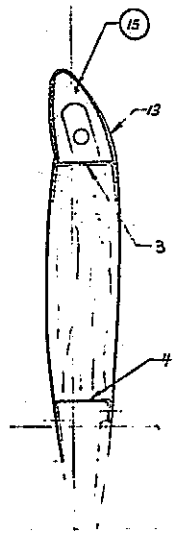

G-G

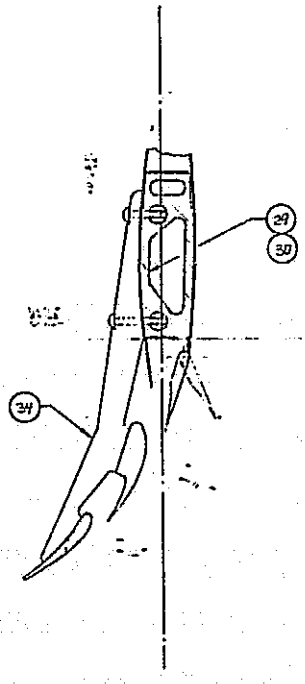

F-F

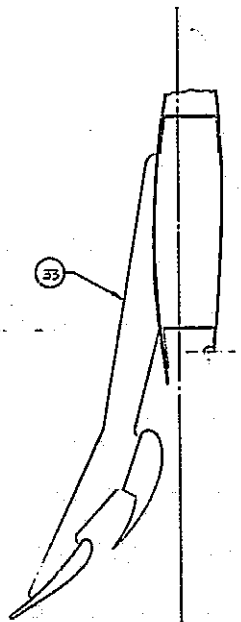

E-E

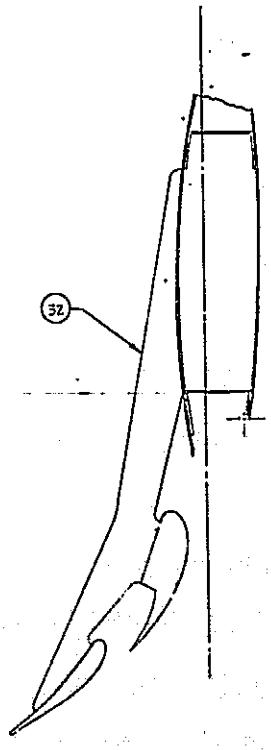

D-D

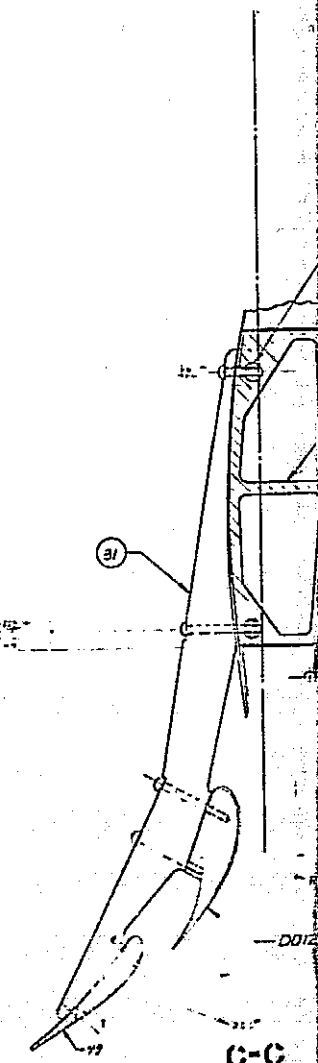

C-C

OLDOUT FRAME

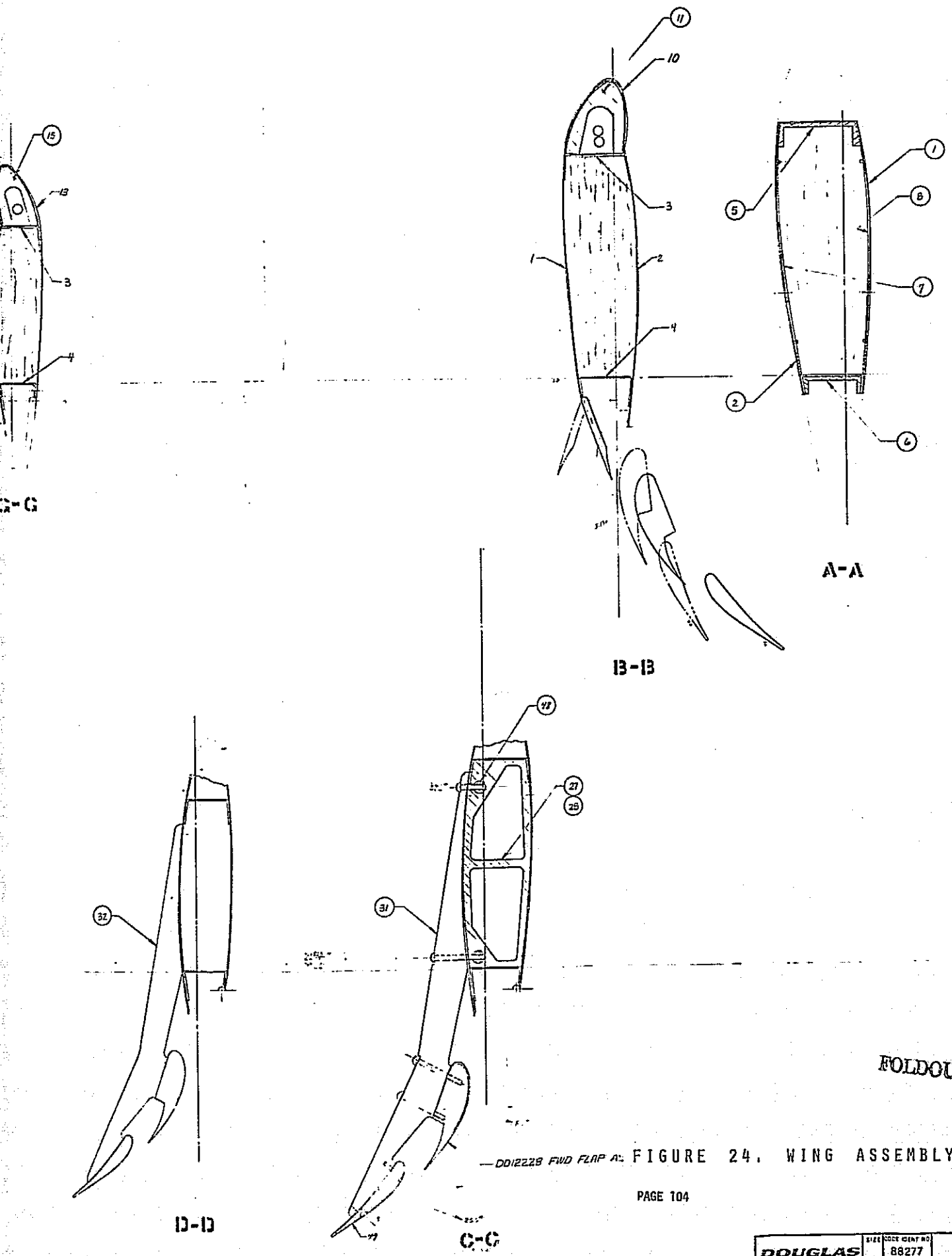

J012226

FOLDOUT FRAME 2

—DD12228 FWD FLAP A: FIGURE 24. WING ASSEMBLY-SECTIONS

DOUGLAS	SIZE	CODE IDENT NO	J012224
		88277	

101555R

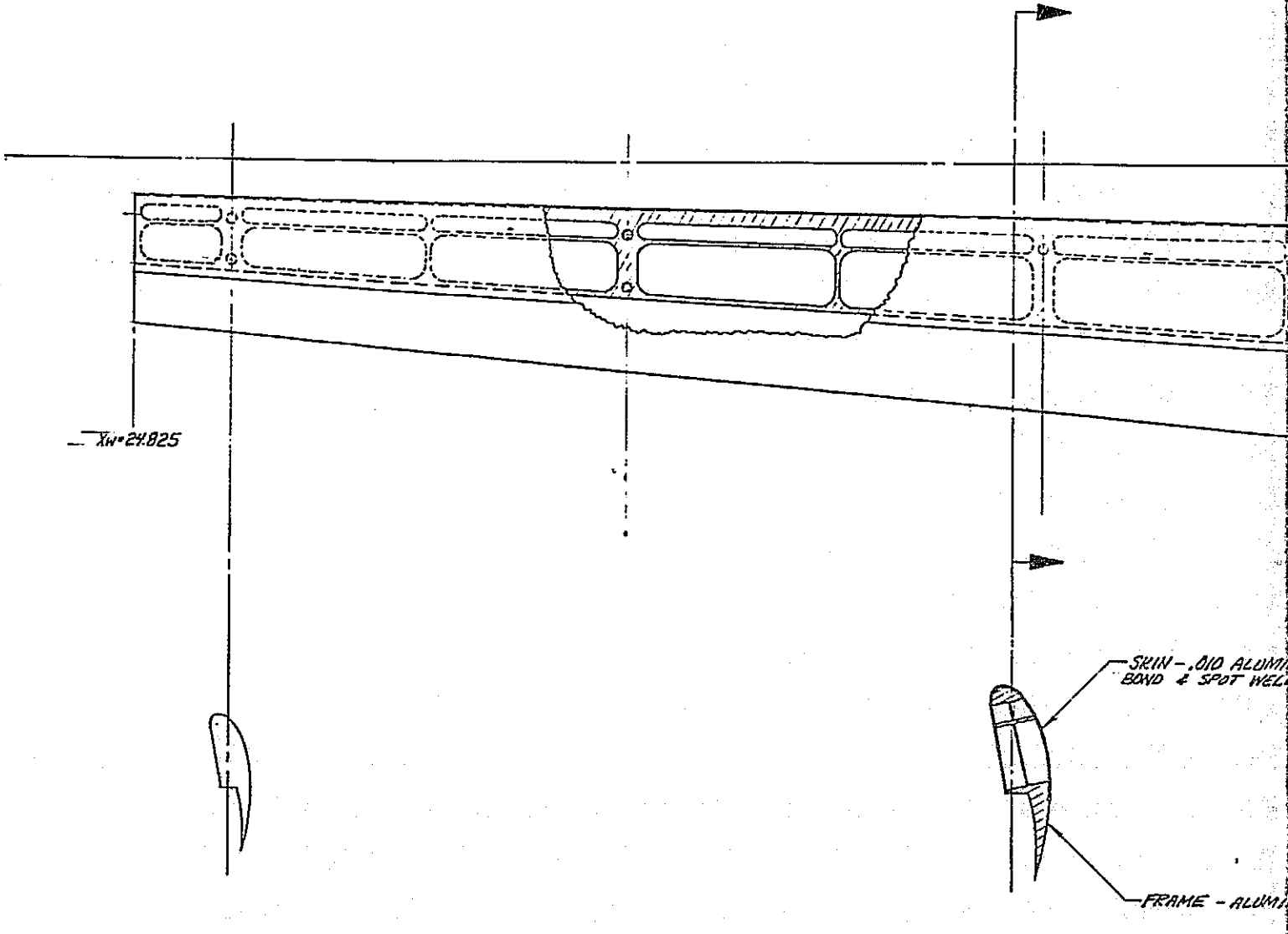

FOLDOUT FRAME 1

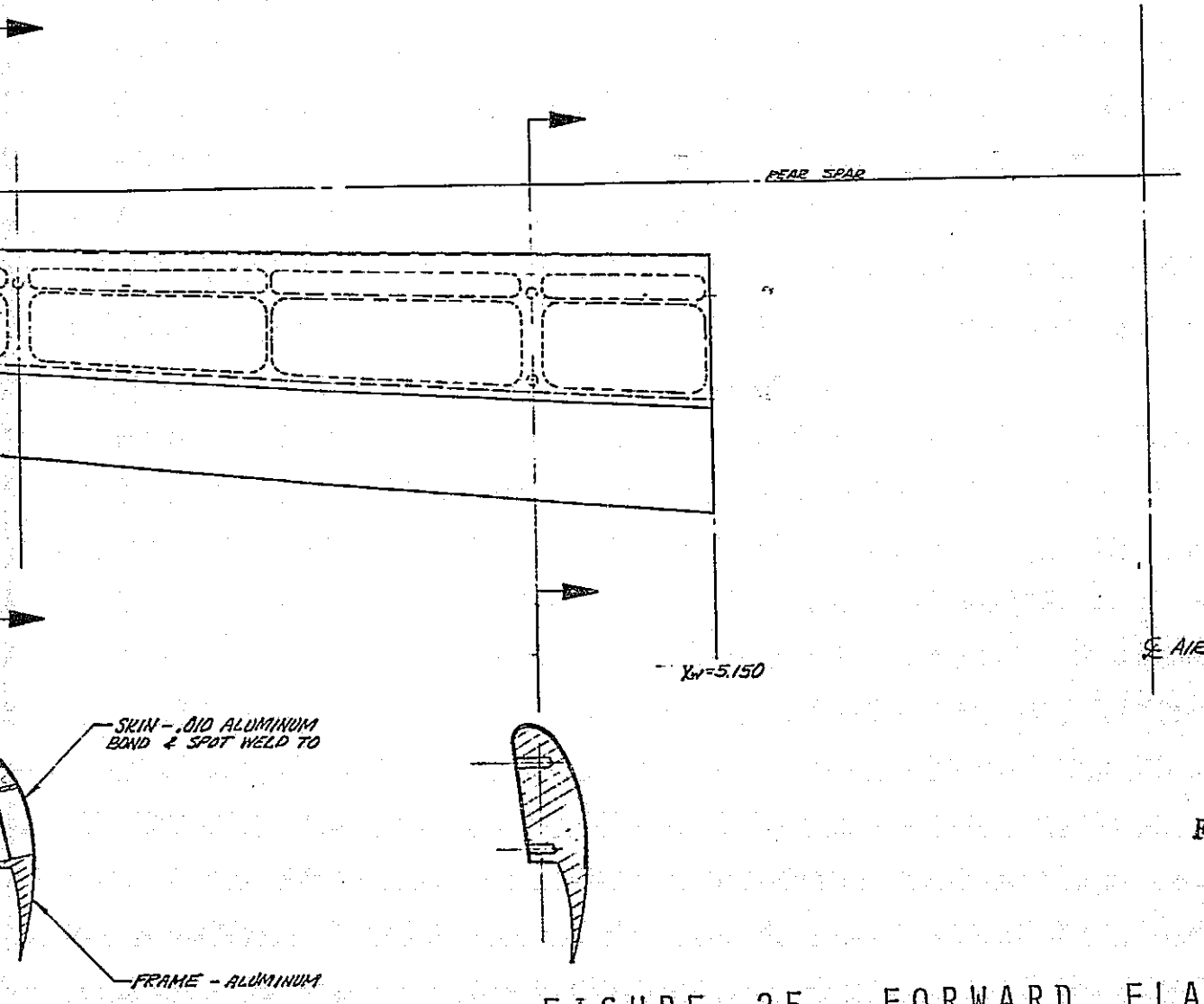

FOLDOUT FRAME 2

FIGURE 25. FORWARD FLAP ASSEMBLY

FWD FLAP ASSY- STOL TRANSIENT GROUND EFFECTS MODEL

ENGR. Fitzee ... NES
DATE JUN 12 1975
SCALE 6

DOUGLAS AIRCRAFT COMPANY
McDONNELL DOUGLAS
LONG BEACH, CALIFORNIA

D012228

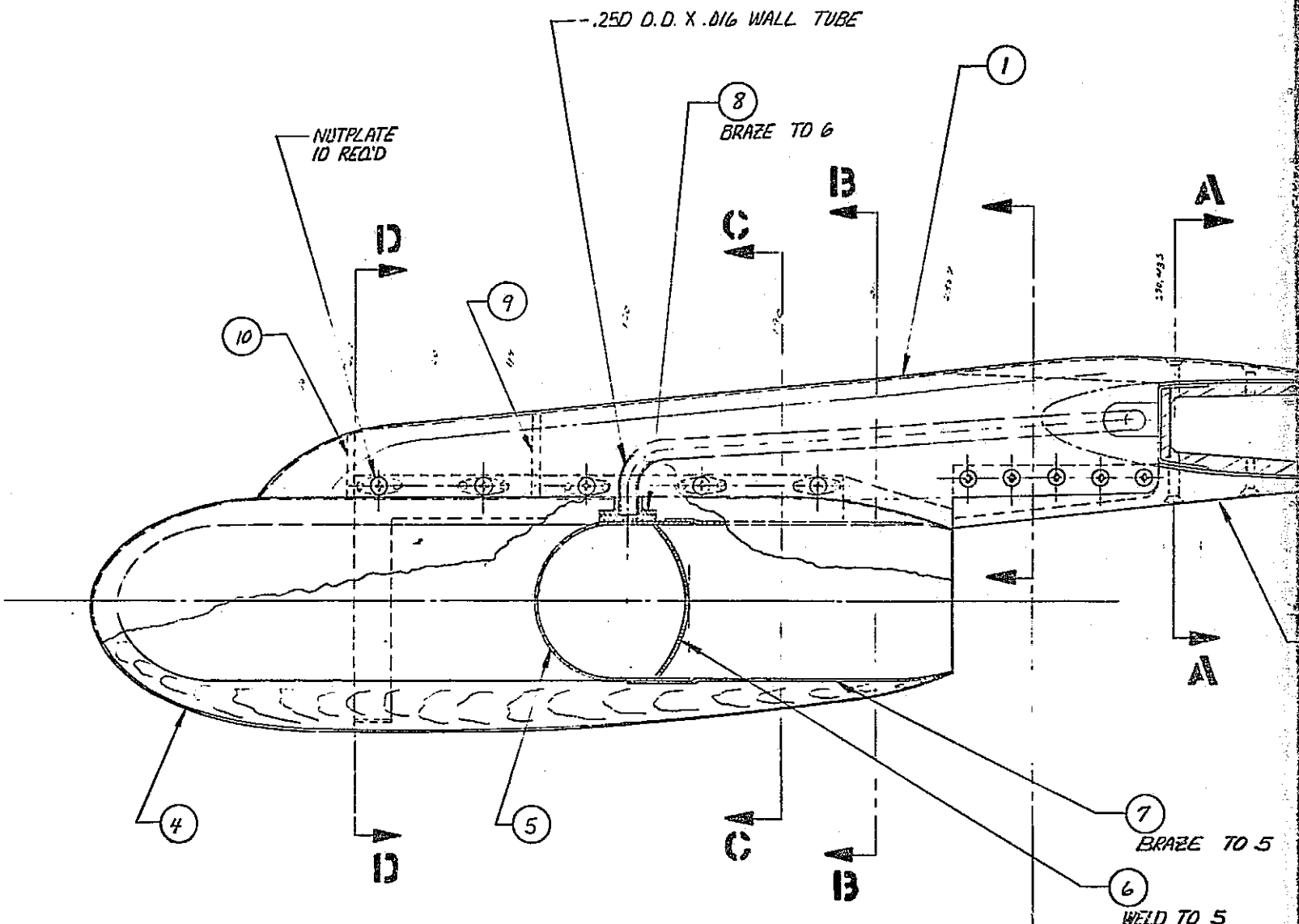

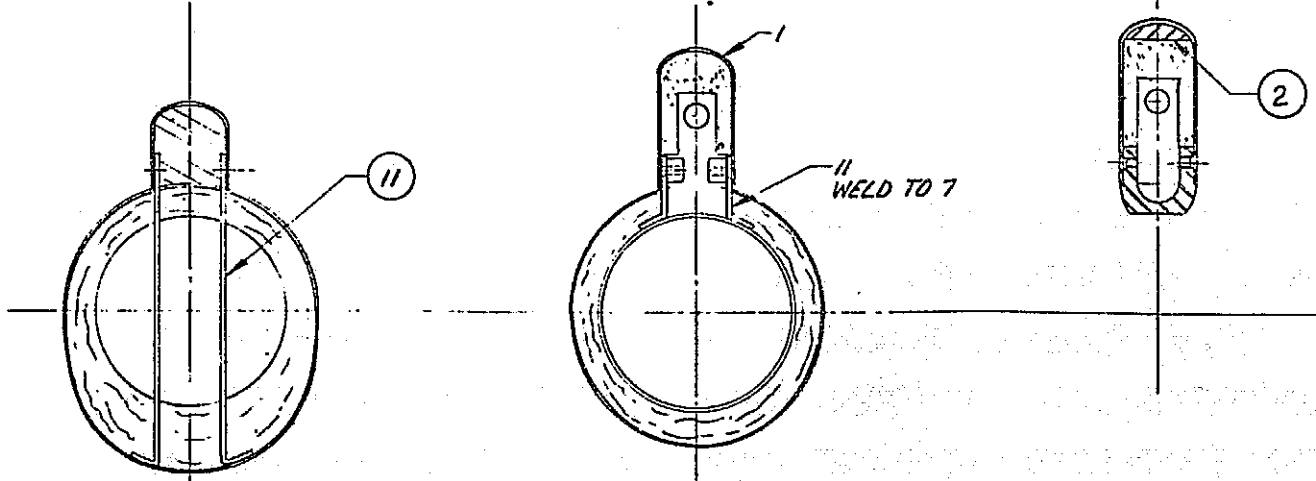

D-D

C-C

OUT FRAME /

F

PAG

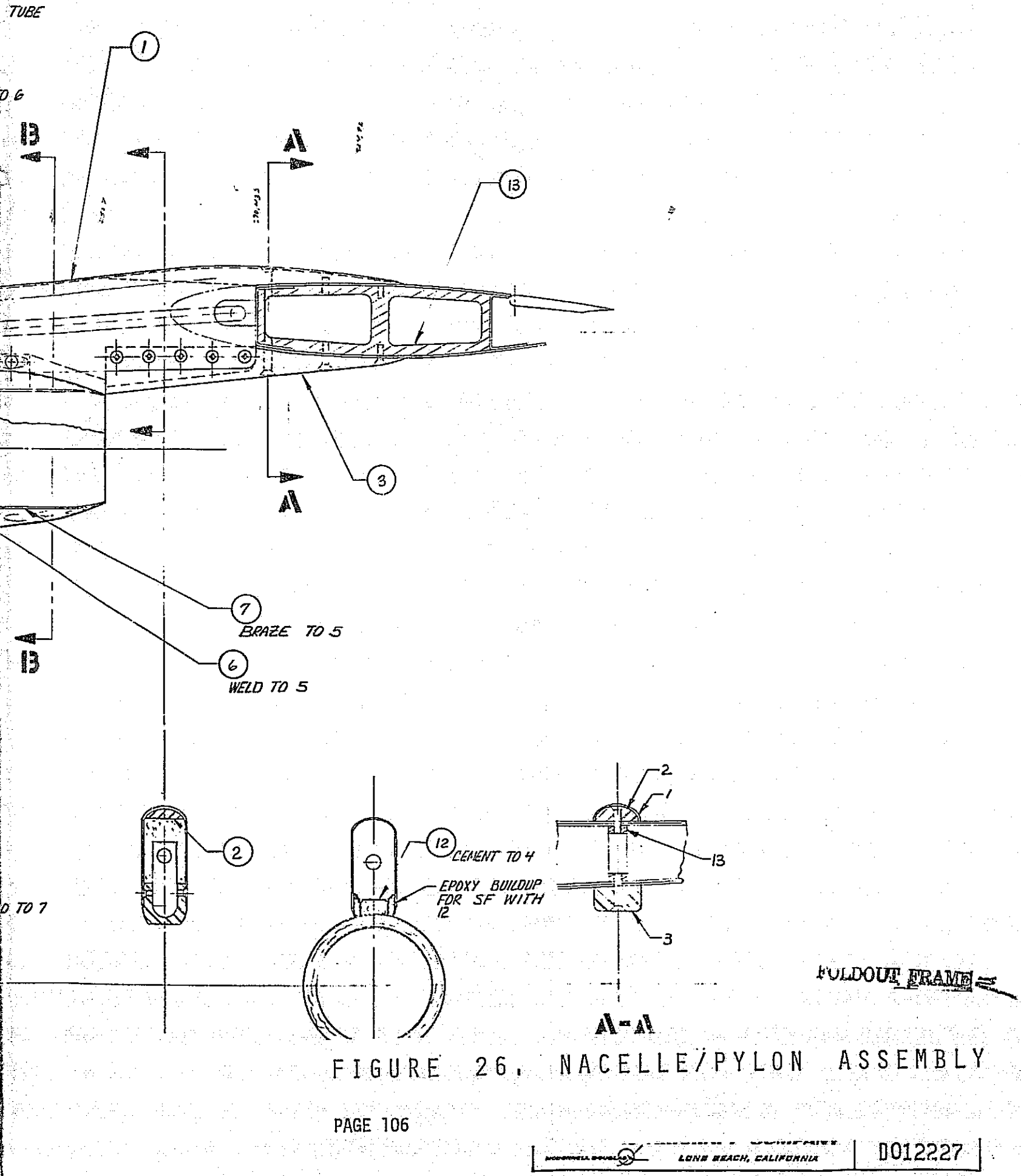

FIGURE 26. NACELLE/PYLON ASSEMBLY

the nozzle. The high pressure plenum is formed of a steel tube with a hemispherical forward end. The chocked baffle is a perforated steel plate with a domed shape that is welded into place at the downstream end of the high pressure plenum. This serves to drop the plenum pressure from about 10 atmospheres to the jet total pressure of less than one atmosphere. The baffle plate forms an array of chocked jets uniformly distributed across the upstream face of the nozzle duct which quickly merge into a uniform stream. The nozzle duct and nozzle is made of aluminum tube in one piece. The high pressure plenum, baffle plate, and supply duct have a constant diameter somewhat larger than the jet exit to allow for some nozzle contraction. If it should prove necessary, smoothing screens can easily be installed in the nozzle duct. The nacelle outer contour is made of fiberglass over a hollow wood core.

The horizontal tail is made by a similar method as the vertical tail. Leading and trailing halves are formed of aluminum, filled with balsa wood, and attached to the main spar which is continuous across the entire span. A partial span forward spar is used with ribs to form a box at the root to accommodate the attachment loads. The horizontal has a fixed elevator deflection and an incidence angle adjustable to several positions.

7.2.2 Model Perturbations

The model perturbations required to satisfy all five experimental systems being considered are small enough that the basepoint model design can be used with appropriate allowances for changes in size and velocity. Pertinent parameters for the test conditions are listed in table 9.

The basepoint model is designed for a maximum lift load of 4.33 kN (973 lb). Its weight is derived from a careful analysis of the component parts and totals 0.31 kN (69 lbs). This is the entire metric mass of the model including the metric balance core.

The model weights for the other test conditions are based on the general

scaling rule derived in section 5.3.2. This specifies that

$$W \sim F_v^2 F_s^3$$

However, judgmental compensations to the scaled weights were included to account for minimum practical weights due to fabrication difficulties and handling loads.

7.2.3 Model Costs

The model cost estimates are presented in table 11 and are expressed in terms of man-hours, material costs, and computer charges. The man-hours estimates are broken down into three categories; model design and coordination, loft line definition, and fabrication including shop management. Total costs are presented based on an average rate of $30 per hour.

The basic cost estimates were prepared; one for the small, blade mounted, model, and the other for the large model. The sting mounted model has a slight increase in cost to allow for the more complicated pitch motion accommodation. The track model is more expensive to fabricate because the overhead blade strut requires a more complicated wing spar carry-through structure. Also, the reduced airloads permit thinner wing skins which require more effort to fabricate.

TABLE 11. MODEL COSTS

	Experimental System				
	A	B	C	D	E
	V/STOL Wind Tunnel Blade Strut Support $F_v = 1.0$, $F_s = 0.053$	V/STOL Wind Tunnel Sting Support $F_v = 1.0$, $F_s = 0.053$	40 x 80 Foot Wind Tunnel Blade Strut Support $F_v = 1.0$, $F_s = 0.11$	Vortex Research Facility with Vertical & Pitch Motion $F_v = 0.54$, $F_s = 0.053$	Vortex Research Facility without Vertical & Pitch Motion $F_v = 0.54$, $F_s = 0.053$
	m-hr $	m-hr $	m-hr $	m-hr $	m-hr $
Model Design	2400	2400	2750	2400	2400
Loft	1230	1230	1230	1230	1230
Fabrication	5880	6000	12920	6680	6680
Materials	$3.5K	$3.5K	$7.7K	$3.5K	$3.5K
Computer Services	$2K	$2K	$2K	$2K	$2K
Total Man-Hours	9510	9630	16900	10310	10310
Total $ @ $30/hr	$291K	$294K	$517K	$315K	$315K

7.3 Model Support and Actuator

The model support and actuator system is the heart of the transient ground effect apparatus. It is this system which provides the motion essential for the trajectory simulation. It is also this system which holds the greatest technical risk for the success of the experiment. The extent and rate of the required motion is close to the ultimate limit for the present state-of-the-art in hydraulic actuator design. The structural dynamics of this system will remain an uncertain area until further detailed analysis can be conducted, but from present indications may present strong limiting conditions for instrumentation frequency response.

Whether or not these limits ever materialize depends, not only on the mechanical performance of the support and actuator system, but on the nature of the transient ground effects under study. Thus even the requirements for the mechanical performance of the system will remain uncertain, probably until the first experiments are conducted.

The present understanding of these requirements, limitations, and uncertainties dictates a conservative approach in the design study of the experimental apparatus, and principally the support and actuator system. Therefore, the principal consideration was to seek the maximum practical mechanical performance by striving for minimum structural mass, maximum stiffness, and as direct as possible load paths.

The descriptions of the support and actuator system design studies are presented in relation to the particular facilities.

7.3.1 V/STOL Wind Tunnel - Blade Strut Support

Figure 27 shows the blade strut support and actuator system installed in the V/STOL wind tunnel. The apparatus is designed for a temporary installation at the upstream end of either of the two test bays. To prevent interference with other wind tunnel uses, the apparatus is sufficiently portable to be easily moved out of the test chamber to an adjacent storage room.

The forward installation location is used in conjunction with the existing wind tunnel floor suction BLC system. This serves to remove the floor boundary layer just ahead of the model. The floor boundary layer then starts growing again underneath the model. It is probable that this small boundary layer growth will not result in large ground plane interference errors for the model power levels involved in the present case. If more powerful BLC provisions are required, a wall-jet blowing BLC system can be installed on a test section cart in the forward test bay and the transient ground effect support apparatus installed immediately downstream of it in the aft test bay. The results of reference 10 indicate that the BLC wall-jet air flow rate is about the same magnitude as the model flow rate. The high pressure air supply system available has sufficient capacity for such flow rates. However, it is likely that the prior BLC removal by the floor suction system will greatly reduce the jet flow required for the wall-jet blowing system.

The strut, as it emerges from the floor, has a constant cross section shape that is designed for minimal floor boundary layer interference. This results in a relatively large chord length with thickness/chord ratio of 10 percent. The shape also reduces the wake interference with the fuselage afterbody. The strut chord length increases at the fuselage seal fairing.

This arrangement produces minimal support interference for test conditions with lateral symmetry. However for tests involving asymmetrical flow, such as engine out, steady side-slip, etc., such an arrangement may result in excessive support interference. For those conditions an alternate strut may be required having a much reduced chord length. This will necessitate a much larger thickness/chord ratio which will produce increased floor boundary layer interference as well as greater wake interference on the fuselage afterbody. These problems are not serious, but may require additional BLC blowing near the strut. In all other respects, an alternate strut presents no further problems and can easily be accommodated by the apparatus.

The maximum motion rate, as shown in table 9 is $\dot{h}$ = 5.2 m/sec (17.0 ft/sec). The actuator system is designed for a maximum deceleration

capability of six "g's". This results in a maximum stopping distance, shown in table 9, of $\Delta h = 0.13$ b. The range of model positions for steady testing is from the ground to a height of $h = 1.0$ b. The range of heights for transient testing is slightly less to allow for the distance required to accelerate the model to the desired descent rate. This acceleration distance is somewhat uncertain and will ultimately depend on the performance of the actuator servo-valves in starting the motion smoothly. Experience with such equipment indicates that, in any event, the starting acceleration capability will certainly be greater than three "g's" which results in a starting distance of less than $\Delta h = 0.26$ b. This still leaves sufficient travel for the expected transient events.

The installation of the apparatus in the test section cart involves cutting a small notch in the upstream edge of it. Otherwise the cart is not affected by the installation. The section of floor surrounding the strut includes a small pop-down panel which is spring loaded to fall away as the model approaches the floor at the end of a run. This provides an additional stopping distance of 0.13 b which permits a high sink rate condition to be maintained closer to the floor before the model deceleration starts.

Beneath the floor the strut attaches to a carriage that rolls in a vertical track. This carriage and track assembly provides the longitudinal and lateral restraint to the model as it moves through the vertical height range. The main hydraulic actuator is located beneath the carriage and the piston rod is connected directly to it. The actuator is supported by a short pedestal resting on the floor. The carriage and track assembly is supported above the actuator by a framework made of structural steel members. This framework forms a cross-shaped platform resting on four posts which bear on the test chamber floor surrounding the actuator pedestal. The floor is modified with a deep concrete footing under the actuator pedestal and anchor bolt inserts for the pedestal and each of the four supporting posts.

In order to remove the apparatus from the wind tunnel, the top of the track is lowered to clear the surrounding wind tunnel structure. The carriage framework is arranged to slide down the four posts to provide the

necessary clearance. A hydraulic jack in each post is used to raise or lower it. When the framework is raised into place, it is securely bolted to the posts, forming a rigid unit. When the apparatus is being moved, it is supported by air bearing pads built into each post. This allows the unit to be easily moved to the adjacent storage area or the alternate test bay.

The main hydraulic actuator incorporates special design features for low friction and fast response. The cylinder is a single-ended type with the piston rod extending from one end only. It operates from a high pressure hydraulic supply system of 21 MPa (3000 lb/in^2) to keep the actuator stiffness to as high a level as possible. The cylinder includes an internal tailstock mounted on the closed end which telescopes into the piston rod to keep the piston area close to the same value for both tension and compression side. The piston has no seals, but relies on carefully maintained tolerances to keep the fluid leakage rate at a low and consistent level for which the servo-amplifiers can be compensated. The low friction piston rod seal includes a continuous scavenging system to recover the blow-by.

Shaped ports are used so that as the piston approaches the end of its travel the fluid flow rate is throttled down by the piston to decelerate the actuator at its maximum rate. This is a fail safe provision which is only used in the event that the positioning logic or servo-systems malfunction and do not properly decelerate the actuator. This eliminates the need for other fail-safe provisions in the drive system. A linear voltage differential transformer (LVDT) is enclosed within the tailstock for the servo system position sensing.

The actuator is operated from an accumulator in a blow-down mode. The maximum hydraulic fluid flow rate is 0.028 m^3/s (440 gpm) but the fluid required per stroke is only 0.0072 m^3(1.9 gal). The high pressure pumping system to charge the accumulator is designed for a cycle time of one minute between runs. The hydraulic servo valve is mounted directly on the cylinder at the compression port. The pitch motion hydraulic actuator is similar in operation to the main actuator, but of greatly reduced capacity. It is

located within the blade strut near the model and the servo valve is at the base of the strut.

The apparatus is operated from a control panel located in the wind tunnel control room. The control panel includes provisions to control and monitor the engine simulator thrust, to manually change the model vertical and pitch position with appropriate readout, and to monitor various dynamic parameters during a run. The DLC spoiler operation is triggered by a switch adjacent to the carriage track. The position of this switch is remotely controlled from the panel. The desired model position trajectory is controlled by data read from a small computer in real time which drives the servo amplifiers.

7.3.2 V/STOL Wind Tunnel - Sting Support

This alternative model support system is considered for the V/STOL wind tunnel as a means of alleviating the possible adverse interference of the blade strut with asymmetric flow conditions as well as permitting the use of the moving belt ground plane. The arrangement of this support shown in figure 28 permits the use of an unusual hydraulic actuator design concept that offers the potential for a significantly simpler system.

The sting is supported from the top of a large diameter column which is the actuator piston rod. This column penetrates the test section floor behind the moving belt ground plane cart and enters the actuator cylinder. The cylinder comprises the upper part of the main support column. The cylinder is double-ended and the piston rod extends through the bottom end into the base of the support column, providing maximum lateral restraint.

The entire support column assembly rests on a deep concrete footing. Two outrigger legs are attached to the top of the column and bolt to the concrete floor. The main column incorporates an air bearing pad to allow the apparatus to be moved from the adjacent storage area.

The sting assembly bolts to a turntable on the top of the piston rod which has provisions to adjust the model side-slip angle. The sting assembly

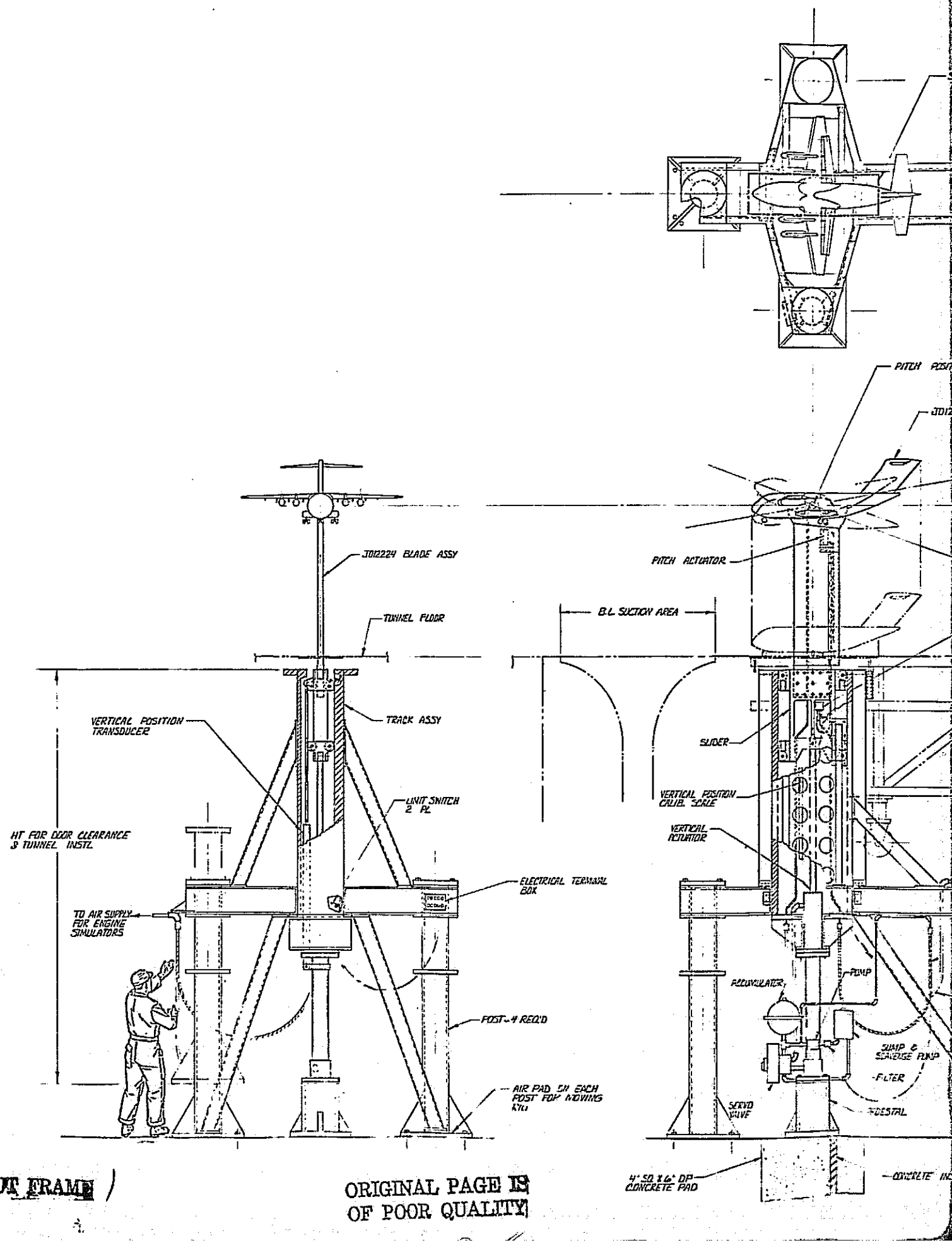

FOLDOUT FRAME

ORIGINAL PAGE IS OF POOR QUALITY

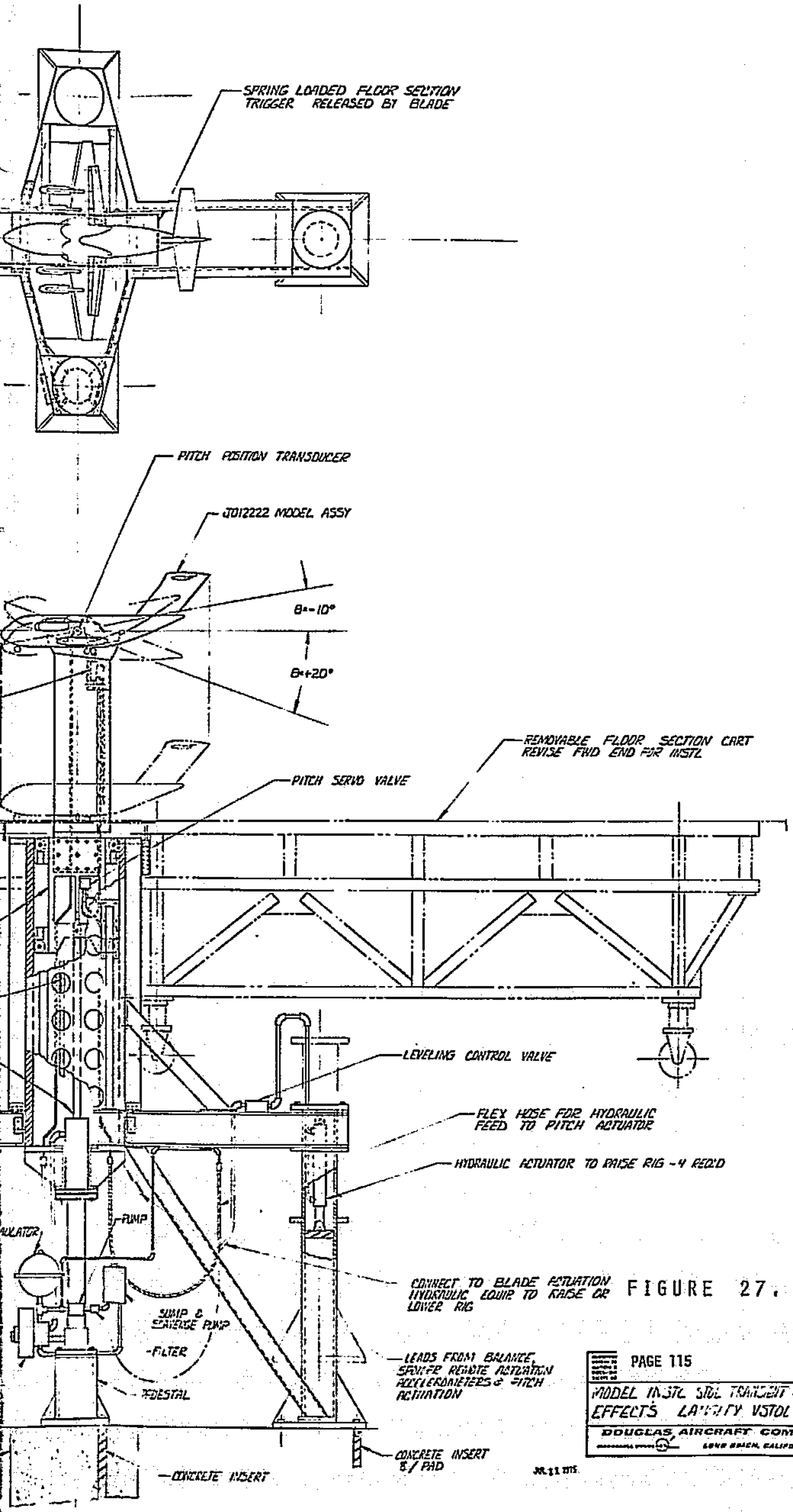

FIGURE 27. MODEL INSTALLATION-NASA LANGLEY V/STOL WIND TUNNEL (BLADE STRUT SUPPORT)

PAGE 115

MODEL INSTL STOL TRANSIENT GROUND EFFECTS LANGLEY VSTOL TUNNEL

DOUGLAS AIRCRAFT COMPANY
LONG BEACH, CALIFORNIA

J012242

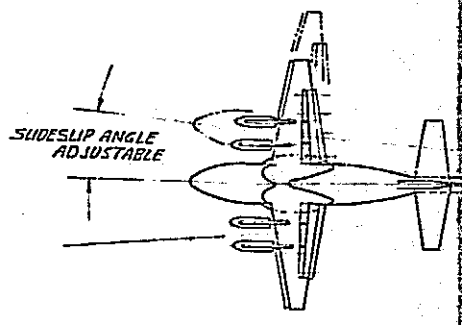

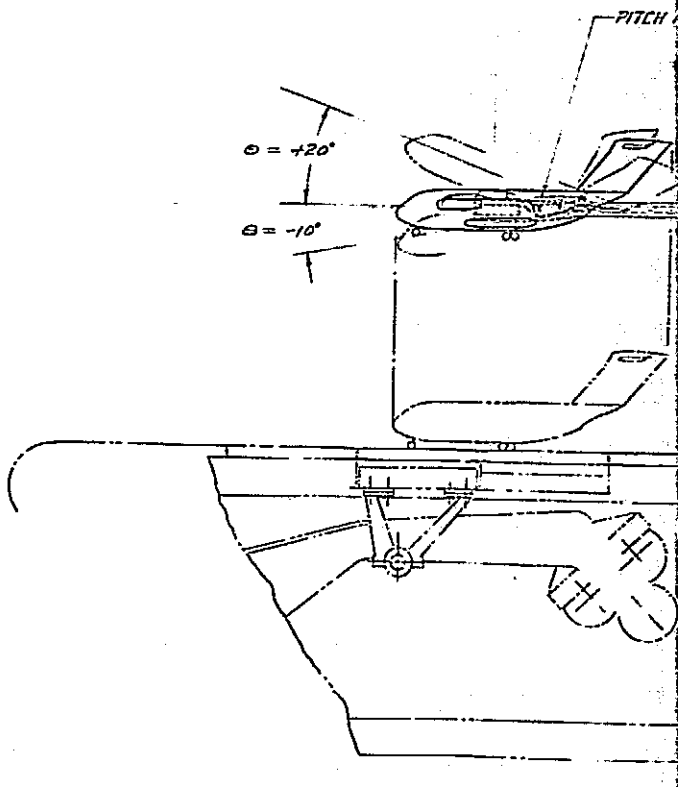

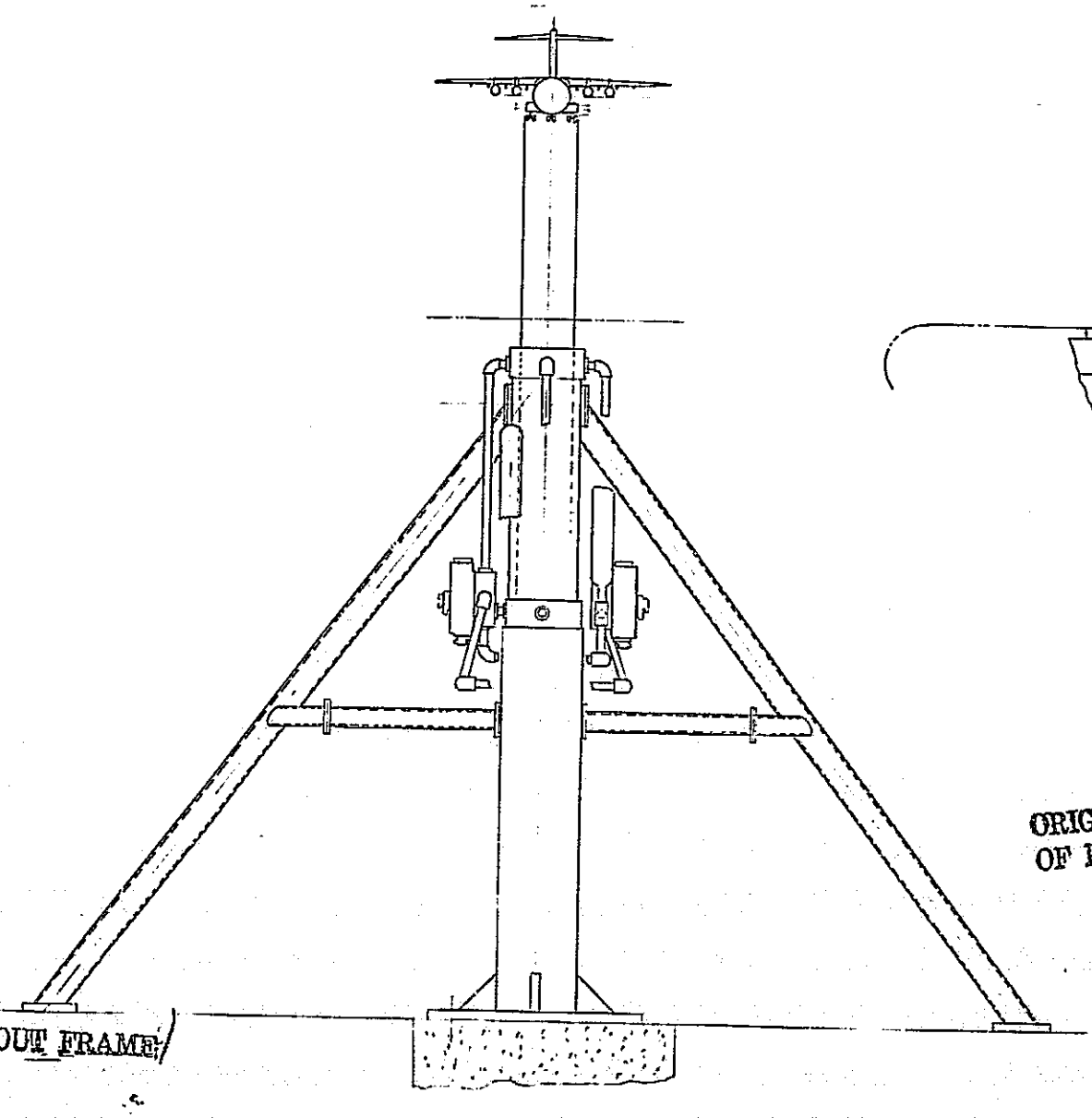

FOLDOUT FRAME

ORIGINAL PAGE IS
OF POOR QUALITY

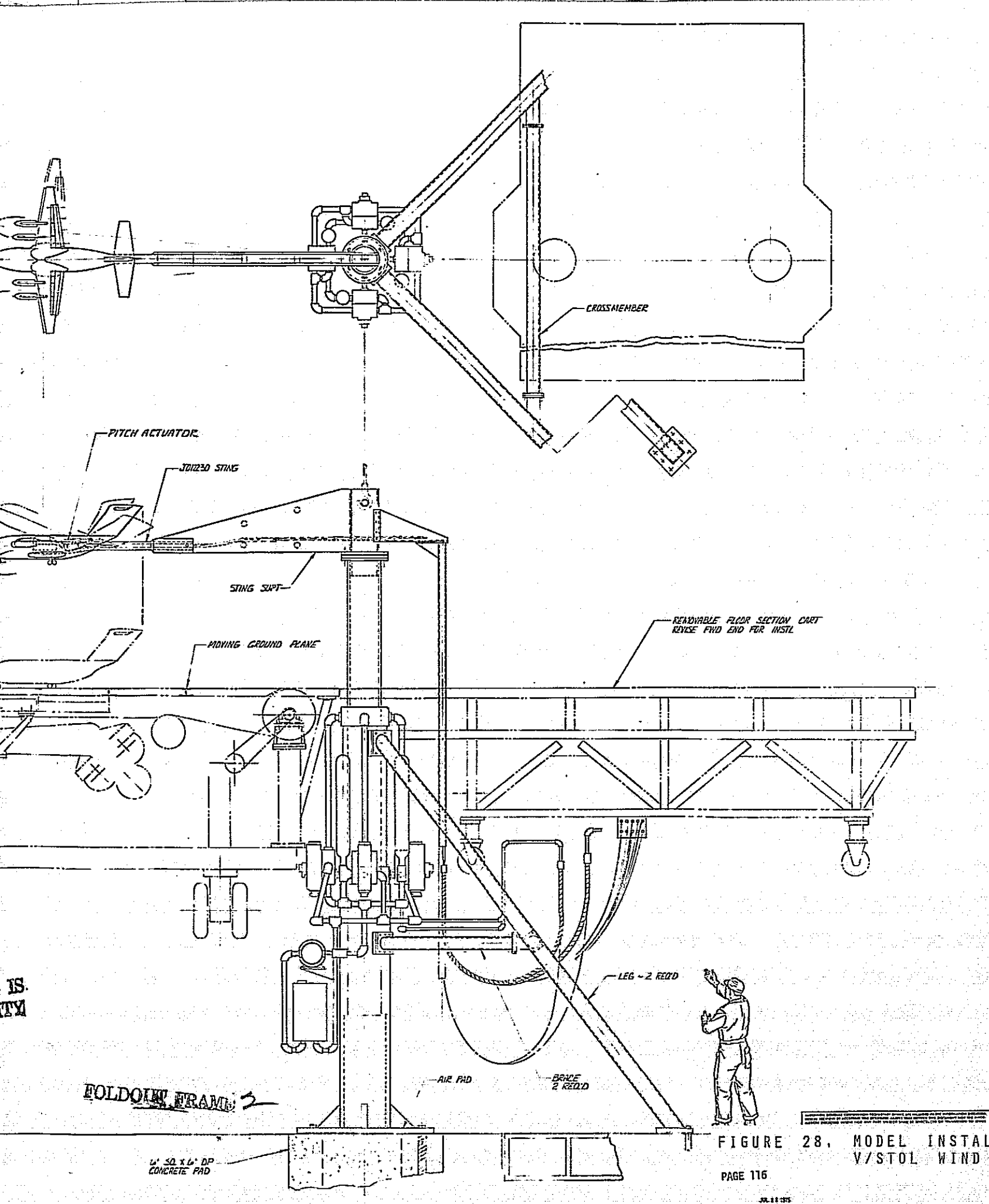

FOLDOUT FRAME 2

FIGURE 28. MODEL INSTALL
V/STOL WIND T

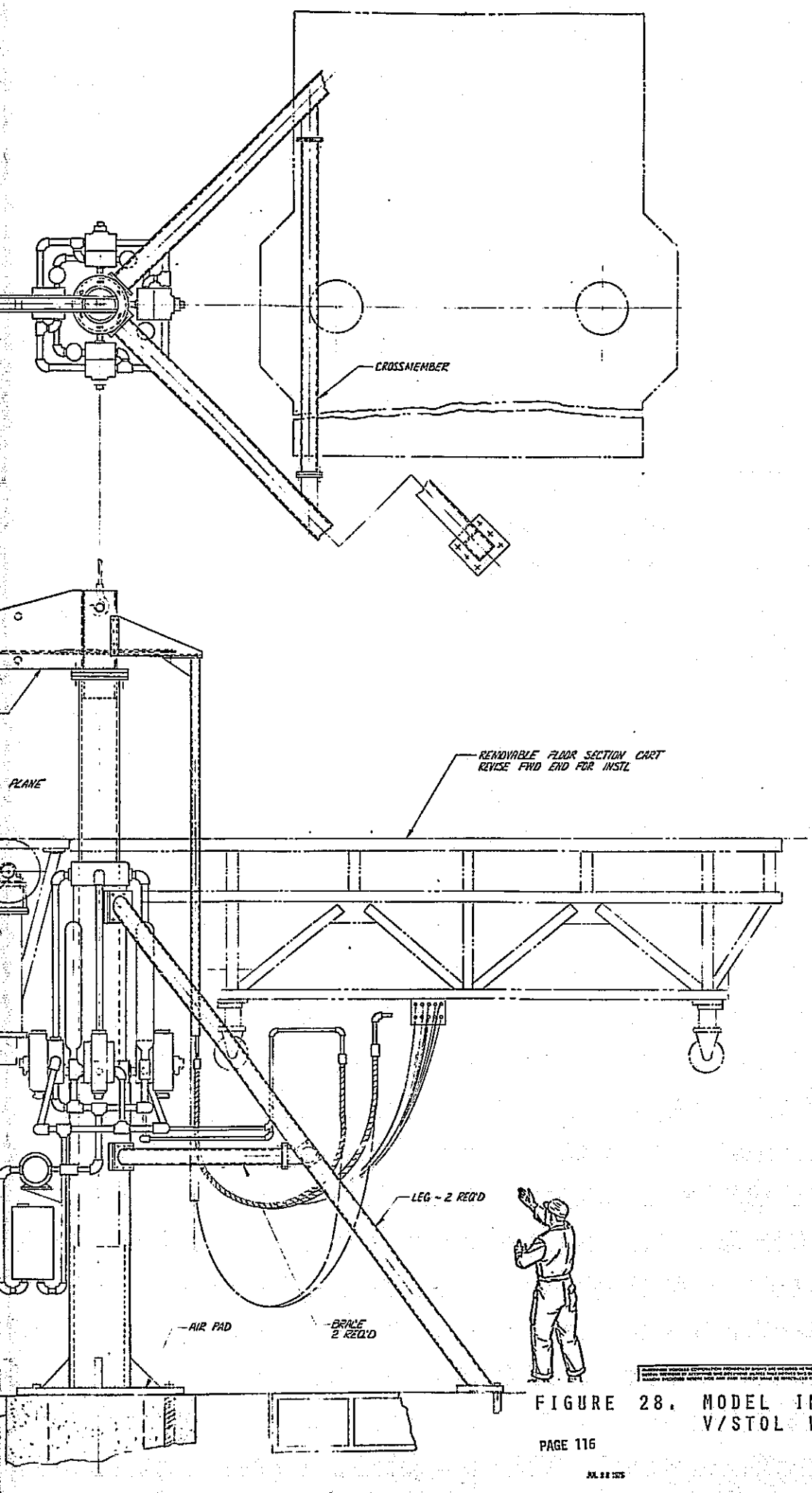

FOLDOUT FRAME 3

4

FIGURE 28. MODEL INSTALLATION-NASA LANGLEY V/STOL WIND TUNNEL (STING SUPPORT)

is made of aluminum plates, bolted together with spacers. It terminates with a short round section that enters the model afterbody under the vertical tail.

The pitch angle pivot is located near the fuselage cutout to keep the base cavity as small as possible. The pitch motion is provided by a hydraulic actuator inside the fuselage. Since the pitch pivot is located some distance from the aircraft center-of-gravity, simulated rotation about that point requires a combined motion of the vertical actuator and the pitch actuator.

The model pitch attitude range of $\theta = -10$ to $+20$ degrees shown in figure 28 probably cannot be achieved with one sting. The rotation required for a simulated transient maneuver is much less than 30 degrees, but this range is needed to encompass all the test conditions of interest for static testing. Different sting adapters can be used to achieve the full range of angles, but with a more limited range of rotation.

The large size of the piston rod may cause a significant interference with the wind tunnel flow. For the present design, the model is located six diameters upstream of the piston rod. The disturbance to the freestream flow will probably be minimal, but there may be a relatively large distrubance where the piston rod emerges from the test section floor, such as boundary layer separation, which may propagate upstream. This can probably be controlled, if necessary, by local BLC blowing near the rod.

The potential advantage of the main actuator system for this installation is tempered by a greater technical risk involved in developing an hydraulic actuator of this size as well as the much greater hydraulic fluid capacity required. The hydraulic fluid flow rate is 0.110 m^3/s (1750 gpm) and the fluid capacity per stroke is 0.026 m^3 (7 gal). This requires four servo valves and accumulators.

Hydraulic cylinders of this size and capacity present difficult design and manufacturing problems. The greatest uncertainty involves the performance

of the piston rod seals and the leakage rate of the piston in the cylinder. Development of such an actuator requires preliminary fabrication of major components such as rod seals and piston/cylinder sections from which operating parameters can be experimentally determined. The additional effort required for such development is very difficult to estimate and has not been included in the cost comparisons for the present study.

7.3.3 40- by 80-foot Wind Tunnel

The blade strut support and actuator system design for the 40- by 80-foot wind tunnel installation is essentially the same as for the V/STOL wind tunnel except that it is about twice as large. The installation is shown in figure 29. One significant difference is that the installation is permanent, but does not interfere with other test objectives of the facility. The equipment is installed upstream of the balance turntable, extending under the test section floor. The vertical carriage and track assembly is attached to the reinforced concrete forward wall of the balance house. The main hydraulic actuator is supported on a raised concrete platform extending beneath the existing floor. A minor amount of modification to the existing facility is required to relocate a stairway and balcony. The test section floor is modified to include a pop-down panel which is spring loaded to fall away as the model approaches the floor to provide additional stopping distance.

Ground effect testing in this facility will require a ground board BLC system because of the large boundary that exists on the test section floor. The study reported in reference 9 identified a wall-jet blowing BLC system as being appropriate for this facility and made a preliminary design of such a system in this facility. The installation location selected for the transient ground effect apparatus can be easily accommodated by that BLC system. Presumably it will be available for this proposed experiment.

A useful consequence of the increased scale for this installation is that relative starting and stopping distances are reduced for a constant acceleration. Table 9 shows the stopping distance for a six "g" acceleration from the maximum sink rate is $\Delta h = 0.06\ b$.

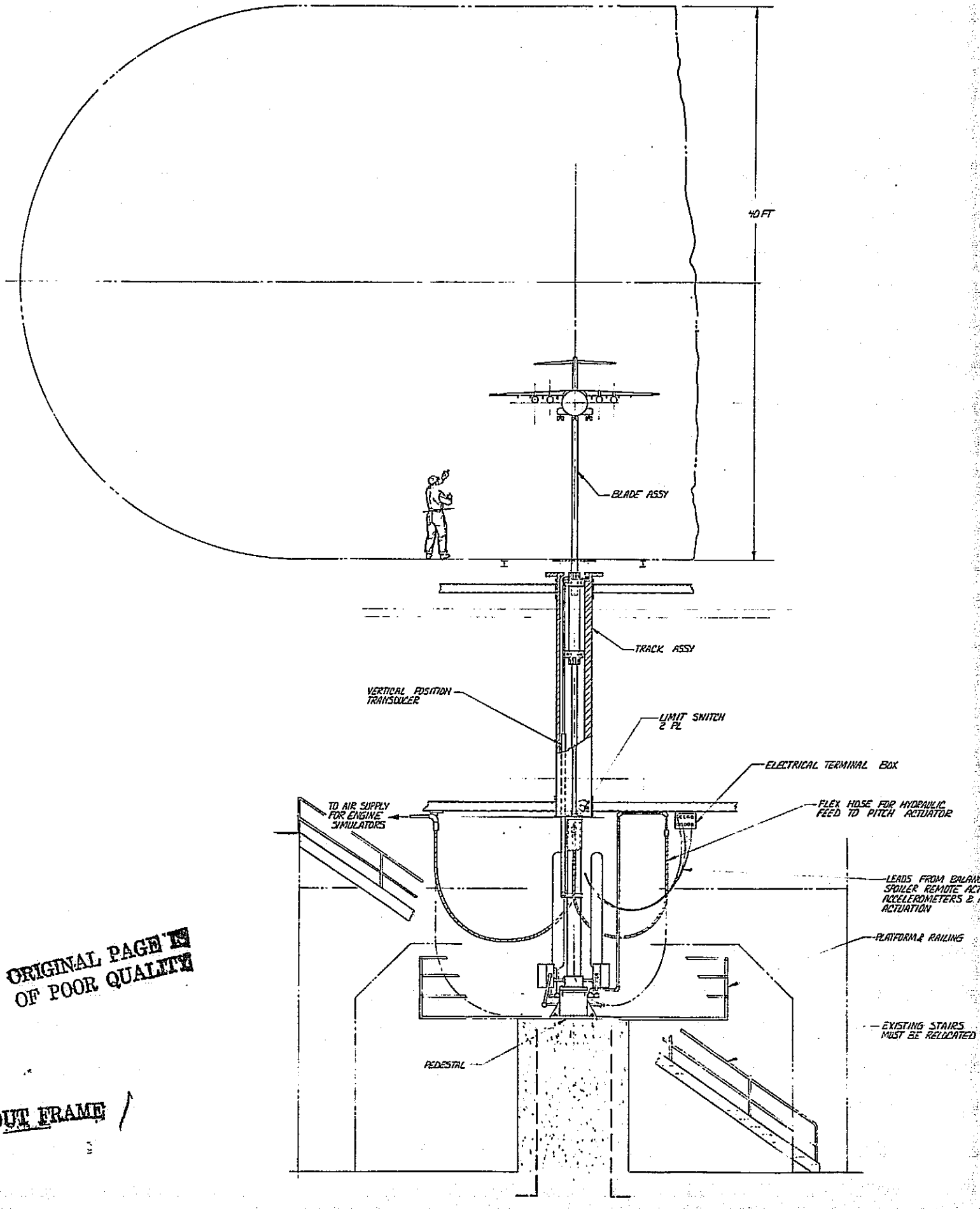

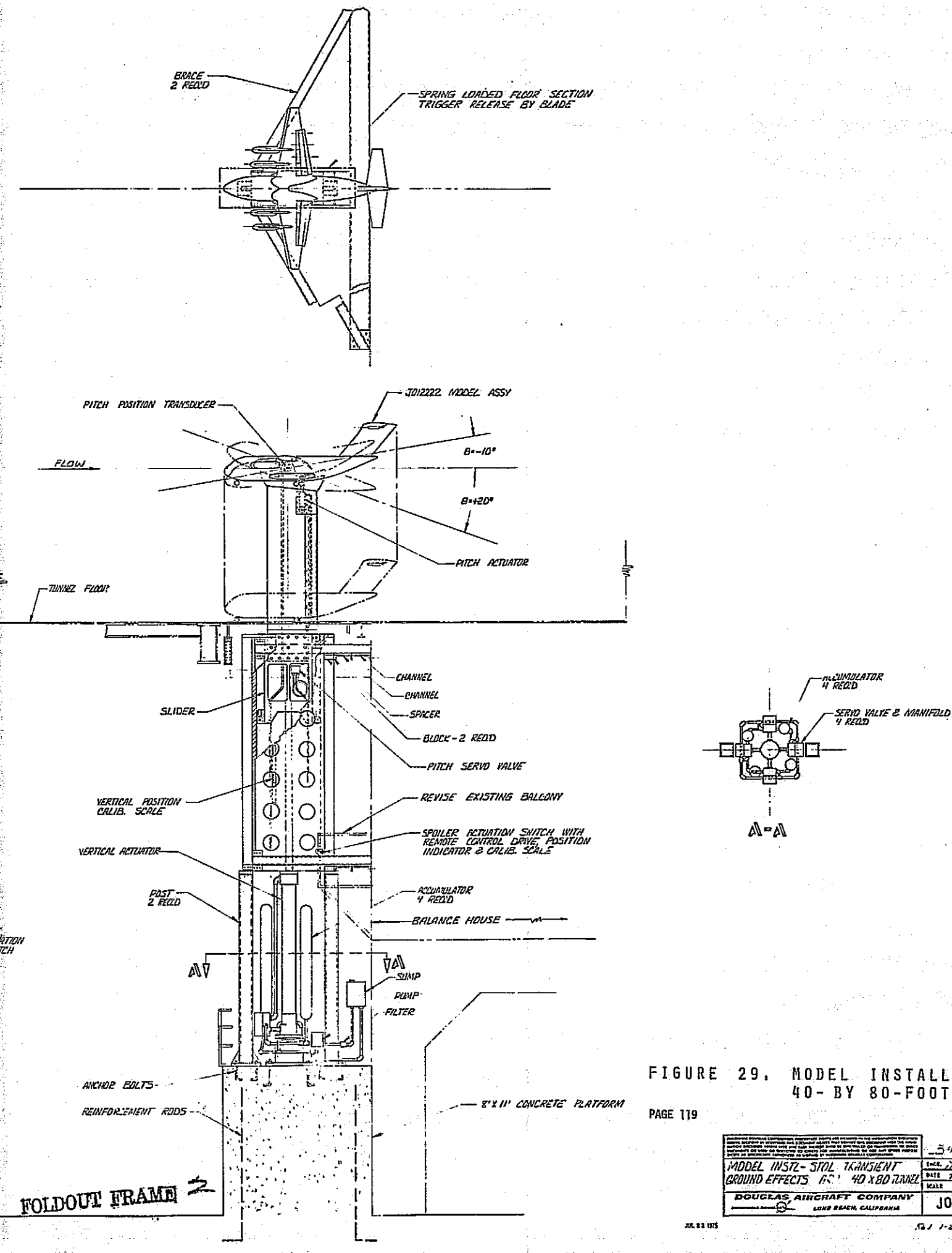

FOLDOUT FRAME 2

FIGURE 29. MODEL INSTALLATION-NASA 40- BY 80-FOOT WIND TU

PAGE 119

MODEL INSTL- STOL TRANSIENT GROUND EFFECTS 40 X 80 TUNNEL	5470
	ENGR. J. JONES
	DATE 7-23-75
	SCALE 1/12
DOUGLAS AIRCRAFT COMPANY LONG BEACH, CALIFORNIA	J012243

FOLDO

JUL 23 1975

7-24

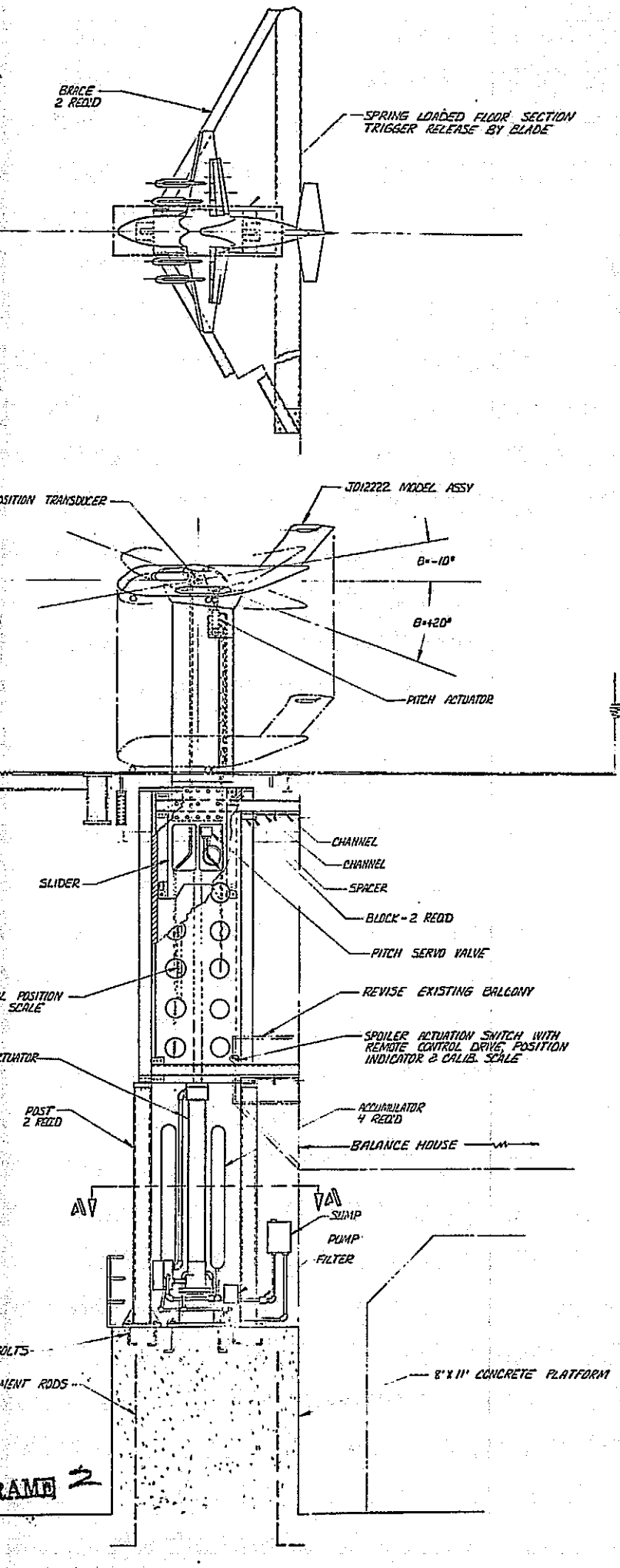

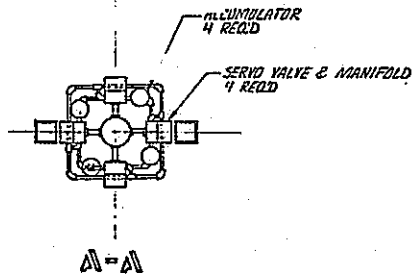

FIGURE 29. MODEL INSTALLATION-NASA AMES 40- BY 80-FOOT WIND TUNNEL

MODEL INSTL- STOL TRANSIENT GROUND EFFECTS AC' 40 x 80 TUNNEL	3470
	ENGR. JAMES LEWIS
	DATE 7-25-75
	SCALE 1/12
DOUGLAS AIRCRAFT COMPANY LONG BEACH, CALIFORNIA	J012243

FOLDOUT FRAME 2

FOLDOUT FRAME 3

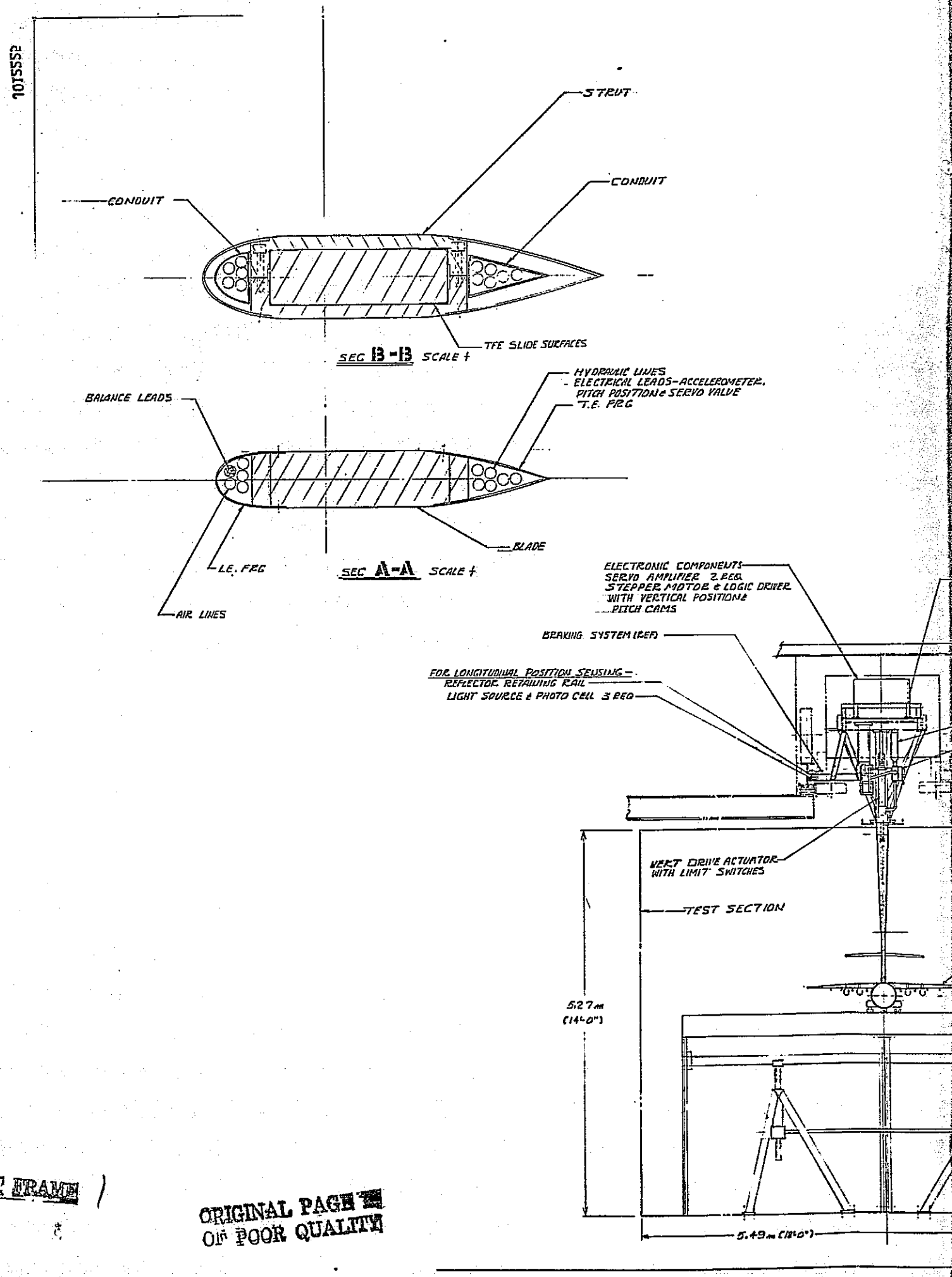

FOLDOUT FRAME

ORIGINAL PAGE IS OF POOR QUALITY

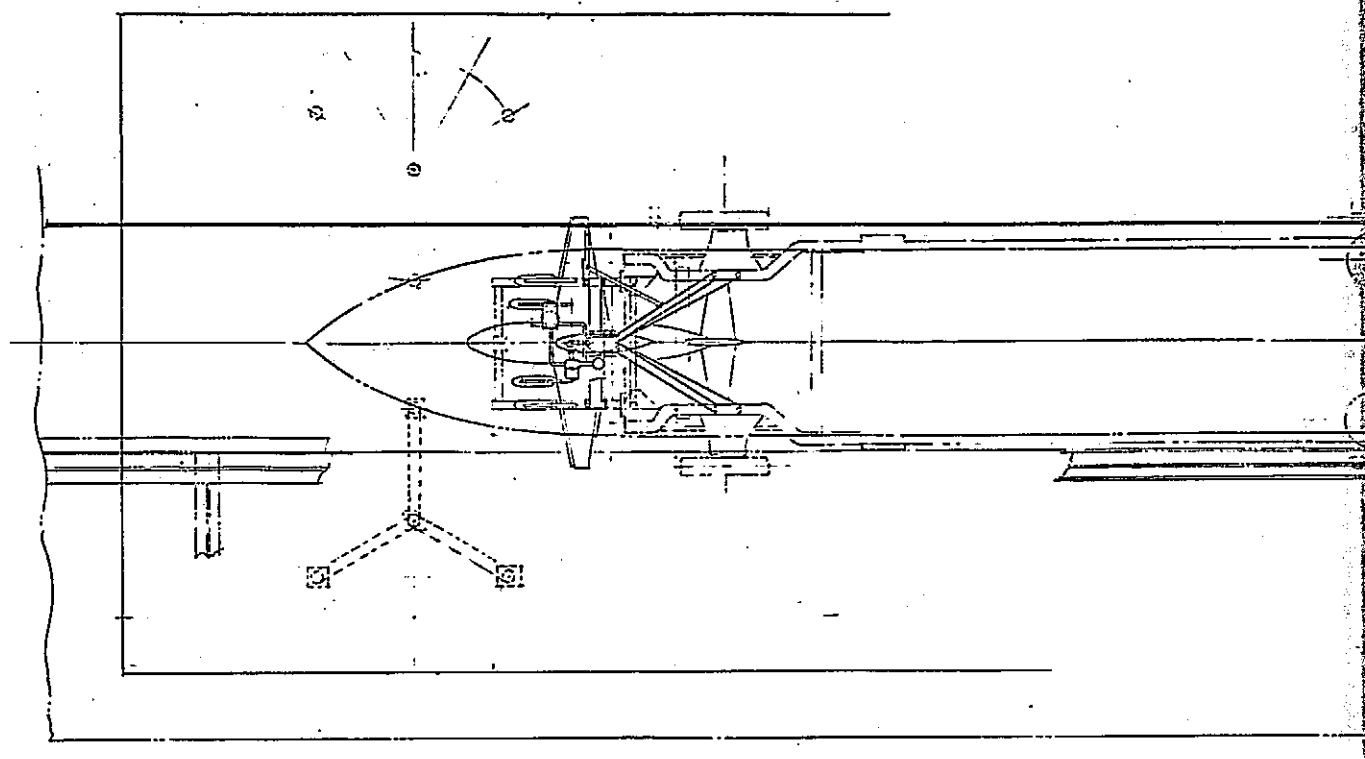

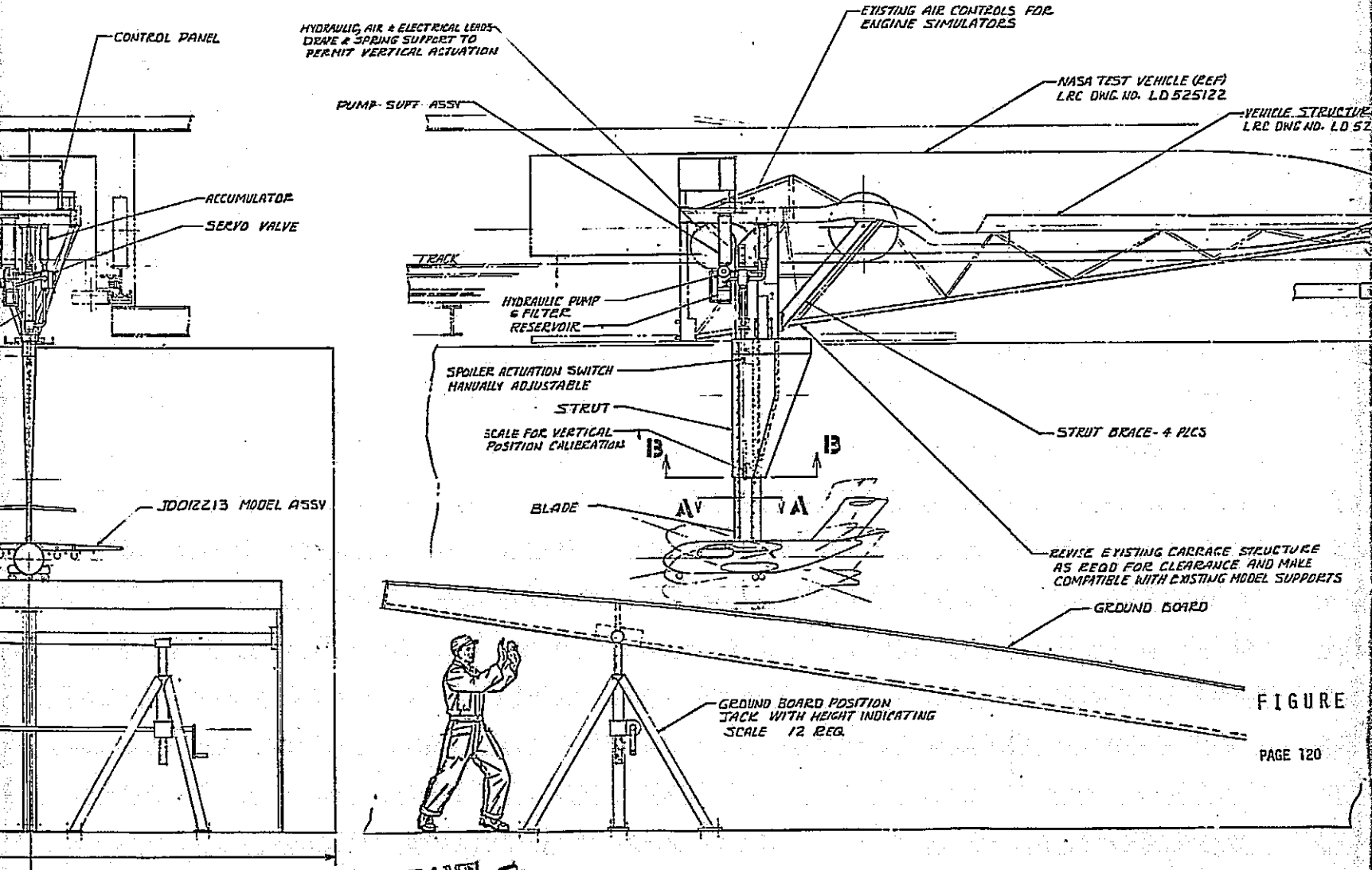

FIGURE

FOLDOUT FRAME 2

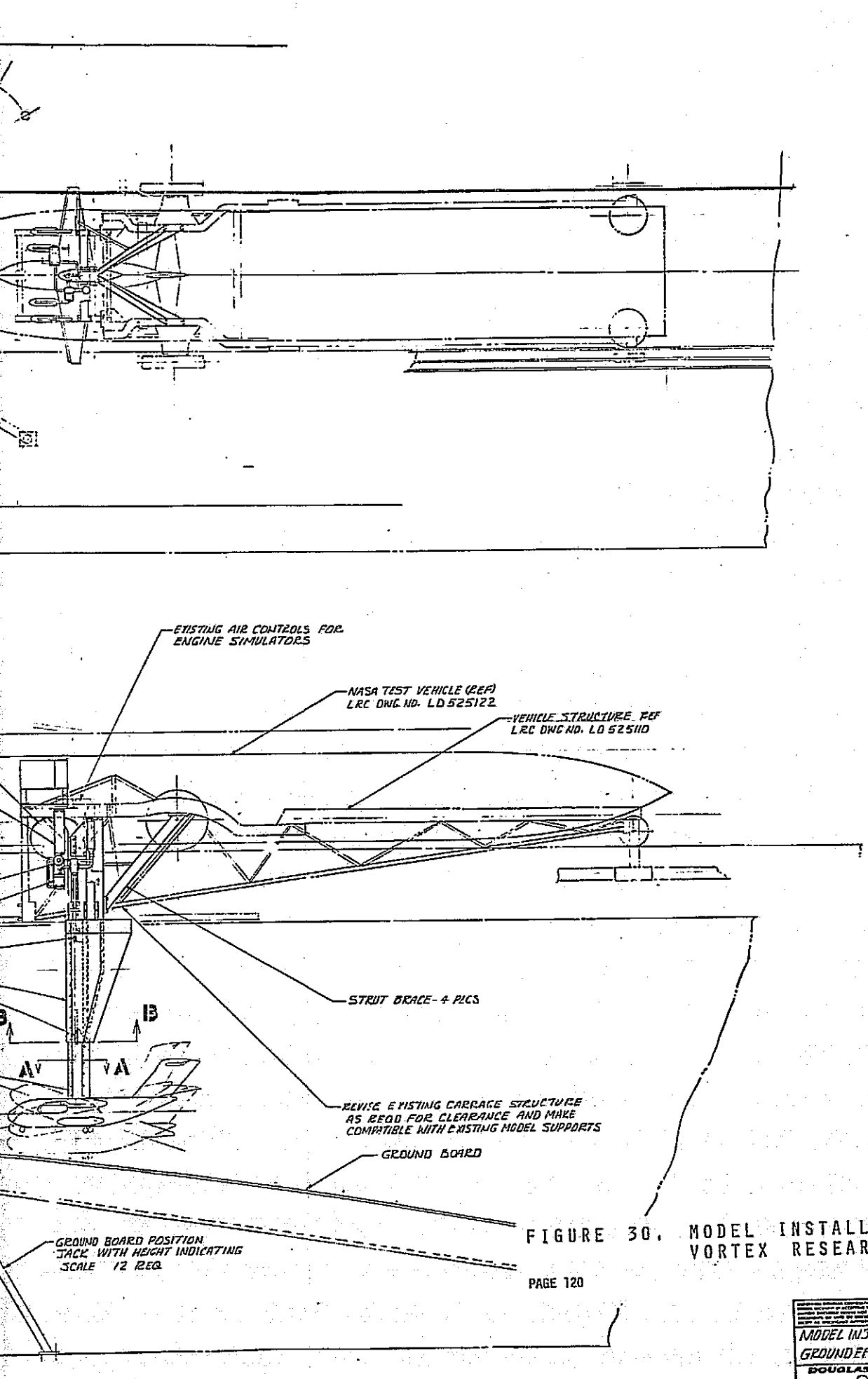

FOLDOUT FRAME 4

FIGURE 30. MODEL INSTALLATION-NASA LANGLEY VORTEX RESEARCH FACILITY

MODEL INSTL-STOL TRANSIENT GROUND EFFECTS IN LRC VRF	LB 469 (4)
	DSGN R. JONES
	DATE 7-30-75
	SCALE 1/2"
DOUGLAS AIRCRAFT COMPANY LONG BEACH, CALIFORNIA	J012225

The hydraulic actuator design concept is the same as for the blade strut installation in the V/STOL wind tunnel. However the equipment is scaled up by a factor greater than two which entails a fluid flow rate and capacity of greater than four times the smaller installation. This requires a greater number of servo valves and corresponding increase in accumulator and pump capacity. Beyond that, there is little difference in the equipment. The larger size of the cylinder and piston does present a slightly greater technical risk. It is not possible to assess the possible cost impact on the present study without a detailed hydraulic actuator design effort.

7.3.4 Vortex Research Facility

Figure 30 depicts the installation of the model and equipment in the Vortex Research Facility. The model is supported from above by a blade strut. It enters the test section through a narrow slit in the ceiling. A baffle plate surrounding the strut acts to seal the slit against disturbances caused by the carriage.

The ground board is comprised of five panels; a single curved panel, as shown in the figure 30 and four straight panels. The length of each panel is about 5.5 wing spans. The four straight panels permit a simulated constant rate descent from a height of $h = 1.0\ b$ at a flight path angle as low as $\gamma = 2.6$ degrees. The curved panel is used in conjunction with flare maneuver simulations.

This facility is examined in the context of two possible motion simulation techniques; a vertically stationary model moving horizontally over a sloped and curved ground board (motion simulation technique number two, experimental system number five) and a model with reduced vertical motion moving over a sloped, straight ground board using vertical motion to simulate the flight path curvature (motion simulation technique number five, experimental system number four). The latter imposes the more stringent condition because of the required vertical model motion. As discussed in Section 5.1.2, this motion is expressed in terms of a vertical perturbation motion from a horizontal reference line and its extent is appreciably reduced from that of motion simulation technique number one. In general, the full

scale flight coordinate system may have any arbitrary orientation to the horizontal reference line, but the landing simulation is most conveniently represented by orienting the approach flight path parallel to the reference line as depicted in the sketch below.

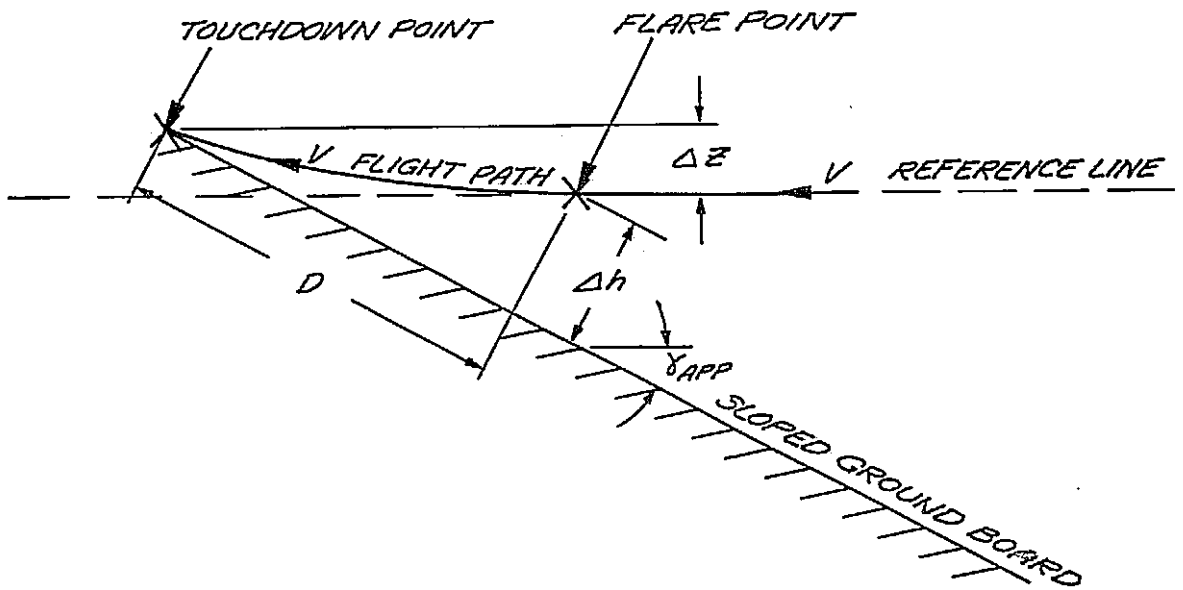

The reference line is horizontal and parallel to the carriage track. The ground plane is inclined at the approach flight path angle, γ_{APP}. For the nominal landing trajectory (section 3.2.1), the approach flight path angle is $\gamma_{APP} = 6.58$ degrees, the flare height is $\Delta h = 0.20$ b, and the distance from flare to touchdown point is $D = 2.18$ b. The vertical perturbation distance, ΔZ, needed to simulate the landing flare is given by

$$\Delta Z = D \sin \gamma_{APP} - \Delta h \cos \gamma_{APP}$$

which yields, for the above conditions, $\Delta Z = 0.051$ b. The vertical perturbation velocity, $\dot{Z}$, is initially zero and increases to a maximum at the touchdown point. It is expressed as

$$\dot{Z} = V \sin (\gamma_{APP} - \gamma) = \dot{h}_{APP} - \dot{h}$$

which is the difference between the instantaneous sink rate and the approach sink rate. For the nominal trajectory, the touchdown flight path angle is $\gamma_{T.D.} = 3.87$ degrees. The required vertical velocity varies over the range

$$0 \leq \dot{Z} \leq 0.047\ V$$

Since the touchdown flight path angle is not zero, the ground board has a break at the touchdown point. In practice the model will continue upward for a short distance as the vertical velocity decelerates to zero.

The takeoff simulation requires more vertical motion than the landing case because the full scale trajectory involves a greater change of flight path angle. Therefore, a slightly different procedure is used to minimize the required motion. The orientation of the flight path, relative to the horizontal reference line, is at an angle half-way between the initial and final flight path angle, as depicted in the sketch below:

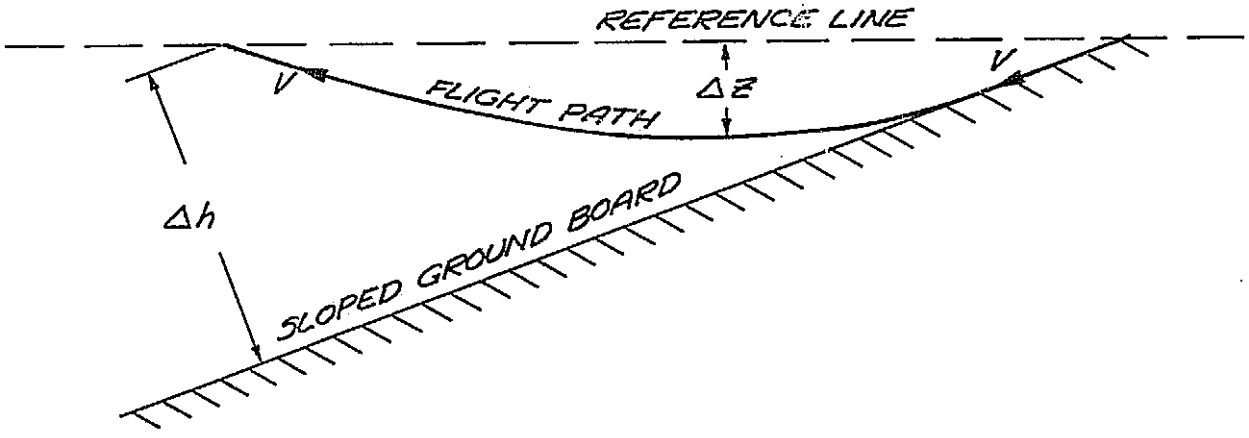

Simulation of the nominal takeoff trajectory (section 3.2.2) to a height of $\Delta h = 0.5$ b, requires a vertical perturbation distance and velocities of

$$\Delta Z = 0.14\ b$$

$$-0.063\ V \leq \dot{Z} \leq 0.054\ V$$

The additional motion capability for starting and stopping the vertical motion is about 0.02 b.

These conditions set the design requirements for the vertical actuator at

$$\Delta Z = 0.3 \text{ m } (1.0 \text{ ft})$$
$$\dot{Z} = \pm 1.9 \text{ m } (\pm 6.3 \text{ ft/sec})$$

The vertical hydraulic actuator and equipment is relatively easily accommodated in the existing volume on the carriage ahead of the drive engine. The strut mounting requires only slight modifications to the carriage frame for additional bracing. The strut assembly consists of a lower blade attached to the model which telescopes into the upper fairing. It is supported and slides in ways coated with Teflon. The vertical actuator is attached to the strut base where it fastens to the main carriage frame. The pitch actuator is located inside the model fuselage.

The hydraulic actuators are operated from high pressure accumulators charged to a 21 MPa (3000 lb/in^2). The accumulators are charged before each run by a hydraulic pump located off the carriage.

The model installation for experimental system number five is greatly simplified in that no provisions for vertical nor pitch motion of the model are included. The model is mounted on a fixed overhead blade strut which is attached to the carriage. A remotely actuated DLC spoiler is included, however, for simulation of landing flare at a constant angle of attack.

7.3.5 Model Support and Actuator Costs

The cost analysis was conducted for two separate aspects of the support and actuator system. The first is concerned with the design and fabrication of the basic equipment, while the second aspect involves the modifications to the facilities and the installation of the equipment. The costs for these two categories are presented in table 12 and are expressed in terms of man-hours and direct dollar outlays for materials and purchased equipment. An additional dollar expenditure is listed under the installation summary for travel and per diem expense of the installation crew.

TABLE 12. MODEL SUPPORT AND ACTUATOR COSTS

	Experimental Systems				
	A	B	C	D	E
	V/STOL Wind Tunnel Blade Strut Support $F_v = 1.0$, $F_s = 0.053$	V/STOL Wind Tunnel Sting Support $F_v = 1.0$, $F_s = 0.053$	40 x 80 Foot Wind Tunnel Blade Strut Support $F_v = 1.0$, $F_s = 0.11$	Vortex Research Facility with Vertical & Pitch Motion $F_v = 0.54$, $F_s = 0.053$	Vortex Research Facility without Vertical & Pitch Motion $F_v = 0.54$, $F_s = 0.053$
	m-hr $	m-hr $	m-hr $	m-hr $	m-hr $
BASIC EQUIPMENT					
Design	3400	3510	3900	2370	1020
Fabrication	7130	5600	7390	4380	1620
Materials	$85.2K	$77.9K	$181.5K	$11.0K	$1.5K
Sub-Total $ @ $30/hr	$401K	$351K	$520K	$214K	$81K
INSTALLATION					
Design	2150	2220	3100	1690	870
Fabrication	2890	2410	7720	4200	2450
Materials	$12.6K	$12.6K	$19.2K	$5.2K	$1.5K
Travel & Per Diem	$18.8K	$17.6K	$27.2K	$12.2K	$3.5K
Sub-Total $ @ $30/hr	$183K	$169K	$371K	$194K	$105K
TOTALS					
Man-hours	15570	13740	22110	12640	5960
Materials + T&PD	$117K	$108K	$228K	$29K	$7K
Total @ $30/hr	$584K	$520K	$891K	$408K	$186K

The relatively large material expenditures shown for the basic equipment of experimental system C, and to lesser extent systems A and B, are largely due to the cost of off-the-shelf hydraulic equipment. This consists principally of the servo valves as well as the pumps and accumulators. The servo valves represent a large cost because the required actuation rates and, hence, the hydraulic fluid flow rates are close to the upper practical limit for large hydraulic actuators.

The larger actuators require proportionally more servo valve capacity. In the case of system B, greater servo valve capacity than system A is required, but the greater simplicity of the apparatus compensates for this, resulting in less dollar outlay as well as a lower total cost.

Both of the track systems include an additional effort for the fabrication and installation of the adjustable ground board equipment. Most of the cost shown under installation for system E is involved with this feature.

7.4 Instrumentation

The instrumentation equipment and measurement techniques are nearly all common to the different facilities. The most notable exceptions to this are for the Vortex Research Facility as noted in the following discussion.

7.4.1 Balance

As mentioned previously the balance is an integral part of the model support system. As such it contributes to frequency response limitations of the system. The design philosophy was therefore to seek maximum stiffness and as high a natural frequency as practical. The results of the balance design study indicate that natural frequencies appreciably greater than the required instrumentation frequency are possible to achieve without undue effort. This approach is thought necessary to limit possible coupling of the balance with other dynamic components.

The balance design adopted in this study is a six-component internal strain gage balance. The metric core is double-ended for rigid attachment to the main fuselage bulkheads. All element gage sections are designed to approximately one-half the stress level considered standard for typical internal strain gage balances. Special high output strain gages are used to prevent the signal levels from decreasing correspondingly. The required size and load capacities result in balance designs with a relatively low length-to-diameter ratio and a small element-spacing-to-diameter ratio. Consequently, single, instead of dual, gage section elements are used for rolling moment and axial force elements, particularly since these components are lightly loaded.

7.4.2 Acceleration and Position Sensors

Acceleration sensors are used principally to determine the inertia forces which must be removed from the balance output to yield the aerodynamic forces. Miniature accelerometers are mounted on the metric side of each balance element to measure the acceleration components directly.

A possibly important additional application of such sensors is to compensate for non-linear dynamic response of the balance at or near resonance conditions. This requires an additional set of accelerometers so that every balance element has a pair of accelerometers at each end of the strain gage beam. Non-linear balance behavior is the result of attenuation or amplification of the motion of one end of a beam with respect to the opposite end and is evident from the difference signal of each accelerometer pair. Twelve miniature accelerometers are used. Utilization of the accelerometers for these purposes will require extensive dynamic calibration of the system. This will entail the use of equipment to excite the apparatus at different locations and orientations over a range of frequencies.

Position sensors are required to indicate model vertical and pitch positions. The pitch position sensor is a precision potentiometer which is mounted on the pitch trunnion in the model. The vertical position sensor is a linear voltage differential transformer (LVDT). This is mounted either within the hydraulic actuator tail stock or adjacent to the vertical carriage

track. Both of these types of position sensors are widely used and are expected to offer sufficient resolution and accuracy for this task. Alternative sensors are available with significantly better performance characteristics such as rotary or linear optical encoders. These could easily be substituted for the sensors selected if necessary, but would entail additional cost for the digital-to-analog convertors.

The Vortex Research Facility installation requires, in addition, a sensor system to determine the carriage position along the track. This is a digital optical system consisting of a light source and photocell pickup on the carriage which senses the passage of reflector targets on the track rail. The targets are located on two inch centers to provide fine spatial resolution. The output of the photocell drives a ten bit binary counter which is used to address a memory device containing the actuator servo system command signals.

The DLC spoiler on the model is activated at a position that is set before each run. In the wind tunnel installations this is accomplished remotely. A microswitch located adjacent to the vertical carriage track is contacted at a certain position. The switch is positioned by a motor driven traverse unit with a position readout potentiometer. In the Vortex Research Facility installation this is accomplished by a photocell sensing a manually positioned reflector target on the track rail.

7.4.3 Servo Control System

The vertical and pitch hydraulic actuators operate in closed loop servo systems. Each system consists of a command signal generator, a position sensor, servo amplifiers, and hydraulic servo valves. Servo power boosters are required for the large servo valves as well.

The command signal generator consists of a digital memory system and a digital-to-analog convertor. For the wind tunnel installations, existing data acquisition and control computers will be used to produce time functions of the vertical and pitch positions. These will be derived from tabular input data loaded prior to the runs.

For the Vortex Research Facility installation, the position command signals are generated in reference to carriage position sensed by the photocell position pickups. The command signals are stored in two 1024-word, eight-bit memories which are addressed by the ten bit binary counter driven by the photocell. The two memories each consist of four 8 by 256 bit erasable-programmable-read-only-memory chips. These chips are programmed from paper tape data using a read-only-memory programmer. They are reusable and are erased by exposure to ultra-violet light for a few minutes.

The command signals and position sensor signals are input to the servo amplifiers which produce drive signals for the hydraulic servo valves.

7.4.4 Engine Simulator Sensors

The direct supply engine simulators require instrumentation to measure jet total temperature and total pressure and the drive air flow rates. Each simulator is individually controllable and so requires a duplicate set of instrumentation. The temperature is measured by a thermocouple probe inserted into the high pressure plenum from the upstream end with the probe body enclosed in the nacelle forebody fairing. A total pressure probe is located in the exit nozzle duct and routed to a pressure transducer in the nacelle forebody. This transducer must be of a type that can tolerate moderate accelerations without producing spurious signals.

The drive air flow rate is measured by standard airflow meters located off the equipment. The importance of flow rate measurements depends, to a certain extent, on the type of powered lift system. Configurations such as the USB or augmentor wing, where the jet exit is located in or near a changing flow field, have a stronger requirement for such measurements than the EBF where the jet exit is relatively remote from the wing flow field. For the nominal STOL configuration in the present example, these measurements may not be necessary. In any event, since such instrumentation in generally available at most wind tunnel facilities, it is not included in the cost estimate presented.

7.4.5 Control Panel

The control panel incorporates all the control and monitor provisions for the model, support, and actuator systems in one central location. For the wind tunnel installation this is in the wind tunnel control room. In the Vortex Research Facility this is located onboard the carriage. Parameters for which monitor provisions are required are vertical and pitch position, engine simulator jet total pressure, and hydraulic system pressure. Also an indicator for the DLC spoiler activation is provided. Control provisions include manual vertical and pitch position, engine simulator jet total pressure, and hydraulic pump controls. A control mode selector is provided to select automatic or manual position control.

Special equipment located in the control panel includes power supplies, servo amplifiers, servo power boosters, and safety interlocks for failsafe shutdown controls.

7.4.6 Instrumentation Costs

Of the instrumentation costs presented in table 13, the largest element is the balance. These costs are based on an informal quotation from an established strain gage balance manufacturer and entail relatively low risk. The costs could be reduced by substituting a three-component balance design.

The major part of the cost for acceleration and position sensors is due to the miniature accelerometers for resolution of inertia forces. These coats are absent for experimental system number five where there is no vertical acceleration.

7.5 Total Cost Summary

The total experimental system costs are presented in table 14, summarized under four separate categories; model, support and actuator basic equipment, support and actuator installation, and instrumentation. The costs are expressed in terms of man-hours and direct dollar outlays for materials and purchased equipment. Total dollars costs are presented based

TABLE 13. INSTRUMENTATION COSTS

	Experimental System				
	A	B	C	D	E
	V/STOL Wind Tunnel Blade Strut Support F_v = 1.0, F_s = 0.053	V/STOL Wind Tunnel Sting Support F_v = 1.0, F_s = 0.053	40 x 80 Foot Wind Tunnel Blade Strut Support F_v = 1.0, F_s = 0.11	Vortex Research Facility with Vertical & Pitch Motion F_v = 0.54, F_s = 0.053	Vortex Research Facility without Vertical & Pitch Motion F_v = 0.54, F_s = 0.053
	m-hr $	m-hr $	m-hr $	m-hr $	m-hr $
BALANCE					
Materials	$40.5K	$40.5K	$55.0K	$40.5K	$40.5K
ACCELERATION AND POSITION SENSORS					
Design & Fabrication	400	400	400	200	100
Materials	$7.4K	$7.4K	$7.4K	$6.9K	$0.5K
SERVO CONTROL SYSTEM					
Design & Fabrication	970	970	970	700	-
Materials	$1.5K	$2.5K	$3.9K	$3.0K	-
ENGINE SIMULATOR SENSORS					
Design & Fab	100	100	100	100	100
Materials	$2.0K	$2.0K	$2.0K	$2.0K	$2.0K
CONTROL PANEL					
Design & Fab	800	800	800	300	-
Materials	$1.5K	$2.0K	$2.5K	$0.5K	-
TOTALS					
Man-Hours	2270	2270	2270	1300	200
Materials	$52.9K	$54.4K	$70.8K	$52.9K	$43.0K
Total @ $30/hr	$121K	$122K	$139K	$92K	$49K

TABLE 14. TOTAL COST SUMMARY

	Experimental System				
	A	B	C	D	E
	V/STOL Wind Tunnel Blade Strut Support $F_v = 1.0$, $F_s = 0.053$	V/STOL Wind Tunnel Sting Support $F_v = 1.0$, $F_s = 0.053$	40 x 80 Foot Wind Tunnel Blade Strut Support $F_v = 1.0$, $F_s = 0.11$	Vortex Research Facility with Vertical & Pitch Motion $F_v = 0.54$, $F_s = 0.053$	Vortex Research Facility without Vertical & Pitch Motion $F_v = 0.54$, $F_s = 0.053$
	m-hr $	m-hr $	m-hr $	m-hr $	m-hr $
MODEL					
Man-Hours	9510	9630	16900	10310	10310
Direct Dollars	$5.5K	$5.5K	$9.7K	$5.5K	$5.5K
Sub-Total @ $30/hr	$291K(.29)	$294K(.31)	$517K(.33)	$315K(.39)	$315K(.57)
SUPPORT & ACTUATOR					
Man-Hours	10530	9110	11290	6750	2640
Direct Dollars	$85K	$78K	$182K	$11K	$1.5K
Sub-Total @ $30/hr	$401K(.40)	$351K(.38)	$520K(.34)	$214K(.26)	$81K(.15)
INSTALLATION					
Man-Hours	5040	4630	10820	5890	3320
Direct Dollars	$31K	$30K	$46K	$17K	$5.0K
Sub-Total @ $30/hr	$183K(.19)	$169K(.18)	$371K(.24)	$194K(.24)	$105K(.19)
INSTRUMENTATION					
Man-Hours	2270	2270	2270	1300	200
Direct Dollars	$53K	$54K	$71K	$53K	$43K
Sub-Total @ $30/hr	$121K(.12)	$122K(.13)	$139K(.09)	$92K(.11)	$49K(.09)
TOTALS					
Man-Hours	27350	25640	41280	24250	16470
Direct Dollars	$175K	$168K	$309K	$87K	$55K
Total @ $30/hr	$996K	$937K	$1547K	$814K	$549K
Relative Total Cost	1.00	0.94	1.55	0.82	0.55

on an average rate of $30 per hour. The sub-total costs shown for each of the four categories have a figure in parentheses indicating the fraction of the total system cost.

The wind tunnel experimental systems all appear relatively similar in terms of the relative costs of the four categories. The model costs are slightly greater than 30 percent, the support and actuator costs total slightly less than 60 percent, and the instrumentation is about 10 percent. For the two track systems, the model cost becomes a greater fraction, the support and actuator costs a smaller part, and the instrumentation costs remain about 10 percent of the total.

The greatest potential for cost reduction appears to be in the model. The design philosophy adopted for this study of striving for minimal model weight results in relatively difficult construction techniques. If a more detailed analysis of the model and support dynamic response shows that greater model weights can be tolerated, the model costs could be reduced somewhat. The greatest model cost reduction would be most probable for track systems. The other cost categories appear to have less potential for cost reduction. A brief examination of the cost sensitivity to the wind tunnel systems test speed indicated little effect.

8.0 RECOMMENDED EXPERIMENTAL APPROACH

8.1 Discussion

In selecting an approach to the experimental investigation of transient ground effects the most important considerations are:

- o Ability to comply with the simulation requirements
- o Cost of developing and installing the apparatus and model
- o Cost of conducting the experiment

Of the experimental systems examined, all comply with the simulation requirements to varying, but what are considered to be satisfactory extents. The system development and installation costs are significant not only in their relative levels, extending over a range of nearly three-to-one, but also in terms of their magnitudes, as great as $1.55 million. The costs of conducting the experiment are only considered in a qualitative manner, since detailed operating costs for the various facilities are not available.

Of the two distinctive types of experimental systems, wind tunnel and test track, the wind tunnel systems have improved simulation potential in one respect, Reynolds number, while the test track systems have an advantage in the exact modeling of the ground plane boundary layer.

The significance of Reynolds number in experimental situations of this type pertains principally to a minimum acceptable value. Operating at Reynolds numbers greater than the minimum value will, in general, improve the quality of the aerodynamic data. However the overall experimental feasibility may not be significantly enhanced. The available evidence suggests that the Reynolds number capability of the test track experimental systems is sufficiently large to provide the necessary aerodynamic data quality. Therefore the greater Reynolds number potential of the wind tunnel facilities may not be a strong advantage.

The importance of the exact ground plane boundary layer simulation provided by the track facility relative to the wall jet BLC system in the wind tunnel is difficult to establish with certainty. The wall jet BLC system can prevent premature ground plane separation, but the condition of the flow under the model exhibits differences from the freestream in velocity

profile, turbulence intensity, and entrainment which may cause significant, though subtle, errors in the flow for some conditions. In addition, neither wind tunnel presently has a wall jet BLC system although one is planned for the 40- by 80-foot wind tunnel. The cost of providing such a system is not included in this study, but could well be an important factor.

Use of the existing moving belt ground plane and boundary layer removal equipment in the V/STOL Wind Tunnel is possible in conjunction with the sting mount apparatus. However, the moving belt is limited to a maximum speed of 30 m/sec (100 ft/sec.). Also the sting mount is less satisfactory than the blade strut in several important respects: poorer dynamic response, large sting interference with the empennage, difficulty of accommodating the entire model pitch range, and increased development risk for the large hydraulic actuator.

It is concluded that, in terms of simulation accuracy, the experimental systems utilizing the Vortex Research Facility have a slight advantage over either of the wind tunnel systems.

Because of the very large cost levels identified for the development and installation of the various experimental systems, the cost differences between them remain relatively large and therefore significant. Some experimental advantages do result from the increased costs and are felt in both the areas of simulation accuracy and experiment conduct.

The most obvious advantage gained by the increased costs is the simulation improvement due to increased Reynolds number. The principal difference between the experimental systems in the two different wind tunnels is an increase in the Reynolds number capability from $1.1\ (10)^6$ to $2.2\ (10)^6$. The cost increase associated with this is from \$1.00M to \$1.55M. As mentioned above, such a Reynolds number increase provides little enhancement to the experimental feasibility and is not thought to warrant the substantial increase in cost required to achieve it.

The cost increment associated with the Reynolds number increment between the V/STOL wind tunnel and the Vortex Research Facility is smaller and the

Reynolds number advantage is greater than in the first example. However, since the lower Reynolds number capability of the track facility is still considered acceptable, the simulation advantage of the exact ground boundary layer modeling becomes the overriding factor in its favor.

The importance of the improved flight path simulation resulting from the cost increment between the two track experimental systems depends principally on the importance of the flight path curvature effects and the ease of estimating appropriate corrections. The results of the analysis of these effects presented in this report suggest that they are relatively small and easily corrected. The accuracy of this assessment will probably not be verified until the first experimental results are in hand. However, the track experimental system for straight flight (system E) can be easily expanded to perform curved flight simulations with little or no wasted effort. Thus, initial experiments can be conducted with the view that if the results appear to warrant the additional cost, the apparatus can be upgraded to provide the complete motion capability.

It is evident that the experimental systems utilizing the Vortex Research Facility have a strong advantage with respect to the cost of developing and installing the apparatus.

The third criterion specified for selecting the experimental approach, i.e., the cost of conducting the experiment, depends principally on the ratio of the utilization rate (i.e., runs per day) of the facility and the charge rate (i.e., $ per day). The latter information is not available, but the general observation is that the 40- by 80-foot Wind Tunnel probably has the highest charge rate and the Vortex Research Facility the lowest, with the V/STOL Wind Tunnel intermediate. The present understanding of the operating characteristics of the facilities and the cycle times of the various experimental systems suggests that the number of runs per day the wind tunnel installations may be capable of is on the order of 100. The Vortex Research Facility, because of cycle time limitations for the basic carriage system, can only accommodate, on the order of, ten runs per day. Thus the wind tunnel facilities may have a cost advantage in this respect, depending on their

charge rates.

The relative importance of these considerations depends on the extent of future experimental studies of transient ground effects. This will depend on the importance of transient effects discerned from the experiments. The present understanding of the problem derived from analytical and limited experimental results summarized in Part I of this report, suggests that the problem is not so great that many STOL configurations will require extensive experimental studies. Therefore, the cost of conducting the experiments cannot, at the present time, be considered as important a factor as the other two criteria.

The experimental systems utilizing wind tunnels apparently have a slight advantage in terms of the cost of conducting the experiment.

The track experimental system without vertical model motion (system E) has an additional advantage in terms of data reduction. Since the model experiences no forced accelerations during the data acquisition, the balance data have no inertia forces superimposed on the aerodynamic forces. Therefore there is no need to provide accelerometers to measure these forces. This eliminates the expense of the sensors, but, possibly more significant, it reduces the experimental risk inherent in separating the inertia and aerodynamic forces and implies a potential for obtaining higher quality aerodynamic data.

In terms of the specified selection criteria, the experimental systems employing the Vortex Research Facility have a slight advantage in simulation accuracy and a strong advantage for the cost of developing and installing the apparatus. The wind tunnel experimental systems probably have an advantage in terms of the cost of conducting the experiment, but the importance of that advantage is not thought to be significant. It is concluded that the Vortex Research Facility offers an overall advantage and therefore provides the basis for the recommendations presented in the next section.

8.2 Recommendations

The recommended approach for the experimental investigation of STOL

aircraft transient ground effects is a two-phase program utilizing the NASA Langley Vortex Research Facility. The initial phase of the program entails testing a powered STOL model traveling along a straight flight path over a sloped and curved ground board. Motion simulation errors due to flight path curvature can be corrected with simple analytical procedures. This approach corresponds to experimental system E.

If transient ground effect phenomena are discovered in the initial phase that appear significant enough to warrant more accurate modeling of the flight path curvature, the second phase of the program would be instituted. This will entail installation of vertical and pitch motion apparatus on the carriage to directly model the correct flight trajectory as with experimental system D.

Prior to commencing this program, careful consideration should be given to a pilot program to acquire preliminary experimental data for correlation with analytical results. This will provide a basis for a rational decision about the importance of investing in a transient ground effect facility. This pilot program should be conducted in the Vortex Research Facility with what amounts to a simplified version of experimental system E (a vertically stationary model moving over a sloped ground board). Attempts should be made to utilize existing model and instrumentation equipment. The pilot program should consist of the following three tasks:

(1) Ascertain dynamic properties of Vortex Research Facility carriage.

(2) Analyze dynamic properties of a simple model installation with an existing balance. If necessary a high stiffness three-component balance could be utilized.

(3) Conduct the transient ground effect experiments over a sloped ground board and correlate the data with analytical methods. This task can be considered a repeat of the experiment reported in reference 1, but with deficiencies of that experiment removed and for a wider range of conditions.

The first two of these three tasks can be accomplished with very modest effort. The third task, involving fabrication or modification of hardware, as well as operation of the facility, is necessarily more expensive.

Accurate estimates of the cost of this program were not prepared as part of this study because of uncertainties regarding the availability of suitable model and instrumentation equipment. However, based on the examination of experimental system E with the cost of the model and balance removed, and allowing for certain experiment simplifications, the cost of the pilot program can confidently estimated to be less than $200k.

9.0 REFERENCES

1. Turner, Thomas R.: Ground Influence on a Model with a Jet-Augmented Flap as Determined by Two Techniques. NASA TN D-658, February 1961.

2. Douglas Aircraft Company: Study of Quiet STOL Aircraft for Short Haul Transportation, Report MDC J4371, June 1973.

3. Parlett, L. P., Smith, C. C., Jr., and Megrail, J. L.: Wind-Tunnel Investigation of Effects of Variations in Reynolds Number and Leading-Edge Treatment on the Aerodynamic Characteristics of an Externally Blown Jet-Flap Configuration. NASA TN D-7194, August 1973.

4. Gentry, G. L., Jr.: Wind-Tunnel Investigation of an Externally Blown Flap STOL Transport Model Including an Investigation of Wall Effects. NASA TM X-3009, September 1974.

5. Vogler, R. D.: Wind-Tunnel Investigation of a Four-Engine Externally Blowing Jet-Flap STOL Airplane Model. NASA TN D-7034, December 1970.

6. Curtiss, H. C., Jr., Traybar, J. J., and Putman, W. F.: The Effect of Ground Proximity on the Lateral/Directional Aerodynamic and Control Characteristics of a Tilt-Wing V/STOL Aircraft at High Lift Coefficients. AFFDL-TR-73-151, December 1973.

7. Hess, J. L. and Smith, A. M. O.: Calculation of Potential Flow About Arbitrary Bodies. Progress in Aeronautical Sciences, Vol. 8, Pergamon Press, New York, 1966.

8. Heyson, H. H.: Linearized Theory of Wind-Tunnel Jet-Boundary Corrections and Ground Effect for VTOL-STOL Aircraft. NASA TR R-124, 1962.

9. Hackett, J. E., Praytor, E. B., Boles, R. A., and Caldwell, E. O.: Ground Effect for V/STOL Aircraft Configurations and its Simulation in the Wind Tunnel. Part I, Introduction and Theoretical Studies, NASA CR-114,495; Part II, Experimental Studies, NASA CR-114,496; Part III, The Tangentially Blown Ground as an Alternative to a Moving Ground: Application to the NASA Ames 40- by 80-foot Wind Tunnel, NASA CR-114,497.

10. Poisson-Quinton, Ph. and Christophe, J.: Special Ground Testing Facilities and Testing Techniques for STOL Aircraft. Von Karman Institute for Fluid Dynamics, Lecture Series 60, STOL TECHNOLOGY, September 1973.

11. DeFrance, S. J.: The NACA Full-Scale Wind Tunnel, NACA Report No. 459, 1933.

12. Cambra, J. M. and Tolari, G. P.: Real-Time Computer Data System for the 40- by 80-Foot Wind Tunnel Facility at Ames Research Center. NASA TN D-7970, May 1975.

13. Patterson, J. C., Jr.: Lift-Induced Wing-Tip Vortex Attenuation. AIAA Paper No. 74-38, January 1974.